University of Alberta

Study of Hydrodynamics in Structured Packing

by

Sharmeen Akhter ©

A thesis submitted to the Faculty of Graduate Studies and Research
in partial fulfillment of the requirements for the degree of

Master of Science

in

Chemical Engineering

Department of Chemical and Materials Engineering

Edmonton, Alberta
Fall 2006

Library and Archives Canada

Published Heritage Branch

395 Wellington Street
Ottawa ON K1A 0N4
Canada

Bibliothèque et Archives Canada

Direction du Patrimoine de l'édition

395, rue Wellington
Ottawa ON K1A 0N4
Canada

Your file Votre référence
ISBN: 978-0-494-22217-1
Our file Notre référence
ISBN: 978-0-494-22217-1

NOTICE:
The author has granted a non-exclusive license allowing Library and Archives Canada to reproduce, publish, archive, preserve, conserve, communicate to the public by telecommunication or on the Internet, loan, distribute and sell theses worldwide, for commercial or non-commercial purposes, in microform, paper, electronic and/or any other formats.

The author retains copyright ownership and moral rights in this thesis. Neither the thesis nor substantial extracts from it may be printed or otherwise reproduced without the author's permission.

AVIS:
L'auteur a accordé une licence non exclusive permettant à la Bibliothèque et Archives Canada de reproduire, publier, archiver, sauvegarder, conserver, transmettre au public par télécommunication ou par l'Internet, prêter, distribuer et vendre des thèses partout dans le monde, à des fins commerciales ou autres, sur support microforme, papier, électronique et/ou autres formats.

L'auteur conserve la propriété du droit d'auteur et des droits moraux qui protège cette thèse. Ni la thèse ni des extraits substantiels de celle-ci ne doivent être imprimés ou autrement reproduits sans son autorisation.

In compliance with the Canadian Privacy Act some supporting forms may have been removed from this thesis.

While these forms may be included in the document page count, their removal does not represent any loss of content from the thesis.

Conformément à la loi canadienne sur la protection de la vie privée, quelques formulaires secondaires ont été enlevés de cette thèse.

Bien que ces formulaires aient inclus dans la pagination, il n'y aura aucun contenu manquant.

Canada

Abstract

Hydraulics experiments, such as, pressure drop, liquid distribution and liquid dispersion were carried out for counter-current two-phase flow in a 0.3 m ID packed column loaded with four elements of stainless steel flexipac-3Y, unperforated corrugated structured packings to understand the flow phenomena inside the packing. Due to the complex geometry and complex, dynamic nature of trickle flow inside the packings, a thorough understanding of flow phenomena inside the column is hard to develop with the aid of experiments alone. Thus a 3-D computational fluid dynamics (CFD) model (UofA's model) based on the experiments was built to predict single-phase (Air) pressure drop and tracer dispersion. Another CFD model based on Zogg's experiments (Zogg, 1972) was developed to predict single and two-phase pressure drop of sulzer mesh-BX structured packings. In most of the cases, the simulation results showed good agreement with that of the experiments. For the simulations, commercial packages, such as, Fluent-6.1.22 and CFX-5.7.1 were used.

Acknowledgment

I gratefully acknowledge my supervisors, Dr. K. Nanadakumar and Dr. K.T. Chuang for their continuous guidance and kind supervision. Special thanks to Dr. Xiaoming Wen and Dr. Ekambara Kalekudithi for their valuable advices and help in doing simulations. I am also indebted to Mr. A. Afacan for his generous help in laboratory during the experiments. Lastly special thanks to my husband, AKM Monjur Murshed for his continuous mental support during my whole research period. The happiness and joy that my daughter Moumita Shasmeen Murshed brought to our lives is also remembered.

To My Parents

for all their love and kindness they gave me throughout my life

Table of Contents

CHAPTER 1 INTRODUCTION 1

CHAPTER 2 LITERATURE REVIEW - PACKED COLUMN 4

2.1 INTRODUCTION 4

2.2 PACKING CHARACTERISTICS 4

2.3 TYPES OF RANDOM PACKINGS 5

2.4 TYPES OF STRUCTURED PACKINGS 6

2.5 GEOMETRICAL FEATURES OF CORRUGATED STRUCTURED PACKINGS 11

2.5.1 Element Geometry *12*

2.5.2 Surface Features *12*

2.6 PACKING MATERIALS 13

2.6.1 Metals *13*

2.6.2 Ceramics *13*

2.6.3 Plastics *14*

2.7 PACKING HYDRAULICS 17

2.7.1 Liquid Holdup *17*

2.7.2 Pressure Drop *18*

2.7.3 Liquid Distribution *21*

2.7.4 Liquid Dispersion *21*

2.7.5 Mass Transfer *22*

2.8 PREVIOUS WORKS ON STRUCTURED PACKING 24

2.9 CONCLUSION 31

CHAPTER 3 MODEL EQUATIONS 32

3.1 INTRODUCTION 32

3.2 CONSERVATION EQUATIONS 32

3.2.1 Closure Relationships *33*

3.3 TURBULENCE MODELING 34

3.3.1 Closure Relationships *35*

3.4 MULTIPHASE MODELING 36

3.4.1 The Concept of Volume Averaging 37
3.4.2 Multi-fluid model 39
3.5 TURBULENT MULTIPHASE FLOW 43
3.6 CONSERVATION OF SPECIES 45
3.7 COMPUTATIONAL FLUID DYNAMICS (CFD) 46
3.7.1 Grid Generation 47
3.7.2 Interpolation and Differencing Scheme 47
3.7.3 Solution of Algebraic System of Equations 48
3.8 CONCLUSIONS 50

CHAPTER 4 EXPERIMENTAL MEASUREMENT OF FLOW HYDRODYNAMICS 51

4.1 INTRODUCTION 51
4.2 EXPERIMENTAL SETUP 51
4.3 EXPERIMENTAL MEASUREMENTS OF DRY AND IRRIGATED PRESSURE DROP 53
4.3.1 Experimental Procedure and Range of Operating Parameters 53
4.3.2 Results and Discussion 54
4.4 EXPERIMENTAL MEASUREMENTS OF LIQUID DISTRIBUTION 55
4.4.1 Introduction 55
4.4.2 Design of Liquid Distributor 55
4.4.3 Design of Liquid Collector 58
4.4.4 Experimental Procedure and Range of Operating Parameters 61
4.4.5 Results and Discussion 62
4.4.6 Quantification of Liquid Maldistribution 81
4.5 EXPERIMENTAL MEASUREMENTS OF LIQUID DISPERSION 84
4.5.1 Introduction 84
4.5.2 Experimental Procedure and Range of Operating Parameters 84
4.5.3 Results and Discussion 85
4.6 CONCLUSION 86

CHAPTER 5 CFD SIMULATIONS OF PRESSURE DROP AND TRACER DISPERSION 91

5.1 Introduction 91
5.2 Description of flow geometry and operating conditions 91
5.2.1 Pressure Drop in Zogg's and UofA's Models 91
5.2.2 Tracer Dispersion in UofA's Model 92
5.3 Assumptions Made During Simulations 92
5.4 Model Equations Solved by CFD Software's 97
5.5 Boundary Conditions used in the Simulations 98
5.6 Initial Values, Discretization Schemes and Flow Field Initialization ... 101
5.7 Simulation of Single-Phase Pressure Drop in Zogg's and UofA's Models 101
5.8 Simulation of Two-Phase Pressure Drop in Zogg's Model 102
5.9 Simulation of Single-Phase Tracer Dispersion in UofA's Model 103
5.10 Results and Discussions 104
5.10.1 Single-Phase Pressure Drop in UofA's Model 104
5.10.2 Single-Phase Pressure Drop in Zogg's Model 111
5.10.3 Two-phase Pressure Drop in Zogg's Model 116
5.10.4 Single-phase Tracer Dispersion in UofA's Model 120
5.11 Conclusions 133

CHAPTER 6 FUTURE WORK 134

6.1 Mass Transfer Modeling 134
6.2 Prediction of Mass Transfer efficiency 134
6.3 Prediction of Residence Time Distributions 135

BIBLIOGRAPHY 136

APPENDIX 141

List of Tables

Table 2.1 Geometric Characteristics of Common Metal Corrugated-Sheet Structured Packings 15

Table 5.1 Physical properties of air, water and carbon-dioxide (CO_2) 96

Table 5.2 Geometrical characteristics of the packings used in the simulation 96

List of Figures

Figure 2.1 Schematic diagram of random packings 7
Figure 2.2 Schematic diagram of structured packings (Kister, 1992) 8
Figure 2.3 Schematic diagrams of three generations of random packings 9
Figure 2.4 Schematic diagrams of common corrugated structured packings 10
Figure 2.5 Simulated and experimental total pressure drop versus gas flow factor, F_s for flexipac (Rocha et al., 1993, 1996) 20
Figure 3.1 A planar sketch of representative elementary volume, ... 38
Figure 4.1 Schematic diagram of experimental setup 52
Figure 4.2 Plot of experimental pressure drop vs. f-factor for flexipac-3Y type packing at different gas and liquid loads 56
Figure 4.3 Comparison of experimental dry and wet pressure drop with Bravo's correlation 57
Figure 4.4 Schematic diagram of liquid distributor 59
Figure 4.5 Schematic diagram of liquid collector 60
Figure 4.6 Liquid distribution for L: 0.004 m^3/m^2s, G: 1.1 m^3/m^2s and bed height: 0.264 m 64
Figure 4.7 Liquid distribution for L: 0.004 m^3/m^2s, G: 2.2 m^3/m^2s and bed height: 0.264 m 65
Figure 4.8 Liquid distribution for L: 0.002 m^3/m^2s, G: 1.1 m^3/m^2s and bed height: 0.264 m 66
Figure 4.9 Liquid distribution for L: 0.002 m^3/m^2s, G: 2.2m^3/m^2s and bed height: 0.264 m 67
Figure 4.10 Liquid distribution for L: 0.004 m^3/m^2s, G: 1.1 m^3/m^2s and bed height: 0.528 m 68
Figure 4.11 Liquid distribution for L: 0.004 m^3/m^2s, G: 2.2m^3/m^2s and bed height: 0.528 m 69
Figure 4.12 Liquid distribution for L: 0.002 m^3/m^2s,G: 1.1 m^3/m^2s and bed height: 0.528 m 70
Figure 4.13 Liquid distribution for L: 0.002 m^3/m^2s, G: 2.2 m^3/m^2s and bed height: 0.528 m 71
Figure 4.14 Liquid distribution for L: 0.004 m^3/m^2s, G: 1.1 m^3/m^2s and bed height: 0.792 m 72
Figure 4.15 Liquid distribution for L: 0.004 m^3/m^2s, G: 2.2.m^3/m^2s and bed height: 0.792.m 73
Figure 4.16 Liquid distribution for L: 0.002 m^3/m^2s, G: 1.1 m^3/m^2s and bed height: 0.792 m 74
Figure 4.17 Liquid distribution for L: 0.002 m^3/m^2s, G: 2.2 m^3/m^2s and bed height: 0.792 m 75
Figure 4.18 Liquid distribution for L: 0.004 m^3/m^2s, G: 1.1 m^3/m^2s and bed height: 1.056 m 76
Figure 4.19 Liquid distribution for L: 0.004 m^3/m^2s, G: 2.2 m^3/m^2s and bed height: 1.056 m 77
Figure 4.20 Liquid distribution for L: 0.002 m^3/m^2s, G: 1.1 m^3/m^2s and bed height: 1.056 m 78

Figure 4.21 Liquid distribution for L: 0.002 m^3/m^2s, G: 2.2 m^3/m^2s and bed height: 1.056 m 79
Figure 4.22 Liquid distribution for L: 0.004 m^3/m^2s G: 2.2 m^3/m^2s and bed height: 1.056 m (single pipe or point flow) 80
Figure 4.23 Plot of maldistribution factor vs. packing height 83
Figure 4.24 Liquid dispersion for L: 0.004 m^3/m^2s, G: 1.1 m^3/m^2s and bed height: 0.528 m 87
Figure 4.25 Liquid dispersion for L: 0.004 m^3/m^2s, G: 1.1 m^3/m^2s and bed height: 1.056 m 88
Figure 4.26 Liquid dispersion for L: 0.002 m^3/m^2s, G: 2.2 m^3/m^2s and bed height: 1.056 m 89
Figure 4.27 Liquid dispersion for L: 0.002 m^3/m^2s, G: 1.1 m^3/m^2s and bed height: 1.056 m 90
Figure 5.1 Schematic diagram of Zogg's model 93
Figure 5.2 Schematic diagram of UofA's model 94
Figure 5.3 Schematic diagram of UofA's model for tracer dispersion 95
Figure 5.4 Comparison of dry pressure drop in UofA's model, experiments vs. simulations 106
Figure 5.5 Contour plots of velocity magnitude (m/s) at X = 0.0 m, Y = 0.0 m and Z = 0.0 m planes 107
Figure 5.6 Contour plots of velocity magnitude (m/s) at (a) X = 0.0 m, (b) Z = 0.0 m and (c) Y = 0.0 m planes 108
Figure 5.7 Contour plots of velocity vectors colored by velocity magnitude (m/s) at plane X = 0.0 m 109
Figure 5.8 Contour plots of velocity vectors colored by velocity magnitude (m/s) at plane Y = 0.0 m 110
Figure 5.9 Comparison of CFD simulation result for single phase pressure drop with Zogg's experiment 113
Figure 5.10 Contour plots of velocity magnitude (m/s) at Z = - 0.003, Z = 0.0 and Z = - 0.003 planes (for Zogg's model) 114
Figure 5.11 Contour plots of velocity vector colored by velocity magnitude at Z = 0.003 m, Z = 0.0 m and Z = -0.003 m planes (for Zogg's model) 115
Figure 5.12 CFD simulation result for two-phase pressure drop vs. f-factor for 117
Figure 5.13 Contour plots of velocity vectors for air colored by velocity magnitude (m/s) at planes Z = - 0.003 m, Z = 0 m and Z = 0.003 m for two-phase flow in Zogg's model 118
Figure 5.14 Contour plots of velocity vectors for water colored by velocity magnitude (m/s) at planes Z = - 0.003 m, Z = 0 m and Z = 0.003 m for two phase flow in Zogg's model 119
Figure 5.15 Contour plot of mass fraction of CO_2 at X = 0.0 m plane 122
Figure 5.16 Contour plot of mass fraction of air at X =0.0 m plane 123
Figure 5.17 Contour plot of mass fraction of CO_2 at Y = - 0.12 m plane 124
Figure 5.18 Contour plot of mass fraction of CO_2 at Y = - 0.11 m plane 125
Figure 5.19 Contour plot of mass fraction of CO_2 at Y = - 0.08 m plane 126
Figure 5.20 Contour plot of mass fraction of CO_2 at Y = - 0.06 m plane 127
Figure 5.21 Contour plot of mass fraction of CO_2 at Y = - 0.04 m plane 128

Figure 5.22 Contour plot of mass fraction of CO_2 at Y = 0.0 m plane 129
Figure 5.23 Surface plot at Y = 0.0 m (birds' eye view) 130
Figure 5.24 Surface plot at Y = 0.0 m plane (3D view) 131
Figure 5.25 Mass fraction of CO_2 at different Y planes 132

Nomenclature

A	area of the column cross section [m^2]
a	specified surface area of the dumped packing [m^2m^{-3}]
a_e	effective interfacial area per unit volume [m^2m^{-3}]
A_f	flow area [m^2]
a_h	hydraulic surface area of the dumped packing [m^2m^{-3}]
A_i	cross sectional area of the i^{th} collecting region/cell perpendicular to the main flow direction of liquid [m^2]
a_p	specific surface area [m^2m^{-3}]
A_{region}	cross sectional area of collecting region [m^2]
b	base length [m]
B	width of packing [m]
C	concentration at inlet [$mollitre^{-1}$]
C_1	constant
C_2	constant
C_3	constant
C_{fM}	friction factor
C_h	hydraulic constant
C_i	concentration at cell i [$mollitre^{-1}$]
c_{p1}	empirical constant
c_{p2}	empirical constant
$C_{\varepsilon 1}$	closure coefficient
$C_{\varepsilon 2}$	closure coefficient
C_μ	closure coefficient
D_e	dispersion coefficient [m^2s^{-1}]
d_{eq}	equivalent diameter [m]
D_H	equivalent diameter [m]
d_h	equivalent diameter [m]
d_h'	equivalent diameter [m]
$D_{i,m}$	diffusion coefficient of species i in the mixture [m^2s^{-1}]

d_L	diameter of the bubbles or droplets of phase L [m]
D_t	turbulent diffusivity [m^2s^{-1}]
f	body force [N]
F_l	laminar coefficient of the friction
f_d	drag function
f_{loc}	local liquid flow rate [kgs^{-1}]
f_P	friction coefficient at packing Reynolds number
Fr	Froude number
F_S	gas flow factor [$ms^{-1}(kgm^{-3})^{0.5}$]
F_α	interphase momentum transfer due to fluid-fluid and/or fluid-solid interactions [Nm^{-3}]
f_∞	friction coefficient at infinite Reynolds number
G	gas superficial flow rate per unit cross sectional area [$kgm^{-2}s^{-1}$]
g	gravitational acceleration vector [ms^{-2}]
g_c	dimensional constant
h	crimp height [m]
H	length of packing [m]
h_L	liquid holdup
i	cell index
J_i	diffusion flux of species i [$kgm^{-2}s$]
k	turbulent kinetic energy [m^2s^{-2}]
K_G	overall mass transfer coefficient [$kmols^{-1}m^{-2}Pa^{-1}$]
k_{inl}	turbulent kinetic energy at the inlet [m^2s^{-2}]
k_α	turbulent kinetic energy of phase α [m^2s^{-2}]
L	length of packing [m]
L	liquid superficial flow rate per unit cross sectional area, [$kgm^{-2}s^{-1}$]
M_A	Molecular weight of component A [$kgkmol^{-1}$]
m	number of cells
n_l	number of gas rising tubes in the collecting region
N_p	total number of phases
P	wetted perimeter [m]

p	pressure [Nm^{-2}]
p_G	pressure of gas phase [Nm^{-2}]
P_k	turbulence production rate per unit dissipation of k [$kgm^{-1}s^{-3}$]
p_L	pressure of liquid phase [Nm^{-2}]
p_α	pressure of phase α [Nm^{-2}]
$P_{k,\alpha}$	turbulence production rate of phase α per unit dissipation of k [$kgm^{-1}s^{-3}$]
q	gas flow rate passing through each of the gas rising tubes [m^3s^{-1}]
r_G	volume fraction of gas phase in the averaging volume
R_i	net rate of production of species i by chemical reaction [$kgm^{-3}s$]
r_L	volume fraction of liquid phase in the averaging volume
r_α	volume fraction of phase α in the averaging volume
Re_g	Reynolds number for gas phase
Re_G	Reynolds number for gas phase
Re_L	Reynolds number for liquid phase
Re_P	Reynolds number for packing
S	side length [m]
Sc_t	turbulent Schmidt number
S_i	rate of creation by addition from the dispersed phase plus any user-defined sources [$kgm^{-3}s$]
S_P	Surface area of packing [m^2]
S_W	Surface area of container [m^2]
$S_{\alpha,mass}$	mass source or sink because of interphase transfer
$S_{\alpha,mom}$	momentum source due to external body forces other than gravity
T	temperature [deg]
t	time [s]
$T_{\alpha\beta}$	interphase transfer term
U	x-component of velocity [ms^{-1}]
u_{av}	average liquid velocity over the empty column cross section [ms^{-1}]
U_G	x-component of velocity for gas phase [ms^{-1}]
u_{ge}	effective gas velocity inside the flow channel of structured packing [ms^{-1}]
u_{gs}	superficial gas velocity [ms^{-1}]

u_i	liquid flowrate based on section area in cell i [$m^3m^{-2}s$]
u_{inl}	velocity at inlet [ms^{-1}]
U_L	x-component of velocity for liquid phase [ms^{-1}]
u_L	liquid velocity [ms^{-1}]
u_{loc}	local liquid velocity [ms^{-1}]
u_{rel}	liquid relative velocity
$\bar{u}$	liquid flowrate based on whole column cross section area [$m^3m^{-2}s$]
$\boldsymbol{V}$	velocity vector [ms^{-1}]
V	y-component of velocity [ms^{-1}]
v	average gas velocity over the i^{th} liquid collecting region [ms^{-1}]
$\boldsymbol{V}'$	fluctuating part of velocity vector [ms^{-1}]
$\boldsymbol{V}_G$	velocity vector of gas phase [ms^{-1}]
V_G	y-component of velocity for gas phase [ms^{-1}]
v'_g	average gas velocity [ms^{-1}]
$\boldsymbol{V}_L$	velocity vector of liquid phase [ms^{-1}]
V_L	x-component of velocity for liquid phase [ms^{-1}]
$\boldsymbol{V}_\alpha$	velocity vector of phase α [ms^{-1}]
W	z-component of velocity [ms^{-1}]
W_G	z-component of velocity for gas phase [ms^{-1}]
W_L	x-component of velocity for liquid phase [ms^{-1}]
y	mole fraction of a component in vapor phase
y_0	mole fraction of a component in vapor phase at the inlet
Y_i	local mass fraction of species i
y_z	mole fraction of a component in vapor phase at the outlet
y^*	equilibrium mole fraction of a component in vapor phase
Z	packed bed height [m]

Greek Letters

γ_L	liquid volume fraction
δ	identity tensor
ΔP	pressure drop [Pam^{-1}]
ΔP_M	pressure drop around packing [Pam^{-1}]
ε	turbulent kinetic energy dissipation rate [m^2s^{-3}]
ε_p	void fraction or porosity
ε_α	turbulent kinetic energy dissipation rate of phase α [m^2s^{-3}]
η_g	gas viscosity [$kgm^{-1}s$]
θ	corrugation angle [deg]
κ	bulk viscosity [$kgm^{-1}s^{-1}$]
μ	molecular viscosity [$kgm^{-1}s^{-1}$]
μ_{eff}	effective viscosity [$kgm^{-1}s^{-1}$]
$\mu_{eff,G}$	effective viscosity of gas phase [$kgm^{-1}s^{-1}$]
$\mu_{eff,L}$	effective viscosity of liquid phase [$kgm^{-1}s^{-1}$]
μ_G	molecular viscosity of gas phase [$kgm^{-1}s^{-1}$]
μ_L	molecular viscosity of liquid phase [$kgm^{-1}s^{-1}$]
$\mu_{laminar,G}$	laminar or molecular viscosity of gas phase [$kgm^{-1}s^{-1}$]
$\mu_{laminar,L}$	laminar or molecular viscosity of liquid phase [$kgm^{-1}s^{-1}$]
μ_t	turbulent viscosity [$kgm^{-1}s^{-1}$]
$\mu_{turbulent,G}$	turbulent viscosity of gas phase [$kgm^{-1}s^{-1}$]
$\mu_{turbulent,L}$	turbulent viscosity of liquid phase [$kgm^{-1}s^{-1}$]
$\mu_{t\alpha}$	turbulent viscosity of phase α [$kgm^{-1}s^{-1}$]
μ_α	molecular viscosity of phase α [$kgm^{-1}s^{-1}$]
$\mu_{\alpha,eff}$	effective viscosity of phase α [$kgm^{-1}s^{-1}$]
ρ	density [kgm^{-3}]
ρ_g	density of gas phase [kgm^{-3}]
ρ_G	density of gas phase [kgm^{-3}]
ρ_L	density of liquid phase [kgm^{-3}]
ρ_α	density of phase α [kgm^{-3}]

σ_k	closure coefficients
σ_ε	closure coefficients
τ	stress tensor [Nm^{-2}]
τ_L	particulate relaxation time [s]
φ^*	point variable associated with a fluid
$\varphi_{\alpha\varepsilon}$	volume averaged point variable

Chapter 1 Introduction

Packed columns have been widely used in industrial separation processes, such as distillation, absorption and extraction. A typical packed bed comprises of a vertical cylindrical container loaded with packing material. Most commonly, the two fluids move counter currently through the column. Liquid enters the top of the column and flows downward while contacting with the upward flowing vapor phase. The packing material is designed to increase the interfacial area for mass transfer between the fluids. Every packing should possess a number of important characteristics, such as, a large wetted surface area per unit volume of packed space which allows a large interfacial area for mass transfer, a large void volume for low pressure drops and good wetting characteristics which give good mass transfer.

The design and scale-up of packed columns have been traditionally based on one-dimensional models which usually need empirical and semi-empirical correlations for capturing interfacial mass transfer. The further improvement of packed columns has been hindered due to the fact that little is known about the flow phenomena prevailing inside packing for given geometry and operating conditions. And the main reason for this is the poor understanding of the complex behaviors of the multiphase flow inside the packing. These practices do not often take into account the actual fluid flow patterns. As a result, the current practices of design and performance analysis of packing are based on experience and empirical correlations. This often leads to unreliable design and limits the application of packed columns, particularly on large scales.

Therefore, the current practice of packing design and performance analysis is facing two major unresolved problems. The first one is what flow patterns to expect for given geometry and operating conditions. The second problem is how to relate these flow patterns to packing performance parameters such as pressure drop and packing efficiency. Once a method or methods are devised to accomplish these two tasks, it will be possible to design packing having desired flow patterns that give rise to the best performance. Over the past years, only experimental methods could be thought of to

solve the problems mentioned. Although experimental predictions are generally expected to give reliable data, the chaotic, three-dimensional and multiphase behaviors of the flow inside packing severely limit the use of these methods and the amount of data they can give. Recently computational fluid dynamics (CFD) is seen as a tool to solve this problem with less time, cost and effort.

In this study the hydrodynamics and mass transfer behavior of structured packings were systematically analyzed. The objectives of this study were

1) To obtain a better understanding of multiphase flow hydrodynamics, liquid distribution, tracer dispersion and mass transfer,

2) To develop CFD based models for predicting pressure drop and tracer dispersion in structured packed columns, and

3) To perform experiments to validate the models obtained through simulations.

Hydraulics experiments have been carried out in University of Alberta's laboratory in a 0.3 m diameter cylindrical column equipped with metal flexipac-3Y type structured packing for air-water flowing counter-currently. Both dry and irrigated pressure drop for different liquid flow rates were investigated. The flow maldistribution was studied by estimating maldistribution factor (*Mf*) for different packed bed heights, and different gas and liquid loads. Liquid dispersion was also studied through tracer experiments for different packed bed heights and different gas and liquid loads.

To predict the results obtained by experiments, a CFD model based on Zogg's experiments (Zogg, 1972) was developed for both single and two-phase flow. Because of the complicated geometry of the packing, only limited success was achieved for two-phase flow using CFX. Large memory requirements placed severe limitations. Simulations for single and two-phase pressure drop were carried out in the Zogg's model developed for sulzer mesh-BX type structured packing according to Zogg's experiment and also in the UofA's model developed for Flexipac-3Y type structured packings based on experiments carried out in University of Alberta's laboratory. The models were solved with the aid of the commercial CFD packages, Fluent 6.1.22 and CFX 5.7.1. In both

cases, single phase pressure drop simulations results showed good agreement with the experiments. Since the predictions agreed well with the experimental data, it indicates the suitability of the proposed models for the simulations of hydrodynamics in structured packed column. But due to lack of availability of two-phase pressure drop data for Zogg's model, simulations for two-phase flow couldn't be compared. The simulations for single-phase tracer dispersion were also carried out with the UofA's model.

The thesis is organized as follows; in chapter 2 a brief literature review on packed column and in chapter 3 model equations used in simulations of packed column will be presented. In chapter 4 a detailed description of the experimental procedures, results and discussions will be given followed by chapter 5 in which a thorough discussion on different simulation results for single and two-phase pressure drop and single-phase tracer dispersion will be given. Finally, in chapter 6 a brief discussion on our future work i.e. mass transfer will be given.

Chapter 2 Literature Review - Packed Column

2.1 Introduction

Separation operations such as distillation, rectification and extraction, are commonplace in many chemical process industries. Also due to increased sensitivity to environmental pollution issues, interest in scrubbing has overtaken, over the years, the traditional realm of separation (Billet, 1989; Strigle, 1994). To cope with the ever-growing demand on cost-efficiency trade-off of contacting devices, researchers and manufacturers have been permanently engaged in a quest for new types of column internals. Among these internals, corrugated packings of the regular type, referred to as "structured packing", have received the greatest attention because of their greater performances. Propensity to structured packings is driven by the minimal pressure drop per theoretical stage attained while achieving high separation efficiency, allowing reduction in energy dissipation, increasing loading capacity, and repelling flooding capacity to higher values.

One of the constraints in structured packing selection is the high cost per unit volume which makes the capital investment on structured packings containing columns much higher than for columns containing random or dumped packings. Therefore, an accurate design of columns equipped with structured packings is very important for minimizing the investment cost, increasing the benefit margins as well as the process competitiveness. This is an important matter because it is estimated that worldwide over 25% of refinery vacuum towers are equipped with structured packings (Brunazzi et al., 1997).

2.2 Packing Characteristics

Packings are generally divided into two classes:

1. Random or dumped packings: These are discrete pieces of packing of a specific geometrical shape which are "dumped" or randomly packed into the column as shown in Figure 2.1.

2. Structured or systematically arranged packings: These are crimped layers of wire mesh or corrugated sheets. Sections of these packings are stacked in the column as shown in Figure 2.2. Grids are also systematically arranged packings, but instead of wire-mesh or corrugated sheets these use an open-lattice structure. The application of grids is limited primarily to heat transfer.

Random packings are by far the most common in commercial practice. Structured packings are less common, but their share of the packing market has rapidly grown over the last decade.

2.3 Types of Random Packings

Historically, there were three generations of evolution in random packings. The first generation (1907 to the 1950s) produced two basic simple shapes, the Raschig ring and the Berl saddle, that became the ancestors of modern random packings. These packings have all been superseded by more modern packing and are seldom used in modern distillation practice.

The second generation (late 1950s to the early 1970s) produced two popular geometries – the Pall ring, which evolved from the Raschig ring, and the Intalox saddle, which evolved from the Berl saddle. The second generation packings are still popular and extensively used in modern distillation practice.

The third generation (the mid 1970s until present) has produced a multitude of popular geometries, most of which evolved from the Pall ring and the Intalox saddle. Examples are, Intalox metal tower packing (IMTP), Cascade mini-rings (CMR), Chempak or

Levapak (LVK), Nutter ring, etc. Schematic diagrams of each generation of random packings are given in Figure 2.3.

2.4 Types of Structured Packings

Structured packings have been around since as early as the 1940s. First-generation structure packings, such as Panapak, never became popular and are seldom used nowadays. The second generation of structured packings began in the late 1950s with high-efficiency wire-mesh packings such as Goodloe, Hyperfil, Montz A and the Koch-Sulzer (KS wire-mesh) packings. Extensive experimentation led by Sulzer provided insight into maldistribution, and the knowledge gained was applied for successful scaleup. By the early 1970s, these packings have made substantial inroads into vacuum distillation, where their low pressure drop per theoretical stage is a major advantage. In these services, they are extensively used till today. Their high cost, high sensitivity to solids, and low capacity hindered application of these wire-mesh packings outside vacuum distillation.

The corrugated-sheet packing, first introduced by Sulzer in the late 1970s, started a third generation of structured packings. With a high capacity, lower cost, and lower sensitivity to solids, while still retaining a high efficiency, these corrugated sheet packings became competitive with conventional internals. In 1980s, an accelerated rise in popularity of structured packings had been seen and they became one of the most popular column internals still in use today. Examples of common corrugated-type structured packings are Mellapak, Fleixpac, Gempak and Montz B1 etc. Schematic diagrams of some of them are given in Figure 2.4.

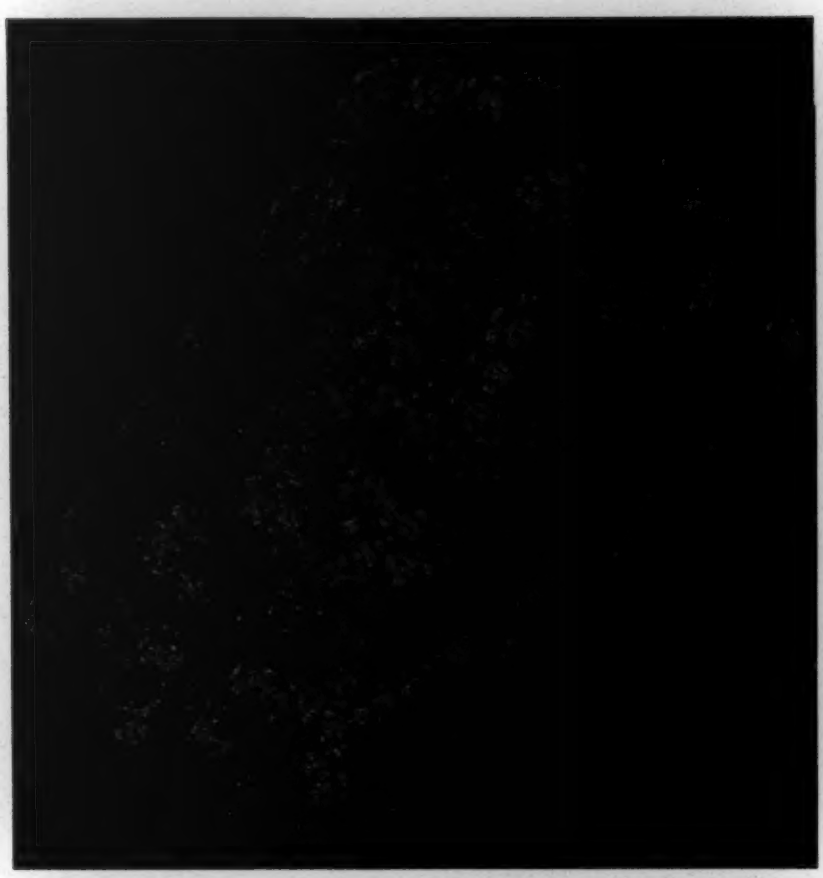

Figure 2.1 Schematic diagram of random packings

Figure 2.2 Schematic diagram of structured packings (Kister, 1992)

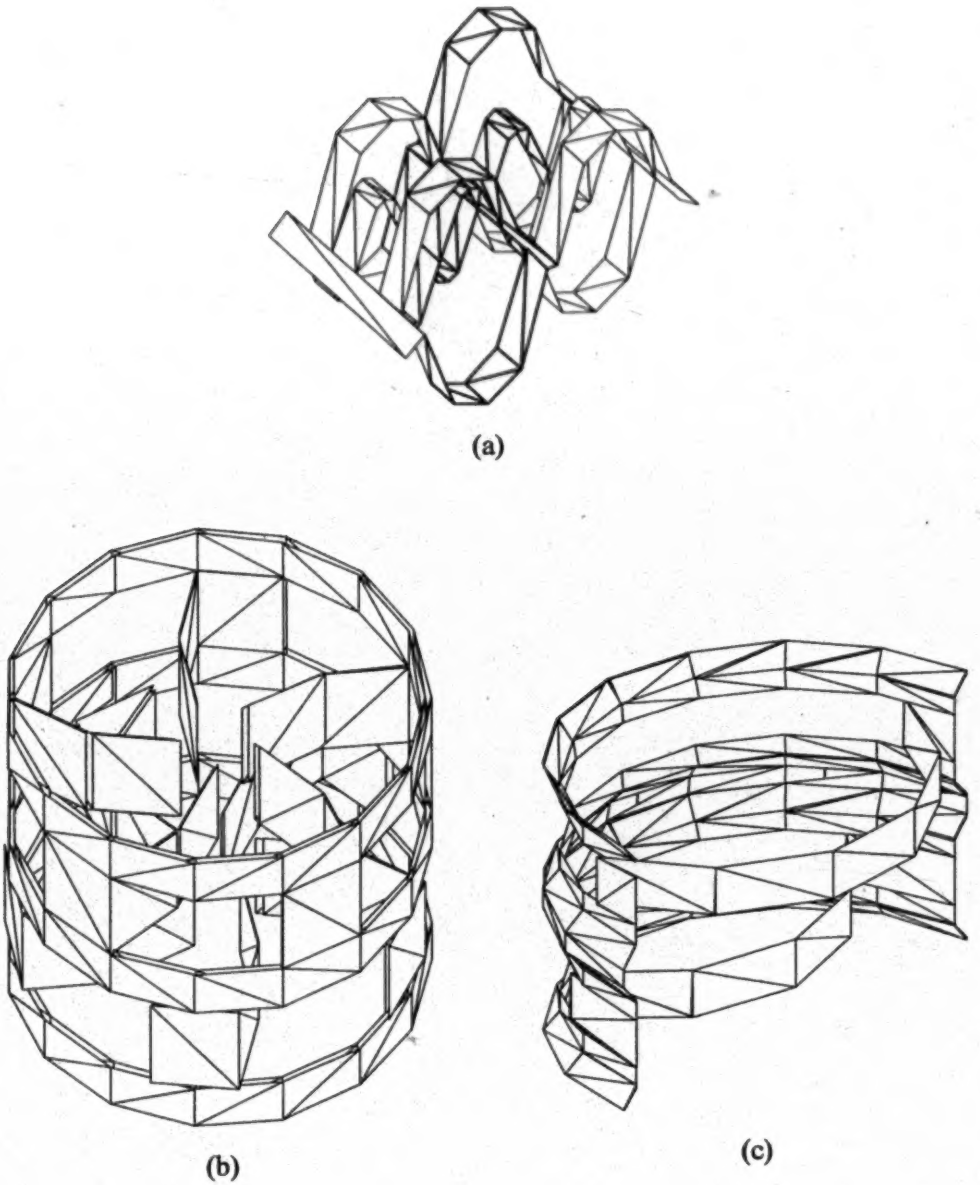

Figure 2.3 Schematic diagrams of three generations of random packings (a) Raschig super-ring, (b) Pall ring and (c) Nutter ring

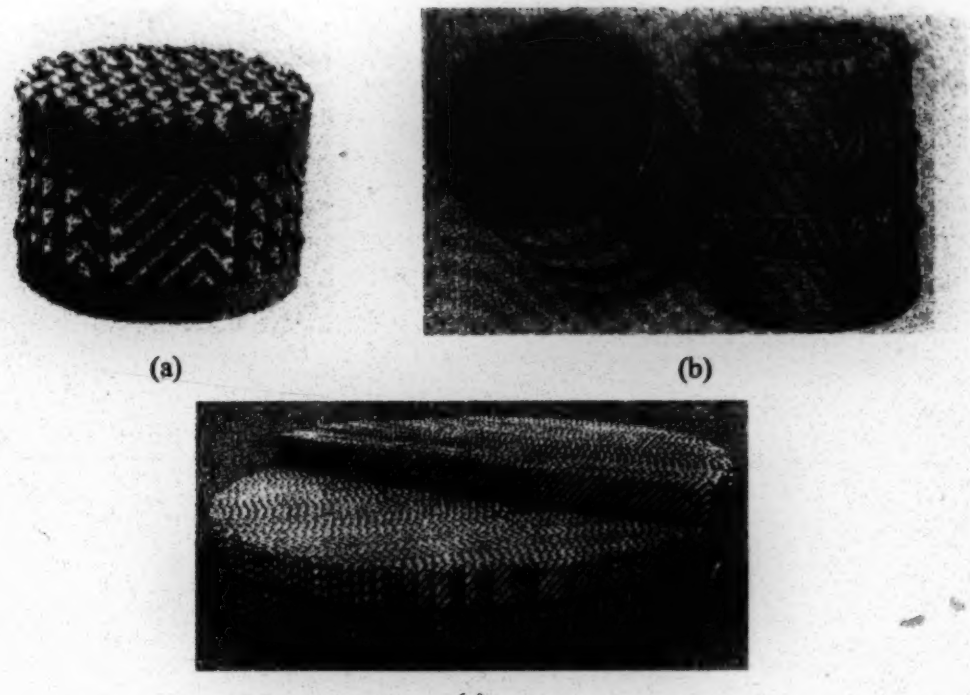

Figure 2.4 Schematic diagrams of common corrugated structured packings (a) Mellapak, (b) Gempak and (c) Montz B1 (Kister, 1992)

2.5 Geometrical Features of Corrugated Structured Packings

Tailoring the geometrical characteristics (crimp geometry, element geometry and surface features) of structured packings is more of an art than an exact science. This explains why different types are available commercially. These variants affect directly the packing performance.

Corrugated structured packings are fabricated from thin, corrugated or crimped metal sheets, arranged in parallel to each other. The surface of the sheets can be grooved, lanced, textured, or smooth and may be perforated or unperforated. They are assembled into an element, typically 8 to 12 in tall. The sheets in each element are arranged at a fixed angle to the vertical. Adjacent elements are rotated so that sheets of one element are at a fixed angle to the layer below. Geometrical characteristics of some common metal corrugated-sheet structured packings are given in Table 2.1.

The crimp size defines the opening between adjacent corrugated layers. The smaller b, h and S are, the narrower the openings, the more sheets (and therefore, more surface area) per unit volume, and the more efficient the packing. On the other hand, narrowing of the interlayer openings reduces void space and raises resistance to gas upflow, leading to a lower capacity and to enhanced sensitivity to plugging and fouling.

The relative ratio of b to h, S to h, and the crimp angle (angle between side, S and base, b) define the geometry of the flow channel and of the vapor-liquid contact zone. This geometry stays relatively uniform within a single packing family, but varies from one packing family to another. Crimp angles vary from 28 to 45° and base-to-height (b-to-h) ratios range from 2:1 to 4:1. In some packings, the sides of the triangle shown in Figure 2.4 are rounded, giving a round top apex. Rounding of the triangle apex reduces friction and prevents concentration of liquids at the corners.

2.5.1 Element Geometry

Due to the corrugations, vapor and liquid flow through a single element spreads in a series of parallel planes. In order to spread the vapor and liquid uniformly in all radial planes, each element is rotated at a certain angle with respect to the element below. The angle of rotation is the angle (in a "horizontal" plane) between the parallel layers in one element and between the parallel layers in an element above (or below).

The angle of rotation and the element height therefore affect the extent of vapor and liquid spread in a structured packing. For this reason, element height is relatively short (typically 8 to 12 in) and the angle of rotation is around 90°.

In each element, corrugated sheets are usually inclined at about 45° to the vertical. This angle is large enough for good drainage of liquid, avoiding stagnant pockets and regions of liquid accumulation, and small enough to prevent gas bypassing the metal surfaces.

2.5.2 Surface Features

The surfaces of a few structured packings are smooth. Most structured packings have a roughened or enhanced surface that assists the lateral spread of liquid, promotes film turbulence, and enhances the area available for mass transfer. Laboratory measurements of absorption rates showed that both mass transfer efficiency and wetted area are enhanced by texturing metal surfaces. The extent to which mass transfer was improved varied with the type of texturing used. Texturing employed by common structured packings includes grooving, lancing, shallow embossing and deep embossing.

The surfaces of most structured packings contain perforations. The holes which usually are of circular shape, serve as communication channels between the upper and lower surface of each sheet. If the holes are too small, or nonexistent, both sides of a sheet will be wet only at low liquid rates. At high liquid rates, "sheeting" or "blanking" will cause

liquid to run down the top surface with little liquid wetting the bottom surface. This may cause a reduction in efficiency as liquid flow rates are raised. A counter-argument by suppliers of packings that contain no holes is that the holes impede the spread of liquid across a sheet, thus adversely affecting the surface action.

2.6 Packing Materials

Packing material selection is primarily based on the corrosion resistance.

2.6.1 Metals

Carbon steel packings are usually the first choice for non-corrosive services. Compared to ceramic and plastic, they normally offer high capacity and efficiency, a wider range of geometries, higher turndown, have a high compression resistance and are unbreakable. Stainless steel and other metal packings, such as alloys, are also used in corrosive services but they are three to five times costlier than carbon steel.

2.6.2 Ceramics

Ceramic packings have declined in popularity ever since low-cost plastic packings became available. Compared to plastic, ceramic packings are breakable, have lower capacity, and are unavailable in many of the popular geometries. Ceramic packings are currently specified only in applications where their high chemical inertness and resistance to high temperature gives them the edge (e.g., in sulfuric acid absorption). However, despite their reputation of high chemical inertness, some grades of ceramic may chemically degrade.

2.6.3 Plastics

A disadvantage of plastic packings is their poor wettability. While the hydrophilic nature of ceramic, and to a lesser degree metal, promotes the formation of thin liquid film on the packing surfaces even at low liquid rates, the hydrophobic nature of plastic makes such a liquid film more difficult to form. Poor wettability can be particularly troublesome in the initial ("aging") period of operation; it may take several days to reach normal efficiency. The ease of handling of plastic packings is an advantage during startup and shutdown. Unpacking techniques such as "sucking and blowing" can easily be used at shutdown. Repacking is easier and faster.

Table 2.1 Geometric characteristics of common metal corrugated-sheet structured packings

Packing	Crimp geometry			Element geometry			Specific surface area, ft^2/ft^3	Void fraction, ε_p	Equivalent diameter, in
	Height h, in	Base length B, in	Side length S, in	Height, in	Rotation angle, deg	Angle to tower axis, θ, deg			
Mellapak									
125Y							38		
250Y	0.47	0.95	0.67	8.27	90	45	76	0.95	
350Y							107		
500Y							152		
Flexipac (Y-type)									
#1	0.49	1.02	0.71	10.5	90	45	68	0.91	0.353
#2								0.93	0.707
#3								0.96	1.414
#4								0.98	2.828
Gempak									
#1A	1.0	2.00	1.44				35	0.96	1.414
#1.5A	0.71	1.41	1.03				49		
#2A	0.49	1.05	0.71	9.75	90	45	67	0.93	0.707
#2AT	0.45	1.07	0.70	9.75			68		
#3A	0.37	0.75	0.53				91	0.92	0.530
#4A	0.24	0.43	0.36				138	0.91	0.353

Table 2.1 Geometric characteristics of common metal corrugated-sheet structured packings (cont'd)

Packing	Crimp geometry			Element geometry			Specific surface area, ft^2/ft^3	Void fraction, ε_p	Equivalent diameter, in
	Height h, in	Base length B, in	Side length S,in	Height, in	Rotation angle, deg	Angle to tower axis, θ, deg			
Intalox 1T 2T 3T	0.41	1.53	0.88	11.0		45	67	0.97	
Montz B1-100	0.59	1.57	0.98	8	90	45	30	0.94	
Montz B1-200							61		
Montz B1-250							76		
Montz B1-300							91		
Sulzer BX (gauge)	0.25	0.5	0.35	7	90	60	150	0.90	0.353

2.7 Packing Hydraulics

2.7.1 Liquid Holdup

The correlation for liquid holdup given by Billet et al. (1999) is valid for both structured and random packings and is given as,

$$h_L = \left(12\frac{1}{g}\frac{\mu_L}{\rho_L}u_L a^2\right)^{\frac{1}{3}}\left(\frac{a_h}{a}\right)^{\frac{2}{3}} \qquad (2.1)$$

where,

$$\frac{a_h}{a} = C_h\left(\frac{u_L\rho_L}{a\mu_L}\right)^{0.15}\left(\frac{u_L^2 a}{g}\right)^{0.1} \qquad \text{for, } \mathrm{Re}_L = \frac{u_L\rho_L}{a\mu_L} < 5 \qquad (2.2)$$

$$\frac{a_h}{a} = 0.85C_h\left(\frac{u_L\rho_L}{a\mu_L}\right)^{0.25}\left(\frac{u_L^2 a}{g}\right)^{0.1} \quad \text{for, } \mathrm{Re}_L = \frac{u_L\rho_L}{a\mu_L} \geq 5 \qquad (2.3)$$

Such correlations are typically used globally in a column providing a single value of holdup everywhere in the column. But it is likely to vary from point to point in the column and CFD models will enable us to track such spatial variations. But CFD models require inlet boundary condition for holdup and they are difficult to measure experimentally. However it can be estimated from the liquid holdup correlation based on the liquid flow-rate equation (2.1) as follows (Kister, 1992)

$$\gamma_L = \frac{h_L}{\varepsilon_P} \qquad (2.4)$$

2.7.2 Pressure Drop

There are many correlations available in literature to determine the pressure drop in any packed column. As an example the following correlation given by Bravo et al. (1986) is applicable to both gauze and sheet metal packings having the same geometry.

$$\Delta P = \left[C_1 + \frac{C_2}{\mathrm{Re}_g} \right] \left[\frac{\rho_g u_{ge}^2}{d_{eq} g_c} \right] \left[\frac{1}{\left(1 - C_3 Fr^{0.5}\right)} \right]^5 \qquad (2.5)$$

Pressure drop through beds of random packings has also been successfully correlated by equation (2.5).

The effective gas velocity inside the flow channel of structured packing, u_{ge}, Reynolds number, Re_g and Froude number, Fr can be expressed as follows,

$$u_{ge} = \frac{u_{gs}}{\varepsilon_p \sin\theta} \qquad (2.6)$$

$$\mathrm{Re}_g = \frac{d_{eq} u_{ge} \rho_g}{\mu_g} \qquad (2.7)$$

$$Fr = \frac{u_L^2}{d_{eq} g} \qquad (2.8)$$

For all packings types, the values of constants C_1 and C_2 in equation (2.5) are 0.171 and 92.7 respectively. By inserting all these values into equation (2.5) and after manipulation it becomes,

$$\Delta P = \left[0.171 + \frac{92.7 \mu_g \varepsilon \sin\theta}{d_{eq} u_{gs} \rho_g} \right] \left[\frac{\rho_g u_{gs}^2}{d_{eq} g_c \varepsilon_P^{\,2} \sin^2\theta} \right] \left[\frac{1}{1 - \frac{C_3 u_L}{\sqrt{d_{eq} g}}} \right]^5 \qquad (2.9)$$

The value of C_3 is packing type dependent and its values were evaluated for a range of gas rate at each liquid rate for different types of structured packings. The value of C_3 for Flexipac 3 is 4.50 (Bravo et al., 1986).

A typical pressure drop curve for different types of flexipac structured packings is given in Figure 2.5. The nature of the curves agreed well with any literature. From Figure 2.5, it can be seen that, at low liquid flow rates, the pressure drop is proportional to the square of the gas flow rate. It may be due to the fact that, at low liquid flow rates, the open cross-sectional area of the packings is about the same as in a dry bed. So, the pressure drop is entirely by frictional losses through a series of openings. In random packings, the openings are randomly sized and located, and pressure drop is due to expansion, contraction, and changes of direction. But in structured packings, the openings are regular and of uniform size, and pressure drop is due to changes in direction (Kister, 1992).

As liquid rates are raised, the liquid occupies some of the cross-section area, making the openings for gas flow smaller. A portion of the energy of the gas is used to support the liquid in the column and pressure drop becomes proportional to the gas rate raised to a power different (usually higher) than 2. For all liquid flow rates, as gas flow rate is raised, a point is reached when the gas velocity begins to interfere with the free drainage of liquid. The slope of the curve increases, until it becomes very steep. Liquid will start to accumulate or "load" the bed until the liquid surface becomes continuous across the top of the packing, giving this region the name "the loading region". The accumulation of liquid reduces the cross-section area available for gas flow and therefore accelerates the pressure drop rise.

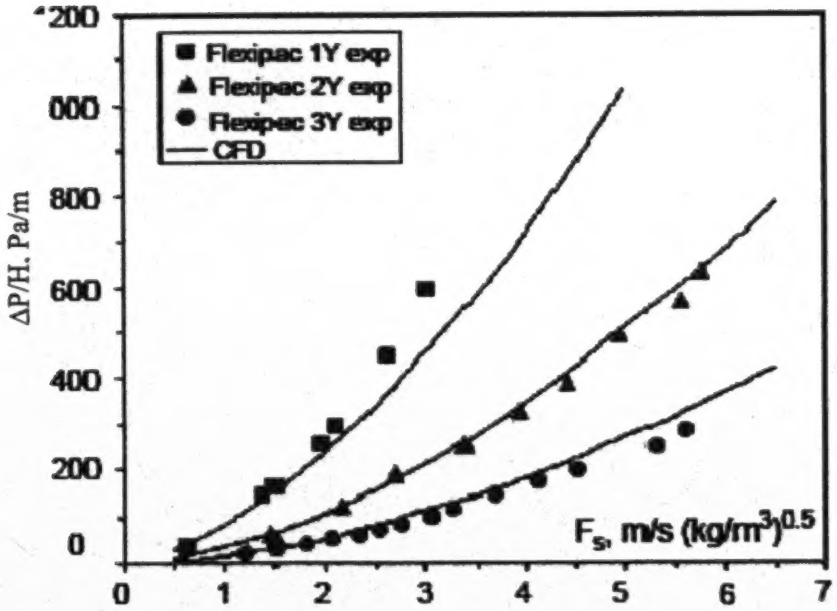

Figure 2.5 Simulated and experimental total pressure drop versus gas flow factor, F_s for flexipac (Rocha et al., 1993, 1996)

2.7.3 Liquid Distribution

Liquid distribution actually affects mass transfer or packing efficiency. The factors which affect liquid distribution can be both structural and operational. Among the structural factors, packing type and geometry, distributor design, and bed height are important and among the operational factors, flow rates of liquid and gas and physical properties of liquid, such as, viscosity, surface tension and density are important(Sun et al., 2000).

2.7.4 Liquid Dispersion

The self-induced mixing process in fluids flowing through various industrially important equipments, such as packed distillation columns, liquid-liquid extraction columns and fixed-bed catalytic reactors can generally be described by dispersion. Axial dispersion tends to reduce driving forces for mass and heat transfer, and thus, has an adverse effect on the performance of such equipments (Yin et al., 2002).

There are three main mechanisms responsible for dispersion in packed columns or porous media:

(1) Molecular diffusion;
(2) Turbulent (or eddy) diffusion; and
(3) Flow maldistribution or uneven convection, both on the pore scale and on the equipment scale due to the packings.

The presence of packings enhances turbulence levels in both the liquid and gas phases and causes the flow redistribution within the packed bed. All these mechanisms, in combination, determine the level and extent of the local mixing of the fluid particles in packed columns (Greenkorn et al, 1969). If the flow is very slow, for example in the creeping flow region, the molecular diffusion dominates the dispersion process, but if the Reynolds number is high (greater than certain critical value), the convective turbulent fluctuation accounts for most of the local self-mixings in packed beds. However, it makes

no difference whether the flow is slow or fast, the dispersion caused by nonuniform flow distribution always exists on the micro-scale in the interstices of porous media and on the macro-scale near confining walls of packed columns.

Dispersion in a packed column is usually studied through tracer experiments. In the tracer experiments, the tracer can be a dye, or another easily detectable inert substance, operating under steady state or unsteady state conditions. Unsteady state experiments are used to measure residence time distributions from pulse response tests in which a pulse is introduced at the inlet and the response of the concentration at some downstream locations is then measured.

The measured tracer concentration profiles can then be used to determine the dispersion coefficient, D_e by fitting the predicted concentration from the following one-dimensional convection-dispersion equation to the measured concentration.

$$\frac{\partial C}{\partial t} + v\frac{\partial C}{\partial z} = D_e \frac{\partial^2 C}{\partial z^2} \qquad (2.10)$$

One of the assumptions in this equation is that the flow is uniform (plug flow) over the entire cross section of a packed column. The main advantage of this model is that it permits analytical solution for the concentration variation with dispersion coefficient, D_e as a parameter. By matching the measured concentration with the predicted one, the best estimate of the dispersion coefficient can be obtained, and its variation with flow rate and other properties can be determined.

2.7.5 Mass Transfer

During design, scale-up and performance analysis for packed columns, homogeneous conditions are assumed along the radial direction. These procedures are usually macroscopic. As a result a design procedure based on unidirectional axial concentration

variation is developed and the concepts of HTU (height of a transfer unit) and NTU (number of transfer unit) are introduced. These concepts rely only on observations made at the macroscopic or equipment scale, i.e., only inlet and outlet flow rate and concentrations are measured (Wankat, 1988).

The standard design equations are, (Kister, 1992)

$$Z = HTU \times NTU \tag{2.11}$$

$$HTU = \frac{G}{K_G a_e p M_A} \tag{2.12}$$

$$NTU = \int_{y_0}^{y_h} \frac{dy}{y^* - y} \tag{2.13}$$

By assuming uniform flow conditions and uniform interfacial mass transfer throughout the packed bed and using macroscopic data, the performance of the column can be analyzed.

Successful design and scale-up of packed columns require a model that captures the basic transport phenomena on the correct length scale. Concepts based on height of a transfer unit (HTU) and number of transfer units (NTU) obtained from the inlet and outlet conditions alone are not adequate for scale-up purposes as both HTU and NTU depend on the flow conditions and interface mass transfer takes place at the scale of the packing, not at the scale of the equipment. The existing design procedures for large diameter packed columns are uncertain due to lack of understanding of liquid flow distribution in such columns (Olujic et al., 1989; Kister, 1992). Height equivalent to a theoretical plate (HETP) which characterizes the mass transfer efficiency of a packed column, varies very strongly and erratically with the change in type and size of packing, liquid and gas flow conditions and fluids physical properties. The complex mechanisms that influence HETP

have not been modeled in a rigorous way in the previous models that assumed homogeneous conditions in the radial direction and neglected dispersion in all directions.

2.8 Previous works on Structured Packing

In spite of the great efforts invested over the past 20 years to study and model the hydrodynamics and mass transfer in structured packing, the design, by and large, still involves some degree of empiricism and semi-empirical equations with uncertain limits of application (Bravo et al., 1986, 1992; Rocha et al., 1993, 1996; Spiegel et al., 1987, 1992; OlujiKc, 1997 and Fair et al., 2000). This comes from the fact that the constants used for describing the hydrodynamics and the mass transfer in structured packings are obtained by calibrating models using laboratory experiments (Bravo et al., 1986; Billet et al., 1999). Not only are these constants case-dependent, but also procurement from lab experiments of a large set of such constants quickly becomes cumbersome and prohibitive and then use for large diameter columns questionable.

A model that is used often for predicting hydrodynamics and mass transfer performance of structured packings was developed several years ago at the Separations Research Program (SRP) of University of Texas at Austin (Bravo et al., 1985, 1992; Rocha et al., 1993, 1996). The basis for the model was a modified wetted-wall flow arrangement through the channels of the packing. An alternate model has been developed more recently at the Delft University of Technology (Olujic et al., 1997, 1999) and is also founded on liquid film flow down inclined corrugated plates and in addition takes into account explicitly several macro geometrical parameters that can affect packing performance. The comprehensive model developed at SRP has been shown to yield acceptable performance but, because of the large number of adjustable parameters, its application in ranges outside the tested region can lead to sizable errors (Brunazzi et al., 1997). The Delft model is based on complete wetting of the packing surface, thus, liquid holdup is determined from the packing surface area and the average liquid film thickness.

As an alternative to these two approaches, Brunazzi et al. (1997) developed a mechanistic model based on mass and momentum conservation equations for a simple geometry. The model approximates the channels within the packing to a bundle of identical columns, inclined with respect to the horizontal axis by an angle equal to the angle formed by the corrugation with the same axis. In this model, the wetted area is not influenced by the gas load. Also, the model requires a priori knowledge of the dynamic liquid holdup.

A consistent set of total reflux distillation test data has been used by Fair et al. (2000) to validate the SRP and Delft models for predicting hydraulic and mass-transfer performance of structured packings. The tests have involved a set of montz packings and covered a wide range of pressures, two corrugation angles, two surface areas, and two surface designs. Experimental results include pressure drop, capacity, and mass-transfer efficiency. The database generated has been used to evaluate generalized performance models developed independently at the University of Texas Separations Research Program (SRP model) and at Delft University of Technology (Delft model). In general, the SRP method over-predicts pressure drop and under-predicts mass-transfer efficiency, both usually considered conservative for design. The Delft method predicts slightly larger HETP values for vacuum conditions than for atmospheric conditions, but not at the expense of overall accuracy, however. Both methods are too optimistic for packings with larger specific surface areas and generally predict too small a difference in mass transfer resulting from the corrugation angle effect. The rather strong effect of this angle on pressure drop is predicted fairly well by both methods. Improved modeling of the effective interfacial area is a key requirement for increasing the reliability and overall accuracy of both methods. A possibility might be adaptation of the Onda (1968) approach to structured packing geometry. In that case, no packing-specific coefficients would be needed.

Zogg (1972) measured the pressure drops of corrugated sheets with smooth unperforated surfaces and different inclinations of the flow channels and extrapolated his results for limited geometries to an infinitely wide geometry to eliminate wall effects. These extrapolated results were expressed as friction factors, together with the friction factor of

a smooth pipe. The characteristic coefficients were obtained by fitting the experimental data using an Ergun type relation.

$$4f_p = 4\frac{F_1}{\mathrm{Re}_p} + 4f_\infty \qquad (2.14)$$

where,

f_∞ = friction coefficient at infinite Reynolds number,

f_p = friction coefficient at packing Reynolds number,

F_1 = laminar coefficient of the friction and

Re_p = Reynolds number for packing

To breakdown the overall single-phase gas flow bed pressure drop in towers containing corrugated sheet structured packings into elementary dissipation mechanisms, a computational fluid dynamics (CFD) methodology was proposed by Larachi et al. (2003). The goal behind was to allow piecewise geometry optimization of such packings in terms of capacity enlargement and efficiency enhancement. The dissipations sorted in order of decreasing importance were:

(1) collision losses by jet streams at criss-crossing junctions within corrugated channels,

(2) elbow loss by form drag at interlayer transition,

(3) elbow loss by jets striking wall and subsequent flow redirection to upper channels, and

(4) elbow loss in bed entrance.

They also showed that, replacement of sharp bends at the interlayer junctions by progressive direction change was beneficial for the reduction of the dissipations at the wall and the interlayer junction and thus stretching capacity of the structured packing. However, this improvement was not spectacular because the most energy-intensive component (criss-crossing) remained unaffected by such modifications.

Recently, Iliuta et al. (2004, 2001 and 2000) developed an implicit, one-dimensional, two-zone, two-fluid mechanistic model for the prediction of the irrigated two-phase pressure drop, the total liquid holdup and the packing fractional wetted area (or the effective interfacial area) in the preloading zone of structured-packing-containing columns operated in countercurrent flow of gas and liquid under partial wetting conditions. The model was an offshoot of the well-known "single-slit" mechanistic approach to co-current down-flow trickle-bed reactors. The model is based on the volume averaged mass and momentum balance equations for the countercurrent gas–liquid flow through structured packings. The model mimicked the actual bed void and the two-phase flow topography by means of two hypothetical, recurrent and geometrically similar inclined slits consisting of a dry and a wet slit. The slits were subject to Couette-Poiseuille gas and liquid flows where the fluid-wall and the fluid-fluid interfacial shear stresses and the (stream-wise) pressure gradient were incorporated. The double slit model approximation was also used for the derivation of the drag force closures needed in the conservation equations. The two model parameters, i.e., the laminar and turbulent Ergun constants, were estimated using a 3-D computational fluid dynamics (CFD) model based on the continuity and the Navier-Stokes equations for the laminar regime or the Reynolds averaged equations for the turbulent regime within a representative elementary unit cell coupled with a combined mesoscale-microscale predictive approach to capture the aerodynamic phenomena occurring at the macroscale in structured-packing-containing columns (Petre et al., 2003). This model has been successful, provided its use is to be restricted to the valid range of the empirical correlations for the turbulent channel wall friction factor developed by Bravo et al. (1986) and Brunazzi et al. (1997).

Model verification and experimental validation were conducted based on a thorough survey of the available pressure drop, liquid holdup and packing fractional wetted area data published over the last two decades for various shapes and sizes of structured packings (Flexipac, Gempak, Mellapak, Sulzer BX and Montz-Pak). A CFD-aided development methodology was also proposed recasting the detailed numerical information into compact macroscopic numerical correlations for the total loss coefficient similar to Ergun equation. The proof-of-concept of the approach was demonstrated by

correlating the laminar, turbulent, and curvature parameters appearing in these correlations as a function of the corrugation angle for Montz B1-250 structured packings. A more traditional approach commonly followed by various researchers has been to develop separate models to predict pressure drop (Bravo et al., 1986; Stichlmair et al., 1989; Robins et al., 1991; Spiegel et al., 1992) and mass-transfer efficiency (Spiegel et al., 1987; Brunazzi et al., 1985; Nardini et al., 1996). These models are semi-empirical in nature and are based essentially on the assumption of liquid flow over an inclined wall. Most of the mass transfer models agree in identifying the area available to the mass transfer as a fraction of the geometrical surface. Provided no ripples develop at the gas–liquid interface, as is the case in the pre-loading zone, the gas–liquid interface is admittedly assumed smooth, so that most mass transfer correlations agree in identifying the area available to the mass transfer as the fractional wetted area of the packing geometrical surface.

In order to describe the countercurrent flow of gas and liquid in column containing conventional cross-channel structured packings, a physically based calculation model has been developed by Ranke et al (2000). A system of equations is presented which characterizes the film flow on the surface as influenced by the countercurrent flowing gas stream and the respective geometric parameters of the packing. The hydraulic operating parameters considered are the pressure drop, the film thickness, and the radial liquid distribution as a function of the column load up to the flooding point. Care was taken to introduce only constants that can be interpreted physically. Their number was reduced to a minimum of three in order to provide the possibility of easy extrapolation to other packing dimensions. Numerical simulations have been carried out for different liquids assuming a fully wetted packing surface. A distribution width is introduced as the parameter characterizing the radial liquid distribution. Its value together with the respective gas split factors are important variables for the inclusion of maldistribution in the calculation of a gas/liquid distillation column.

A macroscopic approach to describe the hydrodynamics of two-phase annular counter-current flow in inclined flow channels was used by Woerlee et al. (2001). This type of

flow is characteristic for gas–liquid contact equipment as applied in packed columns. In this study, a distinction between the pressure drop caused by the geometry of the channels and the pressure drop caused by the friction on the gas–liquid interface was made. It was shown that the frictional forces on the interface have two components that either influence the liquid interface velocity or induce waves on the interface. The gas-liquid interaction was described using an additional term on an undisturbed counter-current flow using a dimensionless expression. A set of three independent equations was derived, describing the liquid hold-up, the interface velocity and the different contributions to pressure drop as function of physical properties of both phases. The description was demonstrated on vertical pipes and packed columns containing either random or structured packing. Because of the general description, it was possible to predict the liquid hold-up and pressure drop induced flood point in this equipment.

Rocha et al. (1996) postulated the generation of effective interfacial area and provided a general correlation for predicting the mass-transfer efficiency as a function of surface type, packing geometry, phase flow conditions, and fluid properties. In particular, separation of interfacial area from the mass-transfer coefficient has been preserved, and independent work by Shi et al. (1985) has been utilized for evaluating the effective interfacial area. Only metal surfaces have been evaluated for structured packing mass transfer, but work reported recently by Uresti-Melendez et al. (1994) indicated that the same model may be used for structured packings fabricated from ceramic materials. The model has been integrated with those for predicting liquid holdup, pressure drop, and flooding capacity of structured packings of the corrugated metal type. It took into account the texturing of the packing surface as well as the wettability of the surface material when in contact with various types of liquids. It had been validated for distillation systems with different structured packings and at operating pressures ranging from 0.02 to 4.14 bars. In principle, it should also be applicable to absorption and stripping systems where transfer is largely unidirectional. It does not account for axial mixing effects, although these are implicitly included in holdup predictions under high loading conditions and at lower pressures.

Baten et al. (2002, 2001) have studied the gas phase mass transfer in empty channels and the liquid-phase mass transfer within the catalyst-packed criss-crossing sandwich structures of KATAPAK-S with the use of computational fluid dynamics. Due to the "upheaval" caused by the flow splitting at the crossovers, the mass transfer coefficient is about 40% larger than for fully developed laminar flow in a single, packed tube. The Sherwood number for the complete structure (sandwich KATAPAK-S structure consisting of 16 triangular tubes and 32 crossovers) almost coincides with that obtained for two triangular tubes with a single crossover. This leads them to conclude that the phenomena of redistribution of streamlines for a single crossover, repeats itself over the whole structure. There are no additional mass transfer effects to be accounted for and single crossover geometry provides an adequate representation of the flow and mass transfer of the complete structure. Mass transfer in a packed triangular KATAPAK-s tube was significantly higher than that of a packed circular tube due to improved convective contribution in the corner regions. Further improvement in mass transfer takes place when the two triangular tubes are made to intersect and exchange mass at the junctions, due to upheaval at the junctions. Through their experiments Baten et al. (2001) showed that, KATAPAK-s structure has excellent radial dispersion characteristics and the radial dispersion coefficient in such structures is about one order of magnitude higher than that for conventional packed (trickle) beds. CFD simulations of the radial dispersion were in good agreement with experiments. At high-liquid loads, there was liquid flow outside the wire gauze envelopes, leading to enhanced axial dispersion. The axial dispersion coefficient of the liquid phase of KATAPAK-S was of the same order of magnitude as the radial dispersion coefficient.

A Composite Structured Packing (CSP) consists of a multi channel framework filled with ordinary catalyst particles, with a square channel-to-particle-diameter ratio (N) of $1 < N < 5$, resulting in a system with a significantly lower pressure drop compared to a randomly packed bed. Romkes et.al (2003) investigated the mass and heat transfer characteristics of a composite structured catalytic reactor packing. They assessed the use of commercial computational fluid dynamics (CFD) software to adequately predict the rate of mass and heat transfer from the catalyst particles to the fluid in a CSP with an average error of 15%

(for Reynolds numbers ranging from 10^1 to 10^5) compared to experimental values, for packed beds of spherical particles with $1.00 < N < 2.00$ and also a simple engineering correlations for this type of packing was also developed.

2.9 Conclusion

The research on understanding the performance characteristics of existing structured packings and development of new ones using emerging CFD tools is an important evolutionary step. It is still pretty tough to understand the complex flow phenomena inside the packings by doing experiments alone.

Chapter 3 Model Equations

3.1 Introduction

The development of a modeling framework to study the complex flow phenomena such as turbulent and multiphase flows in chemical process vessels is maturing rapidly. This has been accelerated by the advent of high-speed and large-memory computers. Computational fluid dynamics (CFD) actually enhances this development. Now-a-days it is possible to investigate the complex flows of industrial interest with the help of CFD. Clearly closure relations are needed and currently they are being obtained from rather crude macroscopic experiments. In this chapter we summarize the model equations and comment on the closure models.

3.2 Conservation Equations

To develop the mathematical models for fluid flow, heat and mass transfer, the conservation of momentum, energy and mass is used. In this work, only hydrodynamics of structured packings were studied and isothermal flow was assumed. Hence only the continuity and momentum equations were considered.

For a single-phase flow, the continuity and momentum equations can be defined as,

Continuity Equation

$$\frac{\partial \rho}{\partial t} + \nabla.(\rho V) = 0 \qquad (3.1)$$

Momentum Equations

$$\frac{\partial}{\partial t}(\rho V) + \nabla.(\rho VV) = -\nabla p + \nabla.\tau + \rho f \qquad (3.2)$$

3.2.1 Closure Relationships

Equations (3.1) and (3.2) represent four transport equations with five unknowns (ρ, three velocity components (U, V, W) and p). In addition, the stress tensor, τ has six unknown components. The body force f is assumed to be given. For closure, two more equations are required.

One equation comes from an equation of state:

$$p = p(\rho, T) \tag{3.3}$$

The second set of equation is a correlation for the viscous stress tensor τ. For a Newtonian and incompressible fluid, τ can be expressed in terms of velocity and fluid properties as:

$$\tau = \mu\left(\nabla V + (\nabla V)^T\right) \tag{3.4}$$

where,

μ = molecular viscosity, and

$(\nabla V)^T$ = transpose of (∇V)

So, for a Newtonian fluid with constant density and viscosity and with gravity as the only body force, equation (3.2) reduces to,

$$\frac{\partial}{\partial t}(\rho V) + \nabla.(\rho VV) = -\nabla p + \mu\nabla^2 V + \rho g \tag{3.5}$$

This is the Navier-Stokes equation.

3.3 Turbulence Modeling

Turbulence consists of random fluctuations of the various flow quantities. It is three-dimensional, chaotic and is characterized by a large range of excited time and length scales. In turbulent flow, the flow field variables vary significantly and irregularly both in time and position.

The governing equations of laminar flows are also applicable for turbulent flows. But for turbulent flows, an enormous amount of information is contained in the equations. Time and length scales of turbulent flows are much smaller than the smallest possible grid size. Thus the direct numerical simulation of these flows would require computing speed and memory that are many orders of magnitude larger than available in the foreseeable future.

Turbulence modeling is used to predict the effects of turbulence. In the most popular approach, the procedure introduced by Reynolds (1895) is followed. In Reynolds approach, all quantities are expressed as the sum of mean and fluctuating components. By time averaging, continuity equation remains the same; the only difference is that the velocity is the mean velocity. But by time averaging of the Navier-Stokes equations, the Reynolds-Averaged Navier-Stokes (RANS) equation is obtained. For an incompressible flow, RANS is:

$$\frac{\partial}{\partial t}(\rho V)+\nabla.(\rho VV)=-\nabla p+\nabla.\tau-\nabla.\rho\overline{V'V'}+\rho g \qquad (3.6)$$

where,

V, ρ and τ are the time-averaged mean quantities and V' is the fluctuating part of velocity vector.

3.3.1 Closure Relationships

As a result of Reynolds averaging of the Navier-Stokes equation, a new quantity, $-\rho\overline{V'V'}$ called the Reynolds stress appears. This is a second order symmetric tensor. With the appearance of this, six more unknowns have been introduced. For closure, these unknowns must be related to the mean flow variables. There are two types of model available for Reynolds or Turbulent Stress, such as,

1) Eddy-viscosity model and
2) Reynolds stress model (Wilcox, 1993)

In the eddy-viscosity hypothesis, for incompressible flow, it is assumed that,

$$-\rho\overline{V'V'} = -\frac{2}{3}\mu_t\rho k\delta + \mu_t\left(\nabla V + (\nabla V)^T\right) \qquad (3.7)$$

where,

μ_t = turbulent viscosity,

k = turbulent kinetic energy and

δ = identity tensor

The k-epsilon (k-ϵ) model (Wilcox, 1993), based on eddy-viscosity hypothesis, is used most commonly and in this model the turbulent viscosity is computed from,

$$\mu_t = C_\mu\rho\frac{k^2}{\varepsilon} \qquad (3.8)$$

To get the values of k and ϵ, the transport equations for k and ϵ are solved.

$$\frac{\partial}{\partial t}(\rho k) + \nabla.(\rho V k) = \nabla.\left(\frac{\mu_{eff}}{\sigma_k}\nabla k\right) + P_k - \rho\varepsilon \qquad (3.9)$$

$$\frac{\partial}{\partial t}(\rho \varepsilon) + \nabla.(\rho V \varepsilon) = \nabla.\left(\frac{\mu_{eff}}{\sigma_\varepsilon}\nabla \varepsilon\right) + \frac{\varepsilon}{k}(C_{\varepsilon 1} P_k - C_{\varepsilon 2}\rho\varepsilon) \qquad (3.10)$$

where,

$$\mu_{eff} = \mu + \mu_t \qquad (3.11)$$

The standard values of the closure coefficients are (Wilcox, 1993):

$C_\mu = 0.09$,

$C_{\varepsilon 1} = 1.44$,

$C_{\varepsilon 2} = 1.92$,

$\sigma_k = 1.0$ and

$\sigma_\varepsilon = 1.3$

3.4 Multiphase Modeling

A multiphase flow system contains a mixture of phases that may have different flow fields; i.e., different velocity, pressure and temperature, etc. Examples of multiphase flow systems are bubbles in liquid, droplets in a gas and solid particles in a fluid i.e., liquid or gas. It is assumed that the phases in multiphase flow are mixed at smaller scales than the scale of the overall system and also at larger scales than the molecular scale.

Ideally, the multiphase flow problem is analyzed by solving the single-phase governing equations for each phase by accounting for interactions between particles in the phase in the flow field. For example, for a dispersed phase flow this would mean solving the single-phase governing equations for the continuous phase by accounting for the effects of each and every individual dispersed phase particle. Computationally, this would

require a grid dimension at least as small as the smallest fluid or solid particle in the field (Crowe et al., 1998). Since this is beyond current computer capability, such an analysis is impractical.

3.4.1 The Concept of Volume Averaging

To overcome this problem, the concept of local volume averaging has been introduced. In this approach, the governing equations are expressed based on average quantities. One considers the average properties in a volume containing many particles and ascribes the average values to a point in the flow enclosed by the volume (Crowe et al., 1998). Volume averaging is carried out by averaging properties at an instant in time over a volume and ascribing the average values to a point in the flow. The single-phase flow conservation governing equations are volume averaged resulting in equations that are expressed in terms of volume-averaged flow variables for the multiphase flow.

Figure 3.1 shows a planar sketch of the Representative Elementary Volume (*REV*) in porous medium. The concept of *REV* is very important in study of porous medium and has been used by various researchers such as Whitaker (1966), Slattery (1969), Bear (1972) and Liu and Masliyah (1996). A *REV* is defined as a minimum volume within which measurable variables (velocity, concentration, density etc.) become continuum quantities inside a porous medium. In the sketch shown in Figure 3.1, S stands for a solid phase, L stands for a liquid phase, and G stands for a gas phase. The solid phase here represents the packing material. According to Slattery, if φ^* stands for the point variable associated with a fluid, then the volume average of this variable can be defined as,

$$\overline{\varphi} = \frac{1}{V}\int_V \varphi^* dV \qquad (3.12)$$

The volume average can also be taken over the partial volume of the individual phase itself as follows,

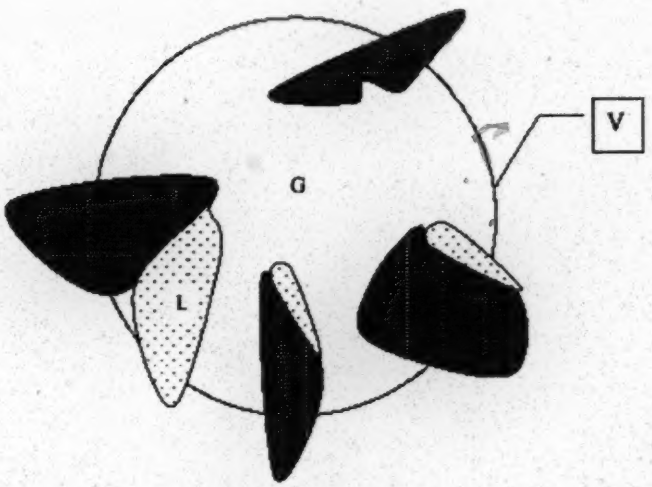

Figure 3.1 A planar sketch of representative elementary volume, S - solid phase, L - liquid phase, G - gas phase and V - volume of REV (Nandakumar et al. (1999))

$$\varphi_{a\varepsilon} = \frac{1}{V_a}\int_{V_a} \varphi^{\bullet} dV \qquad (3.13)$$

3.4.2 Multi-fluid model

In this approach, it is assumed that each phase possesses its own flow field; i.e., velocity, temperature, etc. and the phases are considered as interpenetrating continua; i.e., each point in the mixture is occupied simultaneously (in variable proportions) by each phase. Each phase is governed by its own conservation and constitutive equations; these are then coupled through interphase transfer or interaction terms. The Eulerian-Eulerian multi-fluid model is one of the popular multiphase models.

After volume averaging, the continuity and momentum equations become,

Continuity equation for phase α

$$\frac{\partial}{\partial t}(r_a \rho_a) + \nabla.(r_a \rho_a V_a) = S_{a,mass} \qquad (3.14)$$

where,

$S_{\alpha,mass}$ = Mass source or sink because of interphase transfer,

r_α = Volume fraction of phase α in the averaging volume (arbitrary but well defined)

If there is no interphase transfer, equation (3.14) reduces to,

for gas phase:

$$\frac{\partial(r_G \rho_G)}{\partial t} + \nabla.(r_G \rho_G V_G) = 0 \qquad (3.15)$$

and, for liquid phase:

$$\frac{\partial(r_L\rho_L)}{\partial t}+\nabla.(r_L\rho_L V_L)=0 \qquad (3.16)$$

Momentum equation for phase α

$$\frac{\partial}{\partial t}(r_\alpha\rho_\alpha V_\alpha)+\nabla.(r_\alpha\rho_\alpha V_\alpha V_\alpha) = -r_\alpha\nabla p_\alpha+\nabla.\left[r_\alpha\mu_\alpha\left(\nabla V_\alpha+(\nabla V_\alpha)^T\right)\right]+r_\alpha\rho_\alpha g+S_{\alpha,mom}+M_{\beta\alpha} \qquad (3.17)$$

where,

$S_{\alpha,mom}$ = Momentum source due to external body forces other than gravity

$M_{\beta\alpha}$ = Interphase momentum transfer due to fluid-fluid and/or fluid-solid interactions

If no external body forces other than gravity is present then equation (3.17) becomes,

for gas phase,

$$\frac{\partial}{\partial t}(r_G\rho_G V_G)+\nabla.(r_G(\rho_G V_G V_G)) = -r_G\nabla p_G+\nabla.\left(r_G\mu_{eff,G}\left(\nabla V_G+(\nabla V_G)^T\right)\right)+r_G\rho_G g+M_{LG} \qquad (3.18)$$

and, for liquid phase,

$$\frac{\partial}{\partial t}(r_L\rho_L V_L)+\nabla.(r_L(\rho_L V_L V_L)) = -r_L\nabla p_L+\nabla.\left(r_L\mu_{eff,L}\left(\nabla V_L+(\nabla V_L)^T\right)\right)+r_L\rho_L g+M_{GL} \qquad (3.19)$$

where,

$\mu_{eff,G}$ and $\mu_{eff,L}$ are the effective viscosities of the gas and liquid phases, respectively, and can be defined as,

$$\mu_{eff,G} = \mu_{laminar,G} + \mu_{turbulent,G} \quad (3.20)$$

$$\mu_{eff,L} = \mu_{laminar,L} + \mu_{turbulent,L} \quad (3.21)$$

The volume fractions summation constraint adds one more equation:

$$\sum_{\alpha=1}^{N_p} r_\alpha = 1 \quad (3.22)$$

where,

N_p = total number of phases and

r_α = volume fraction of phase α

So, for two-phase (gas and liquid) system equation (3.22) becomes,

$$r_G + r_L = 1 \quad (3.23)$$

It is also assumed that both phases have the same pressure, i.e,

$$p_G = p_L \quad (3.24)$$

In order to solve equations (3.14) to (3.21) for velocities, pressure and volume fractions, additional closure equations are needed that relate the interphase momentum transfer term M_{GL}. The interphase momentum transfer term, M_{GL} is basically inter-phase drag force per unit volume and can be defined as,

$$M_{LG} = K_{LG}(V_L - V_G) \quad (3.25)$$

where,

K_{LG} = exchange co-efficient

For fluid-fluid flows, each secondary phase is assumed to form droplets or bubbles. This has an impact on how each of the fluids is assigned to a particular phase. For example, in flows where there are unequal amounts of two fluids, the predominant fluid should be modeled as the primary fluid, since the sparser fluid is more likely to form droplets or bubbles. The exchange coefficient for these types of bubbly, liquid-liquid or gas-liquid mixtures can be written in the following general form:

$$K_{LG} = -K_{GL} = \frac{r_G r_L \rho_L f_d}{\tau_L} \qquad (3.26)$$

where,

f_d = drag function which is defined differently for the different exchange-coefficient models and

τ_L = particulate relaxation time which is defined as ,

$$\tau_L = \frac{\rho_L d_L^2}{18\mu_G} \qquad (3.27)$$

where,

d_L =diameter of the bubbles or droplets of phase L

Nearly all definitions of f_d include a drag coefficient C_D that is based on the relative Reynolds number, Re. It is this drag function that differs among the exchange-coefficient models. For all situations, K_{LG} should tend to zero whenever the primary phase is not present within the domain.

To define the interphase momentum transfer term or the interphase drag force per unit volume in the two-phase simulations in CFX, built-in Schiller-Naumann model were used. It is acceptable for general use for all fluid-fluid pairs of phases. For the model of Schiller and Naumann,

$$f_d = \frac{C_D \, \mathrm{Re}}{24} \tag{3.28}$$

where,

$$C_D = \frac{24\left(1 + 0.15\mathrm{Re}^{0.687}\right)}{\mathrm{Re}} \qquad \text{for Re<1000} \tag{3.29}$$

and, $C_D = 0.44$ for Re>1000 (3.30)

and, *Re* = relative Reynolds number

The relative Reynolds number for the primary phase α and secondary phase β is obtained from,

$$\mathrm{Re} = \frac{\rho_\beta \left|\vec{V}_\beta - \vec{V}_\alpha\right| d_\alpha}{\mu_\alpha} \tag{3.31}$$

and the relative Reynolds number for secondary phases *p* and *r* is obtained from,

$$\mathrm{Re} = \frac{\rho_{rp} \left|\vec{V}_r - \vec{V}_p\right| d_{rp}}{\mu_{rp}} \tag{3.32}$$

where,

μ_{rp} = mixture viscosity of the phases *p* and *r and can be defined as,*

$$\mu_{rp} = \alpha_p \mu_p + \alpha_r \mu_r \tag{3.33}$$

3.5 Turbulent Multiphase Flow

Turbulence in multiphase flow is another stage of modeling which is still underdeveloped. Currently turbulence averaging is performed on the already averaged

conservation equations. Volume fraction weighted Favre averaging is preferred in order to eliminate complications arising from correlations of volume fraction with velocity. Due to turbulence averaging, a new term called 'Reynolds stress' appeared in the momentum equations for each phase. In order to close the system of equations, the Reynolds stresses in each phase have to be expressed in terms of mean flow variables. The k-epsilon turbulence model for the single phase may be generalized for a multiphase system. An effective viscosity is used in the momentum equations and the eddy-viscosity hypothesis is applied to each phase,

$$\mu_{\alpha,eff} = \mu_\alpha + \mu_{t\alpha} \tag{3.34}$$

and, for the k-ε model,

$$\mu_{t\alpha} = C_\mu \rho_\alpha \frac{k_\alpha^2}{\varepsilon_\alpha} \tag{3.35}$$

Thus the equations for k_α and ε_α are,

$$\frac{\partial}{\partial t}(r_\alpha \rho_\alpha k_\alpha) + \nabla.(r_\alpha \rho_\alpha V_\alpha k_\alpha) = \nabla.\left(r_\alpha\left(\mu_\alpha + \frac{\mu_{t\alpha}}{\sigma_k}\right)\nabla k_\alpha\right) + r_\alpha(P_{k,\alpha} - \rho_\alpha \varepsilon_\alpha) + T_{\alpha\beta}^{(k)} \tag{3.36}$$

$$\frac{\partial}{\partial t}(r_\alpha \rho_\alpha \varepsilon_\alpha) + \nabla.(r_\alpha \rho_\alpha V_\alpha \varepsilon_\alpha) = \nabla.\left(r_\alpha\left(\mu_\alpha + \frac{\mu_{t\alpha}}{\sigma_\varepsilon}\right)\nabla \varepsilon_\alpha\right) + r_\alpha \frac{\varepsilon_\alpha}{k_\alpha}(C_{\varepsilon 1} P_{k,\alpha} - C_{\varepsilon 2} \rho_\alpha \varepsilon_\alpha) + T_{\alpha\beta}^{(\varepsilon)} \tag{3.37}$$

where, $T_{\alpha\beta}^{(k)}$ and $T_{\alpha\beta}^{(\varepsilon)}$ are inter-phase transfer terms that need to be specified, if any exist.

3.6 Conservation of Species

To solve the conservation equations for chemical species, the local mass fraction of each species, Y_i, is predicted through the solution of a convection-diffusion equation for i-th species. The general form of this conservation equation is as follows:

$$\frac{\partial}{\partial t}(\rho Y_i) + \nabla.(\rho \vec{v} Y_i) = -\nabla.\vec{J}_i + R_i + S_i \qquad (3.38)$$

where,

R_i = net rate of production of species i by chemical reaction,

S_i = rate of creation by addition from the dispersed phase plus any user-defined sources and

J_i = diffusion flux of species i, which arises due to concentration gradients

For full multi-component diffusion in laminar flows, the Maxwell-Stefan equations is solved, but for dilute approximation, the diffusion flux can be written as,

$$\vec{J}_i = -\rho D_{i,m} \nabla Y_i \qquad (3.39)$$

For turbulent flows, the mass diffusion can take the following form,

$$\vec{J}_i = -\left(\rho D_{i,m} + \frac{\mu_t}{Sc_t}\right)\nabla Y_i \qquad (3.40)$$

and, the turbulent Schmidt number, Sc_t, the default value of which is 0.7 can be defined as,

$$Sc_t = \frac{\mu_t}{\rho D_t} \qquad (3.41)$$

where,

J_i = diffusion flux of species i which arises due to concentration gradients,

$D_{i,m}$ = diffusion coefficient of species *i* in the mixture,

∇Y_i = gradient of concentration,

μ_t = turbulent viscosity, and

D_t = turbulent diffusivity

Generally, turbulent diffusion overwhelms laminar diffusion, and so the specification of detailed laminar diffusion properties in turbulent flows is generally not needed.

An equation of this form will be solved for *N-1* species where *N* is the total number of fluid phase chemical species present in the system. Since the mass fraction of the species must sum to unity, the *N-th* mass fraction is determined as one minus the sum of the *N-1* solved mass fractions. To minimize numerical error, the *N-th* species should be selected as that species with the overall largest mass fraction.

3.7 Computational Fluid Dynamics (CFD)

The differential equations of momentum, energy and mass transfer form a system of coupled non-linear partial differential equations, which have no known general analytical solutions. Analytical solutions are possible only for a few simple special cases where the equations can be made linear through simplifications. The equations can, however, be discretized and solved numerically. Another approach to the problem is to measure the flow variables experimentally. Although experimental measurements are generally expected to give reliable data, they give a limited amount of data, and are expensive, time-consuming and less flexible. Compared to experiments, the numerical model gives a large amount of data, and is cheap, fast and more flexible.

Computational fluid dynamics (CFD) is concerned with obtaining numerical solutions to the basic governing equations using the computer. The advent of high-speed, large-

memory computers, the evolution of precise numerical algorithms, and developments in complex flow phenomena modeling have enabled CFD to obtain numerical solutions to flows of industrial interest. CFD obtains numerical solutions through two steps:

1) Discretization of the partial differential equations over the flow domain, and
2) Solution of the large set of algebraic system of equations those results from the discretization process.

The finite volume method is the most common solution methods used in CFD codes. It is the method used in the commercial CFD packages, i.e., CFX-5 and fluent, the packages used for the CFD analysis of this work.

3.7.1 Grid Generation

In the finite volume method, the flow domain is divided into small sub-regions known as control or finite volumes. The grid could be structured or unstructured. In the former case, transformation from physical space into computational space is performed. This will give grid lines that are orientated regularly in three directions so that coordinate transformations of curvilinear lines result in a cube for three-dimensional problems. The partial differential equations are then discretized and solved using the simplified computational space coordinate system. Unlike structured grids, in unstructured grids, coordinate transformation is not performed and as a result they can be used for irregular geometries but at the expense of more complex computer programming. Both structured and non-structured grids are used in Fluent and CFX-5. Unstructured grid is used in our model of the structured packings since the geometry is quite complicated.

3.7.2 Interpolation and Differencing Scheme

The finite volume method uses the integral form of the conservation equations. Integration is carried out for each finite or control volume (CV). This requires

approximations of surface and volume integrals. The surface integration process requires values of variables at one or more faces and/or corners. Since variables are evaluated and stored at the center of each CV or cell, methods of interpolating values of variables at faces or corners from the CV centers are required. The methods of interpolation are known as differencing schemes.

One of the popular ones is upwind differencing scheme, first put forward by Courant et al. (1952). In this scheme, CV face value of a variable is set equal to the CV center value upstream of the CV face. The scheme is first order accurate. In this study, for all simulations using Fluent-6, first-order upwinding differencing scheme was used for all the equations except for the pressure equations where the standard scheme was used and the pressure-velocity coupling was obtained using the SIMPLE algorithm (Van Doormal et al., 1984). Also, in the simulations using CFX-5, first order upwinding differencing scheme was used for all the equations. But for some cases, the results obtained using the first order upwinding scheme were further run using higher order schemes in order to check the sensitivity of the simulation results to the given order of the differencing scheme.

3.7.3 Solution of Algebraic System of Equations

The algebraic system of equations resulting from the discretization process is solved by using any of the two solution algorithms available in Fluent. The manner in which the governing equations are linearized may take an "implicit" or "explicit" form with respect to the dependent variable (or set of variables) of interest. In the implicit option, for a given variable, the unknown value in each cell is computed using a relation that includes both existing and unknown values from neighboring cells. Therefore each unknown will appear in more than one equation in the system, and these equations are solved simultaneously to give the unknown quantities. In our simulations, the segregated solver was used and only the implicit option is available for that.

In the segregated solution method, each discrete governing equation is linearized implicitly with respect to that equation's dependent variable. This will result in a system of linear equations with one equation for each cell in the domain. Because there is only one equation per cell, this is sometimes called a "scalar" system of equations. A point implicit (Gauss-Seidel) linear equation solver is used in conjunction with an algebraic multigrid (AMG) method to solve the resultant scalar system of equations for the dependent variable in each cell. For example, the x-momentum equation is linearized to produce a system of equations in which u velocity is the unknown. Simultaneous solution of this equation system (using the scalar AMG solver) yields an updated u-velocity field. In summary, the segregated approach solves for a single variable field (e.g., p) in an iterative manner by considering all cells at the same time. It then solves for the next variable field by again considering all cells at the same time, and so on.

Using the segregated solver numerical scheme, the governing equations are solved sequentially (i.e., segregated from one another). Because the governing equations are non-linear (and coupled), several iterations of the solution loop must be performed before a converged solution is obtained. Each of the iteration consists of some of the steps which are continued until the convergence criteria are met. The steps are outlined below:

1. Fluid properties are updated, based on the current solution. If the calculation has just begun, the fluid properties will be updated based on the initialized solution.

2. The u, v, and w momentum equations are each solved in turn using current values for pressure and face mass fluxes, in order to update the velocity field.

3. Since the velocities obtained in Step 2 may not satisfy the continuity equation locally, a "Poisson-type" equation for the pressure correction is derived from the continuity equation and the linearized momentum equations. This pressure correction equation is then solved to obtain the necessary corrections to the pressure and velocity fields and the face mass fluxes such that continuity is satisfied.

4. Equations for scalars such as turbulence and species (where appropriate) are solved using the previously updated values of the other variables.

5. A check for convergence of the equation set is made.

3.8 Conclusions

In this chapter, the mathematical and numerical modeling of fluid flow was reviewed. An overview of the mathematical model was given which started with single-phase laminar flow and ended up with turbulent multiphase flow. The concept and necessity of computational fluid dynamics was illustrated. The development of computer technology and availability of computational fluid dynamics (CFD) techniques constitute now a days an incontestably powerful route to enable accurate predictions of the hydrodynamics in structured packings by solving locally the rigorous fluid transport equations. Combined with minimal laboratory testing, CFD is foreseen to yield very detailed flow field solutions of all relevant variables, such as velocities, pressure, eddy viscosity, etc. Such detailed solutions are expected to yield better understanding of the phenomena occurring in structured packing-containing columns.

Chapter 4 Experimental Measurement of Flow Hydrodynamics

4.1 Introduction

In this chapter, the experimental set-up used in our laboratory to measure the flow hydrodynamics in structured packed distillation column is described. The experimental results obtained are presented, discussed and the important conclusions are given. The motivation for doing such experiments is that although pressure drop data is easily available in literature, liquid distribution and tracer dispersion data for structured packings are not easily available.

4.2 Experimental Setup

The experimental apparatus consisted of a 0.3 m ID cylindrical column, an air blower with variable speed DC motor, a liquid feed pump, a U-tube manometer (to measure pressure drop around the packings), a commercially designed liquid distributor (to measure liquid flow distribution), a specially designed liquid collector (also served as support plate and gas distributing device) and the necessary flow rate indicating and controlling meters. A schematic diagram of the experimental set-up is shown in Figure 4.1. Water was pumped at the top of the column. It then flowed downward through the packings and exited at the bottom of the column. The liquid flow rate was measured and controlled by a calibrated rotameter. The gas (air) flow to the column through the gas inlet pipe was supplied by an air blower which was normal to column axis. Air was distributed across the bottom of the packed column via a number of gas rising tubes (chimneys) fixed to the inside of the liquid collector. Each gas rising tube had a small cap fixed on the top that prevented liquid from entering it. The flow rate of air was measured by a hot-wire anemometer which was located on the gas inlet pipe adjacent to the column.

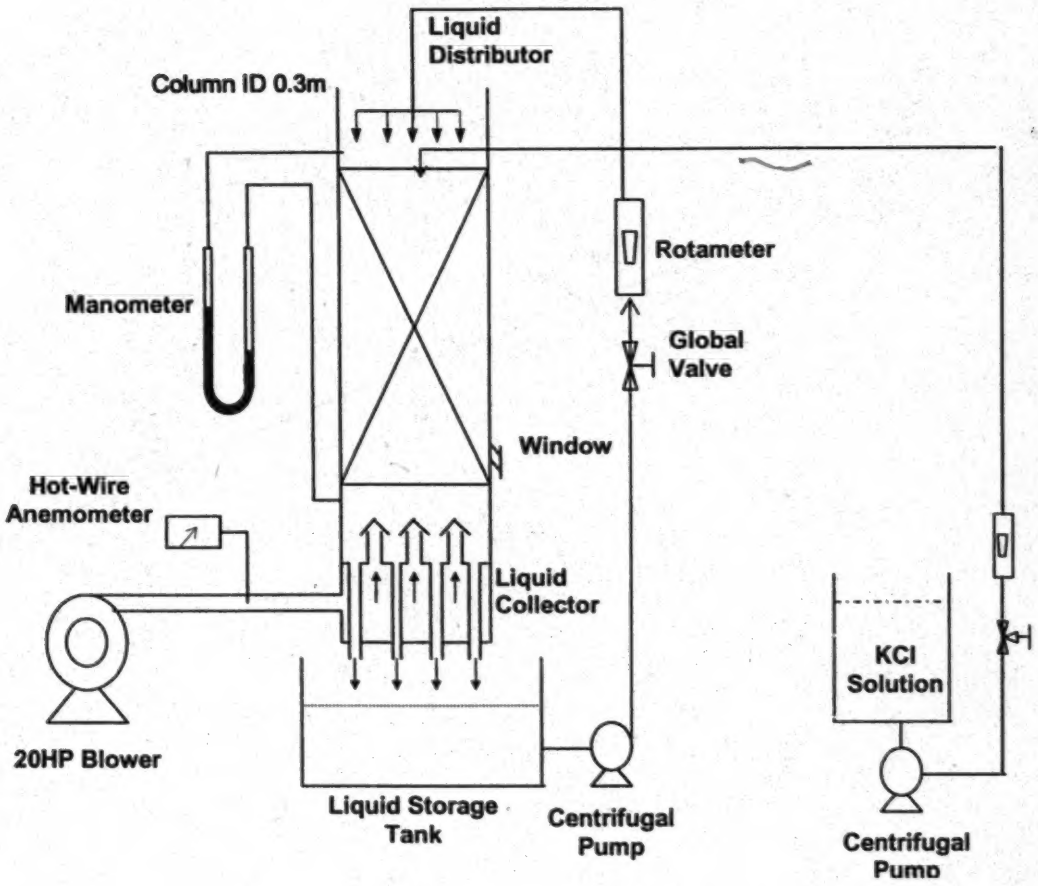

Figure 4.1 Schematic diagram of experimental setup

The column itself consisted of a number of transparent Plexiglass™ cylindrical sections. Each Plexiglass™ section had an inside diameter of 0.3 m and a height of 1.5 m. The use of transparent Plexiglass™ sections allowed for visual observation of the flow behavior in the packed column. The base of the column was made of stainless steel.

The column was dry-packed by hand with the four elements of smooth, unperforated flexipac-3Y type metal corrugated structured packings. Schematic diagram is shown in Figure 2.4. Orientations of the packings are such that consecutive elements are rotated by 90 degree with respect to the previous one. The specifications of the packings are given in Table 2.1.

4.3 Experimental Measurements of Dry and Irrigated Pressure Drop

4.3.1 Experimental Procedure and Range of Operating Parameters

Pressure drop experiments were conducted with the packings being loaded into the dry column. Four elements of flexipac-3Y type packings with a total height of 1.056 m were installed in the column. The first pressure drop experiment was carried out without any liquid flow, i.e., dry pressure drop experiment. Dry pressure drop was measured with air flowing upward through the column at different rates. The rest of the experiments were done with both the gas and liquid flow, i.e., irrigated pressure drop. Irrigated pressure drop was done for air-water countercurrent flow in the column at different gas and liquid flow rates.

For the irrigated pressure drop experiments, water was first introduced into the column through a pipe and its flow rate was set to a predetermined value. The air blower was then started to provide air to the column. The air flow rate was adjusted to the desired value by adjusting the speed of the air blower. A check was regularly made on the gas

and liquid flow rates to ensure that the conditions did not vary during the operation. Pressure drop around the packing was measured with a U-type manometer attached to the column. The flow rates of air and water were increased simultaneously until the flooding points were detected.

Liquid velocities were varied from 0.002 m/s to 0.006 m/s and for gas velocity starting from 1.1 m/s experiments' were continued till the flooding points occur for any given liquid rate.

4.3.2 Results and Discussion

Both the dry and wet pressure drop data are analyzed by plotting them as pressure drop per unit length of packing vs. f-factor ($v\sqrt{\rho}$) as shown in Figure 4.2. The nature of the graphs agreed well with any literature. From the nature of the plot, it was seen that for a given gas flow-factor the pressure drop per unit length increased with the increase in liquid rate and for a given liquid rate pressure drop increased gradually / linearly with the increase in gas flow-factor up to the flooding or loading point.

Again, with the increase in liquid flow rate, liquid holdup on the packings builds up quicker and so its loading point comes earlier than the lower liquid flow rate for the same gas flow factor and it can also be visualized from the nature of the plots shown in Figure 4.2. Above the flooding point, for a small increase in gas rate, pressure drop increased abruptly. Since flooding point is the indication of maximum operating region for any packed bed without flooding, so we can use this graph for determining the operational range of that particular packed column.

The experimental pressure drop data were compared with Bravo's correlation (Equation 2.9) and shown in Figure 4.3. It can be seen that, for any liquid rate, the values of experimental pressure drop per unit length is little bit higher than the pressure drop from Bravo's correlation. Also, for the same liquid rate, flooding occurs at low gas flow factor

in experiments. This may be due to the error in manometer reading and sensitivity of the flow rate indicating and measuring devices, such as, anemometer, rotameter etc.

4.4 Experimental Measurements of Liquid distribution

4.4.1 Introduction

Most of the studies on liquid distribution were carried out in small diameter columns packed with Raschig rings and Berl saddles without gas flow. Few years back, Sun et al. (2000) studied liquid flow maldistribution in random packed columns filled with 25 mm stainless steel Pall rings with gas-liquid (air-water, air-isopar) countercurrent flow. But still there is a dearth of experimental data on liquid distribution in large-scale columns filled with commercially important structured packings, such as Flexipac, Mellapac, Gempak, etc.

The same experimental set-up described in section 4.2 was used to measure the liquid flow distribution in the column for the counter current operation of two-phase flow (gas and liquid).

4.4.2 Design of Liquid Distributor

A commercially designed 0.2 m diameter liquid distributor of 20 drip points was used in the liquid distribution experiments. The schematic diagram of the liquid distributor is shown in Figure 4.4. The liquid distributor is usually quantified in terms of drip point density, defined as

$$\text{Drip point density} = \frac{\text{Number of drip points}}{\text{Cross - sectional area of column}} \qquad (4.1)$$

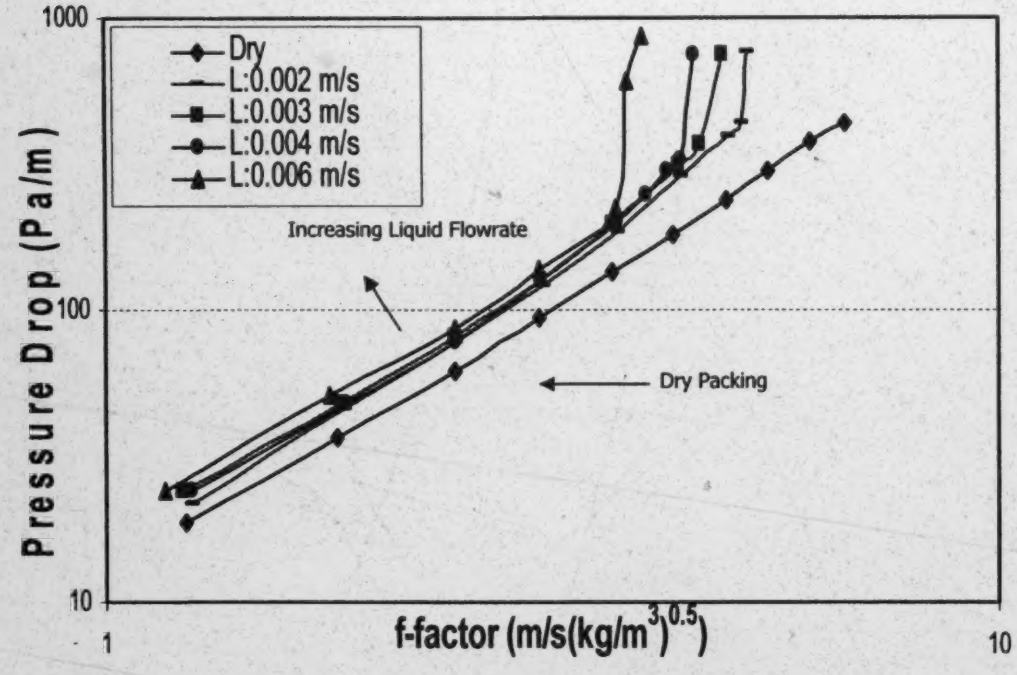

Figure 4.2 Plot of experimental pressure drop vs. f-factor for flexipac-3Y type packing at different gas and liquid loads

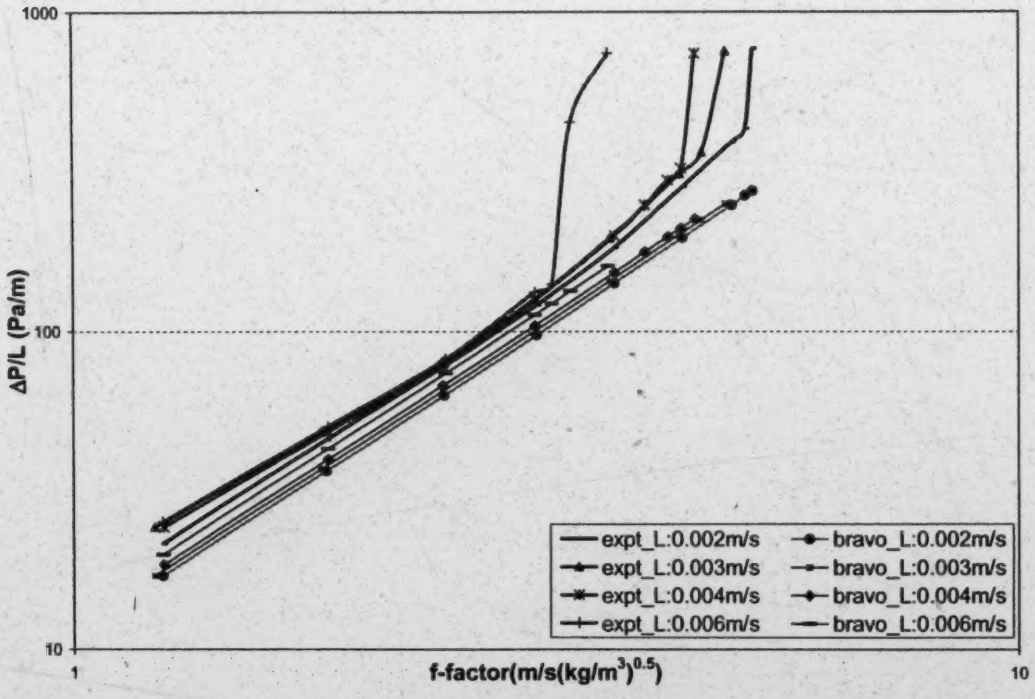

Figure 4.3 Comparison of experimental dry and wet pressure drop with Bravo's correlation

Based on the above definition, this distributor had a drip point density of 283 points per square meter. A distributor with drip point density this high is considered to distribute liquid uniformly over the top of the packing (Olujic et al., 1989). So, the distributor used in our experiments was uniform type.

In addition to the value of drip point density, the uniformity of any liquid distributor can be measured by measuring the flow rate of liquid from each drip points or holes as shown by Sun et al. (2000). They used ladder type liquid distributor and showed that, if for any given liquid distributor, the flow rate of the liquid from each holes is same then that distributor can be considered as uniform type.

4.4.3 Design of Liquid Collector

A specially designed liquid collector with 24 collecting cells was used to measure the liquid flow distribution at the bottom of the column. As the liquid flowed out of the packings, it was collected through each of the cells of the liquid collector. The schematic of the liquid collector is shown in Figure 4.5.

The liquid collector also acts as a support plate for packings and gas distributing device. The uniform initial gas distribution over the bottom column cross section was ensured by the appropriate arrangement of the gas rising tubes. For the ease of construction, each gas rising tube was designed with the same diameter (25.4 mm). There is one gas rising tube and one liquid collecting tube in each cell.

Assuming that the cross sectional area of the i^{th} collecting region is A_i and the number of gas rising tubes in this region is n_i, then from the simple mass balance, we can get

$$n_i q = A_i v \qquad (4.2)$$

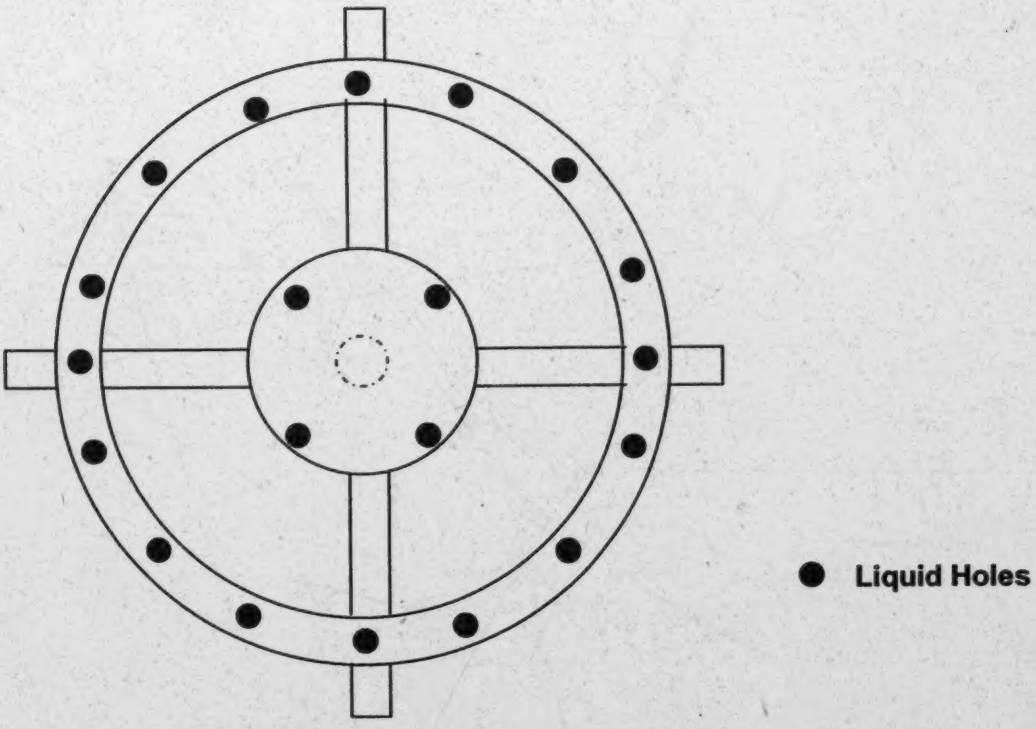

Figure 4.4 Schematic diagram of liquid distributor

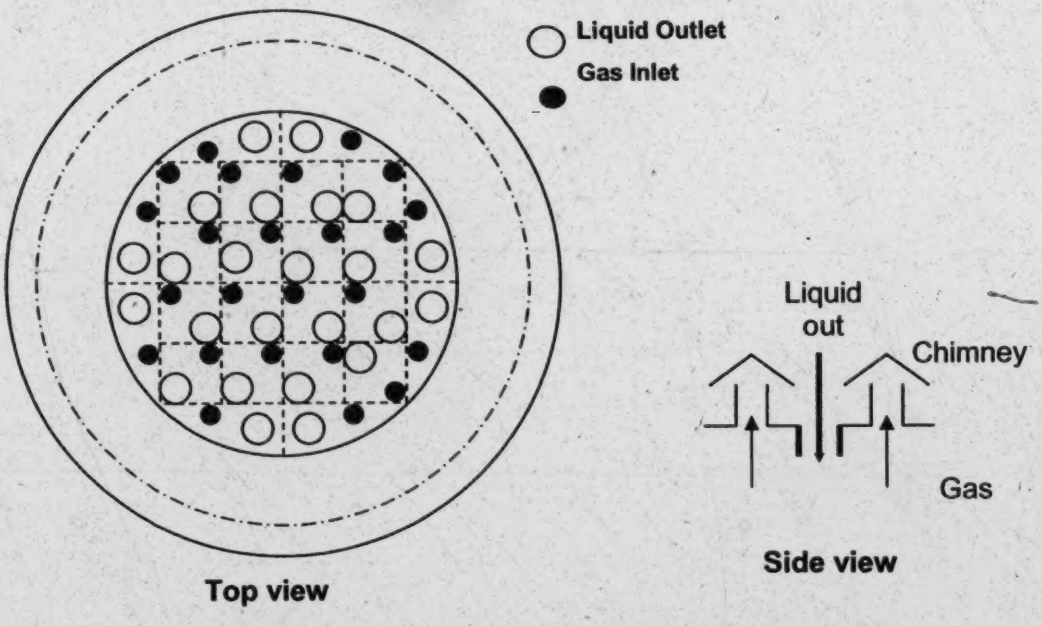

Figure 4.5 Schematic diagram of liquid collector

where,

q = gas flow rate passing through each of the gas rising tubes,

v = average gas velocity over the i^{th} liquid collecting region

To ensure uniform gas distribution over the total column cross section, the above relationship should be satisfied for each region.

4.4.4 Experimental Procedure and Range of Operating Parameters

Experiments on liquid flow distribution were carried out with water trickle flow. In the first experiment, for the four packing elements, water was introduced into the column through a single pipe. And for the rest of the experiments, a uniform liquid distributor was installed on top of the packings.

At the fixed packed bed height, water was first introduced into the column through the liquid distributor and its flow rate was set to a predetermined value. The air blower was then started to provide air to the column for the study of counter-current gas-liquid flow. The air flow rate was adjusted to the desired value by adjusting the speed of the air blower. A check was regularly made on the gas and liquid flow rates to ensure that the conditions did not vary during the operation.

About 20 minutes were needed for the liquid to reach a steady state in the column after flow rates were set. It was found that the liquid flow rate through each liquid drain tube was almost independent of time after 20 minutes.

The packed bed height was varied from 0.264 m (1 element) to 1.056 m (4 elements). The position of the liquid distributor was adjusted accordingly with the variation of the packed bed height. Two liquid flow rates, such as, 1.996 kg/m^{2}s and 3.992 kg/m^{2}s and two gas flow rates, such as, 1.1302 kg/m^{2}s and 2.6059 kg/m^{2}s were used in the

experiments. The ambient pressure and temperature conditions were used. The effects of operating condition and packed bed height on the liquid distribution were observed.

To measure the flow distribution, liquid was collected from each cell of the liquid collector with the time interval measured. The collected liquid samples were weighed and the liquid flow rates were then calculated. From the measurement of the local liquid flow rate for each collecting cells, the local liquid velocity can thus be calculated as,

$$u_{loc} = \frac{f_{loc}}{\rho_L A_{region}} \tag{4.3}$$

where,

f_{loc} = local liquid flow rate in kg/s, and

A_{region} = cross sectional area of the collecting region.

4.4.5 Results and Discussion

To analyze the liquid distribution data, it was plotted in terms of the liquid relative velocity against the coordinates of each of the measuring cells after the liquid flow rate from each collecting region had been measured. The liquid relative velocity (u_{rel}) is defined as the ratio of the local liquid velocity (u_{loc}) to the average liquid velocity (u_{av}) over the empty column cross section, that is,

$$u_{rel} = \frac{u_{loc}}{u_{av}} \tag{4.4}$$

The three-dimensional liquid flow distribution profiles are shown in Figures 4.6 to 4.22 which illustrate the development of the liquid flow patterns at various bed heights. It can be seen from the figures that, starting with a 20-point initial distribution at the top of the column that only irrigates a small fraction of the column section, liquid spreads well at Y

direction after one element of the packing (Figures 4.6 to 4.9). Then after two elements, liquid distributes reasonably well all over the column section (Figures 4.10 to 4.13). Those demonstrate the good spreading ability of the packings. The development of liquid wall flow after the second elements can be visualized from Figures 4.14 to 4.21.

Figures 4.6, 4.10, 4.14 and 4.18 show the three-dimensional profiles of the measured liquid flow distributions at the liquid load of 0.004 m^3/m^2s and the gas load of 1.1m^3/m^2s for different packed bed height of the packings. It can be seen from the figures that after one layer of the packing, liquid distributes well along Y direction (Figure 4.6) and a good distribution is achieved through two layers (Figure 4.10). Then the flow rates at the wall increased as shown in Figure 4.14 and 4.18.Figure 4.20 shows the distribution profile at the liquid load of 0.002 m^3/m^2s and the gas load of 1.1 m^3/m^2s for four elements of the packings (packed bed height = 1.056 m). By comparing Figure 4.18 with Figure 4.20, it can be seen that there is no significant difference between the liquid flow distributions at the two different liquid loads.

From the nature of the liquid flow distribution bar plots showing in Figures Figure 4.6 to Figure 4.22, it can be seen that although a uniform liquid distributor was stalled on top of the packings to distribute liquid, liquid was not evenly distributed for the whole cross section of the column. So, maldistribution occurred.

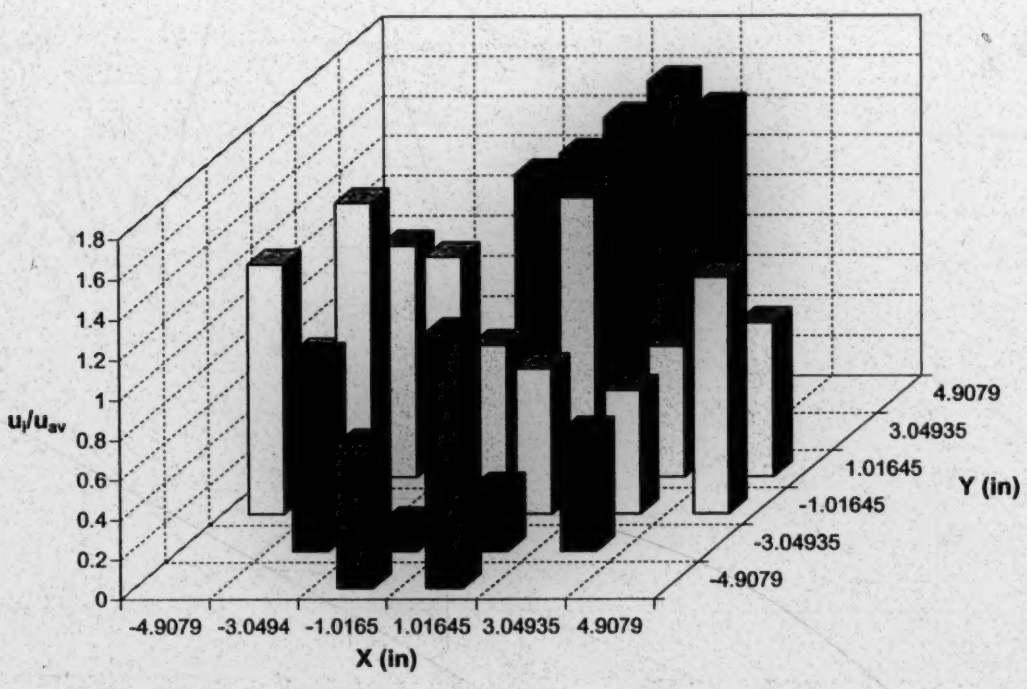

Figure 4.6 Liquid distribution for L: 0.004 m^3/m^2s, G: 1.1 m^3/m^2s and bed height: 0.264 m

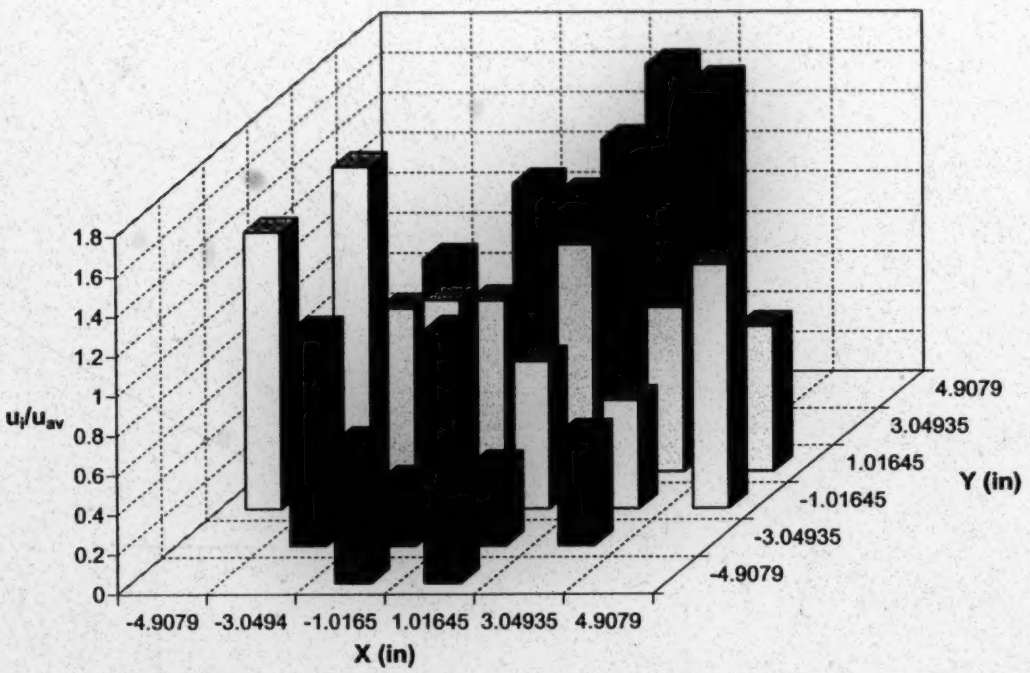

Figure 4.7 Liquid distribution for L: 0.004 m^3/m^2s, G: 2.2 m^3/m^2s and bed height: 0.264 m

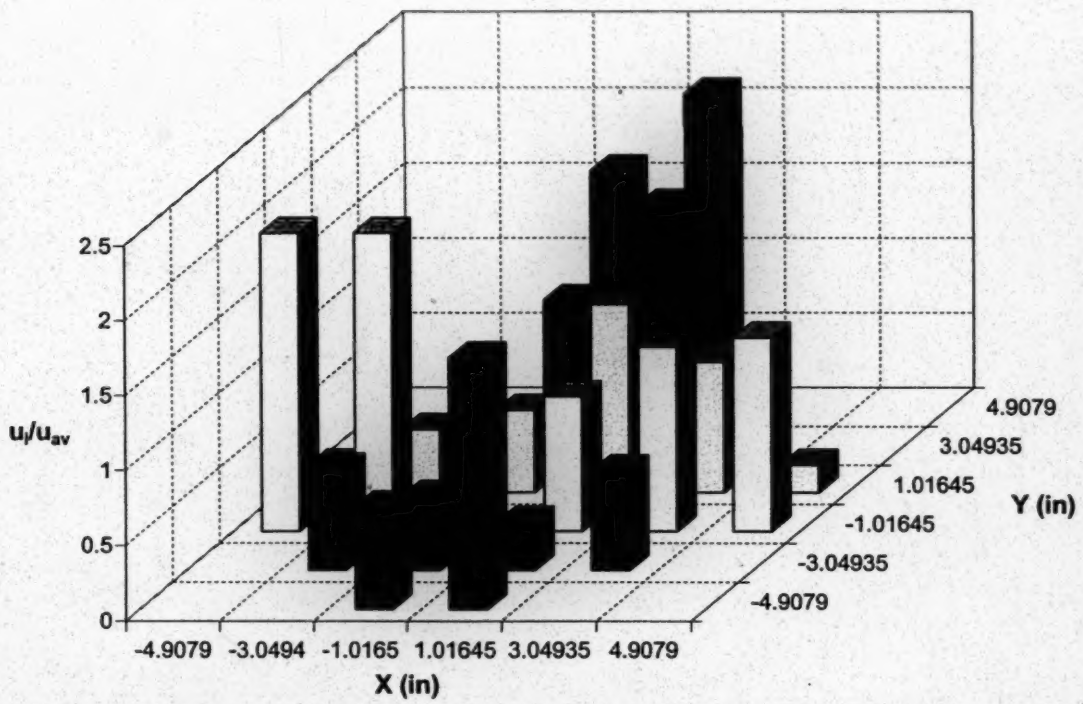

Figure 4.8 Liquid distribution for L: 0.002 m^3/m^2s, G: 1.1 m^3/m^2s and bed height: 0.264 m

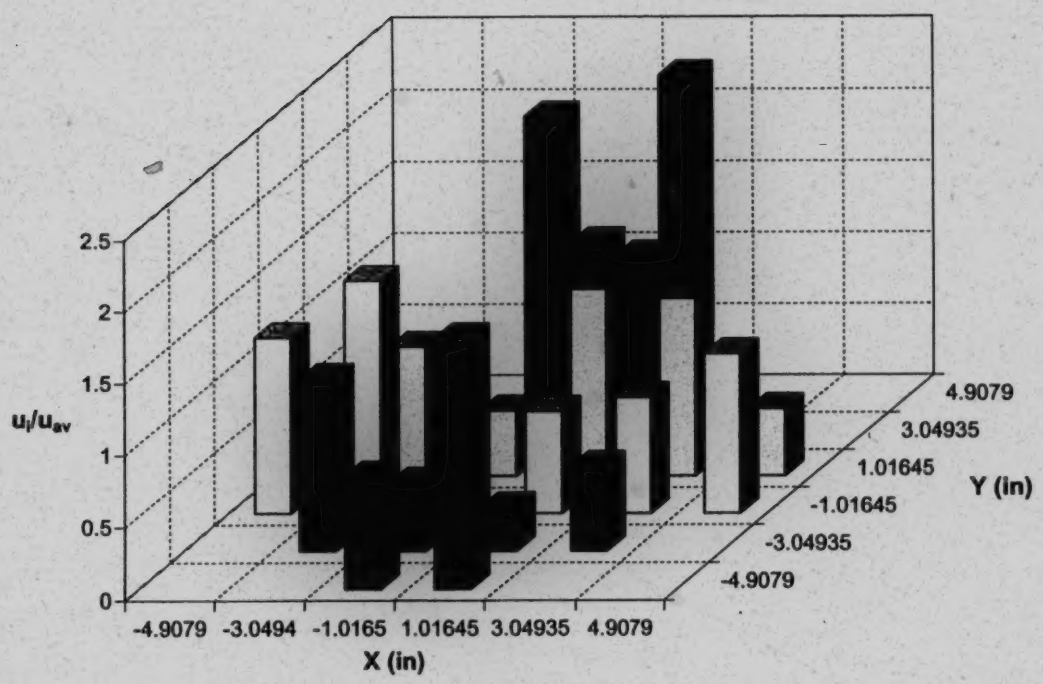

Figure 4.9 Liquid distribution for L: 0,002 m^3/m^2s, G: 2.2m^3/m^2s and bed height: 0.264 m

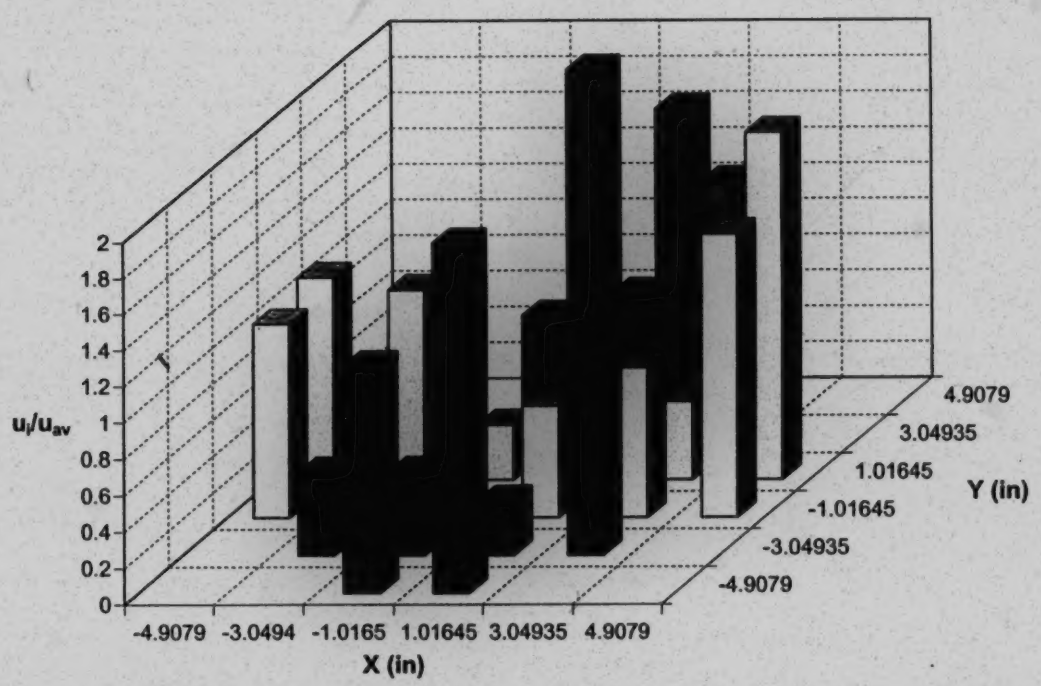

Figure 4.10 Liquid distribution for L: 0.004 m^3/m^2s, G: 1.1 m^3/m^2s and bed height: 0.528 m

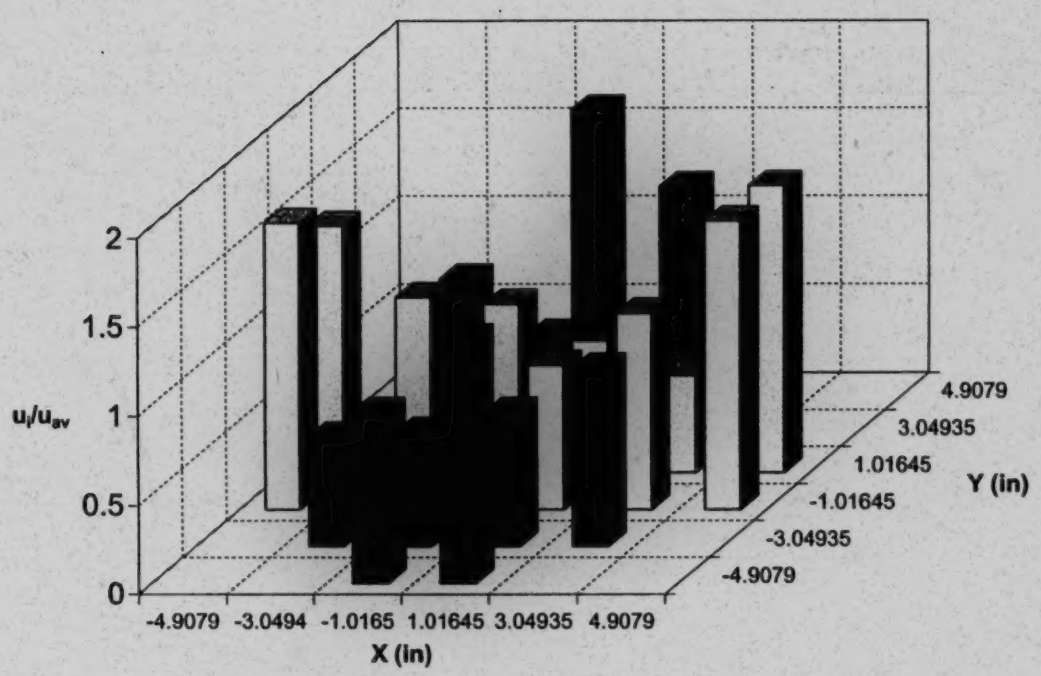

Figure 4.11 Liquid distribution for L: 0.004 m^3/m^2s, G: 2.2m^3/m^2s and bed height: 0.528 m

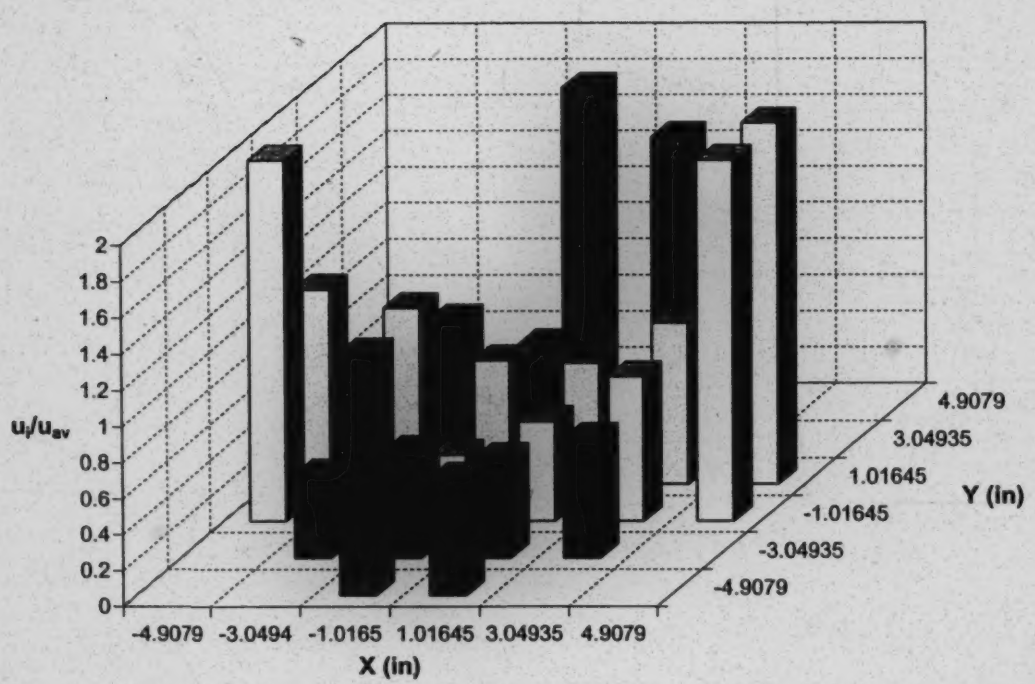

Figure 4.12 Liquid distribution for L: 0.002 m^3/m^2s,G: 1.1 m^3/m^2s and bed height: 0.528 m

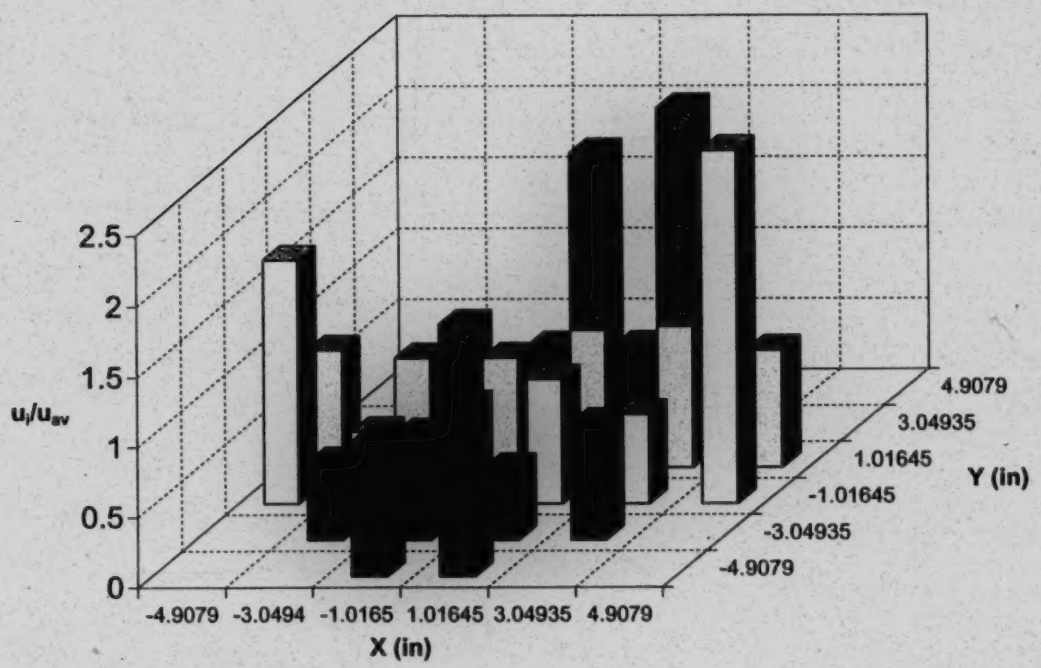

Figure 4.13 Liquid distribution for L: 0.002 m^3/m^2s, G: 2.2 m^3/m^2s and bed height: 0.528 m

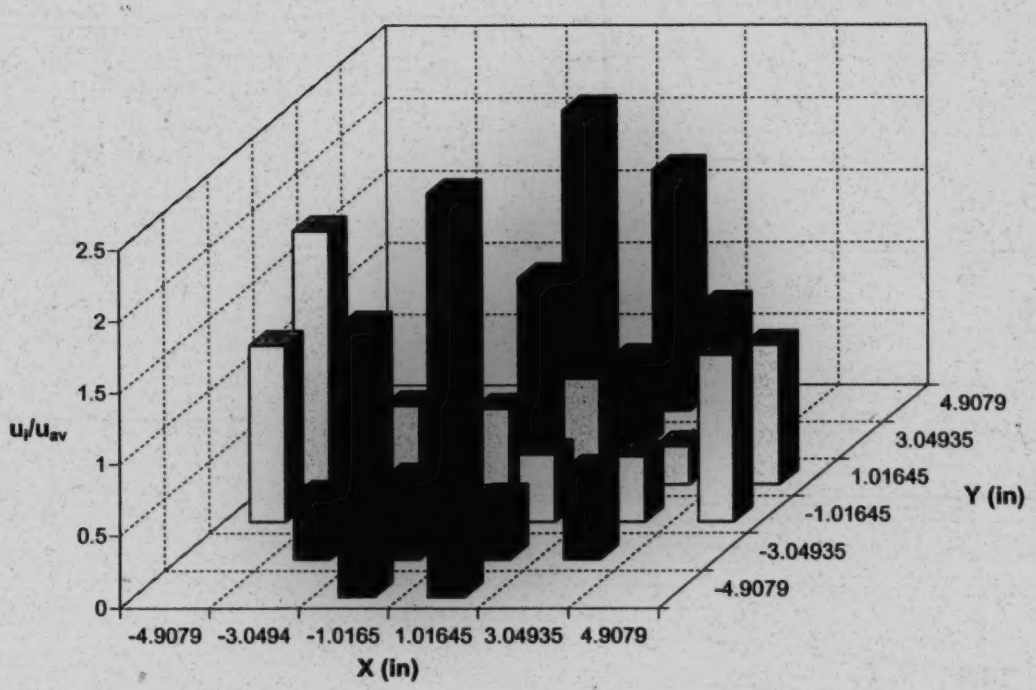

Figure 4.14 Liquid distribution for L: 0.004 m^3/m^2s, G: 1.1 m^3/m^2s and bed height: 0.792 m

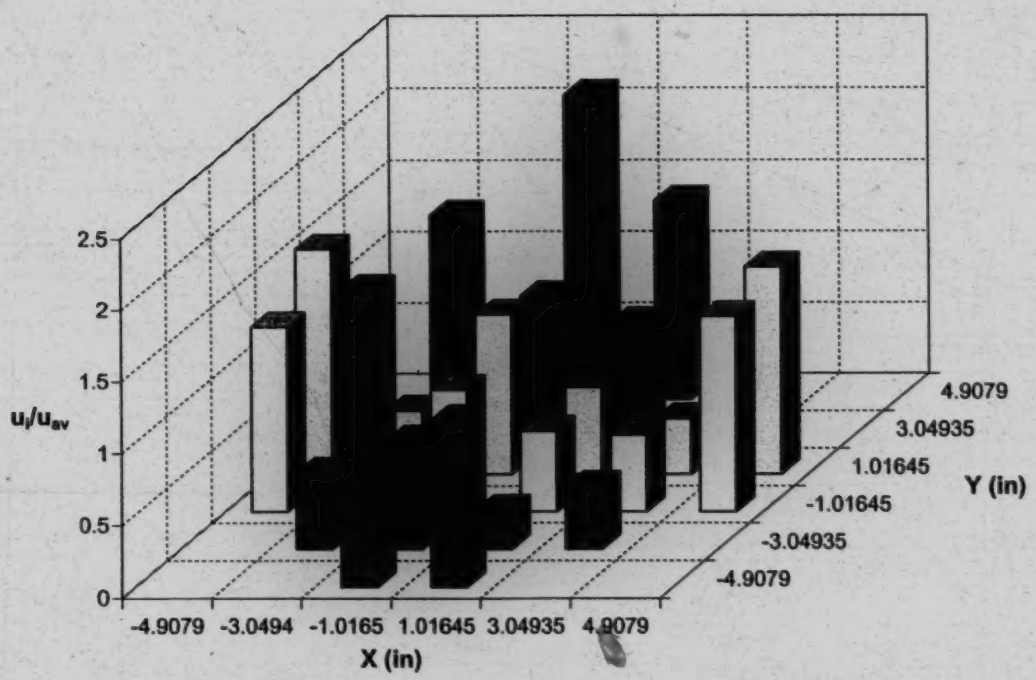

Figure 4.15 Liquid distribution for L: 0.004 m^3/m^2s, G: 2.2.m^3/m^2s and bed height: 0.792.m

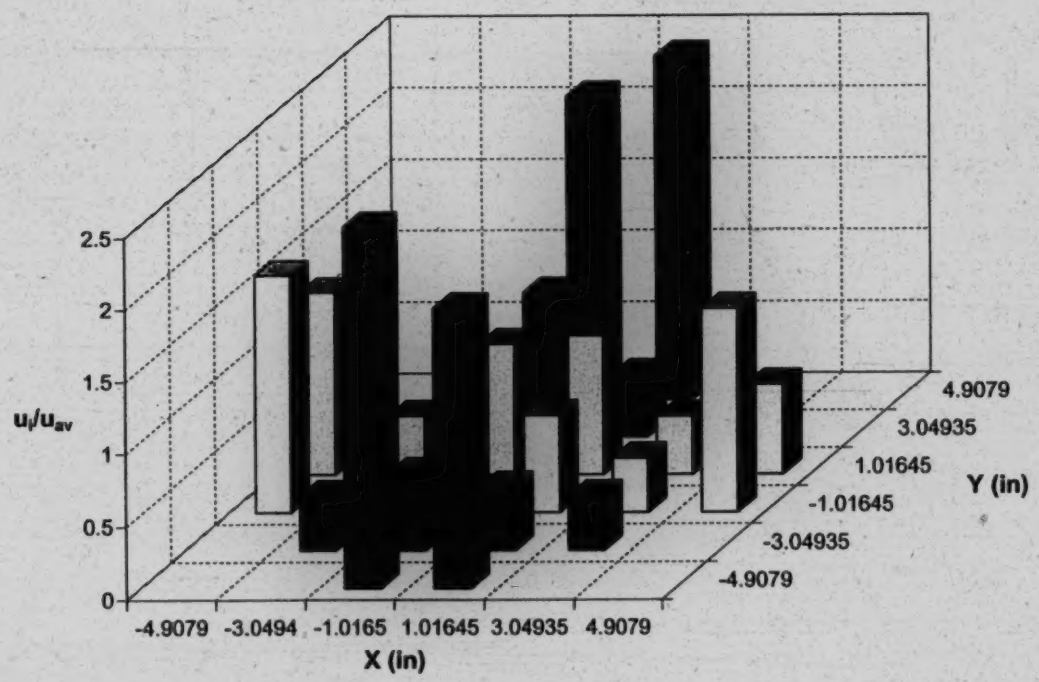

Figure 4.16 Liquid distribution for L: 0.002 m^3/m^2s, G: 1.1 m^3/m^2s and bed height: 0.792 m

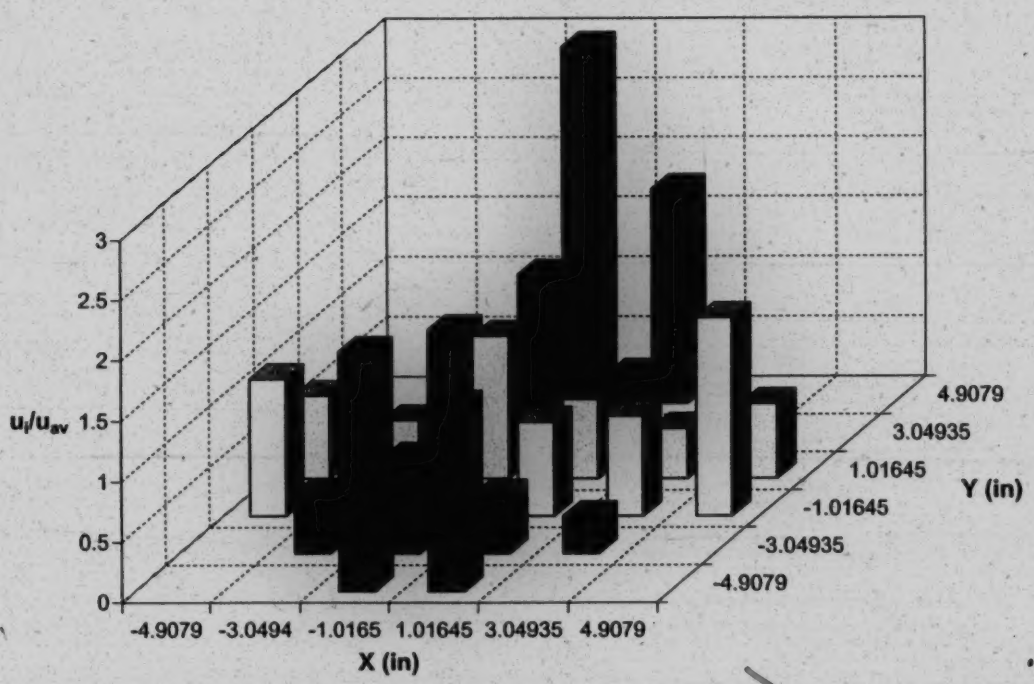

Figure 4.17 Liquid distribution for L: 0.002 m^3/m^2s, G: 2.2 m^3/m^2s and bed height: 0.792 m

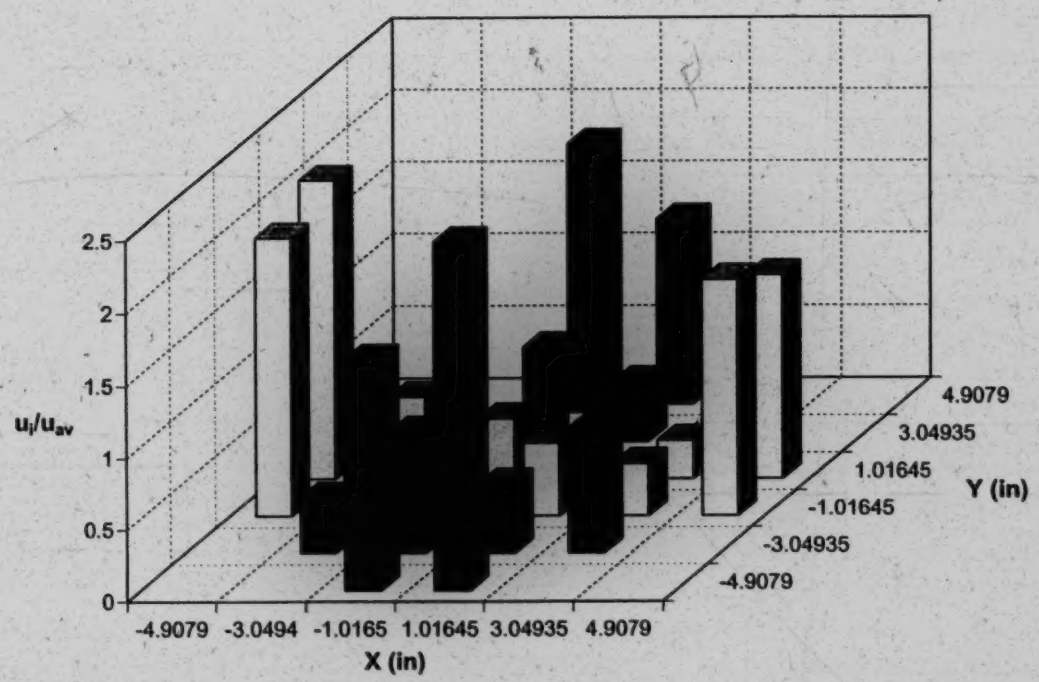

Figure 4.18 Liquid distribution for L: 0.004 m^3/m^2s, G: 1.1 m^3/m^2s and bed height: 1.056 m

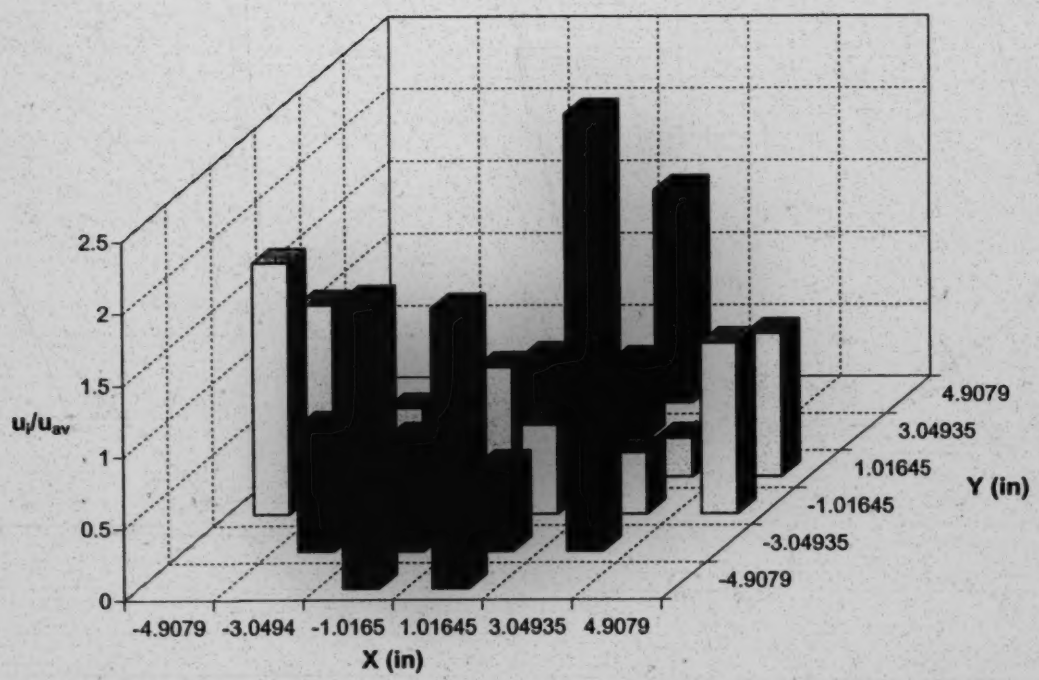

Figure 4.19 Liquid distribution for L: 0.004 m^3/m^2s, G: 2.2 m^3/m^2s and bed height: 1.056 m

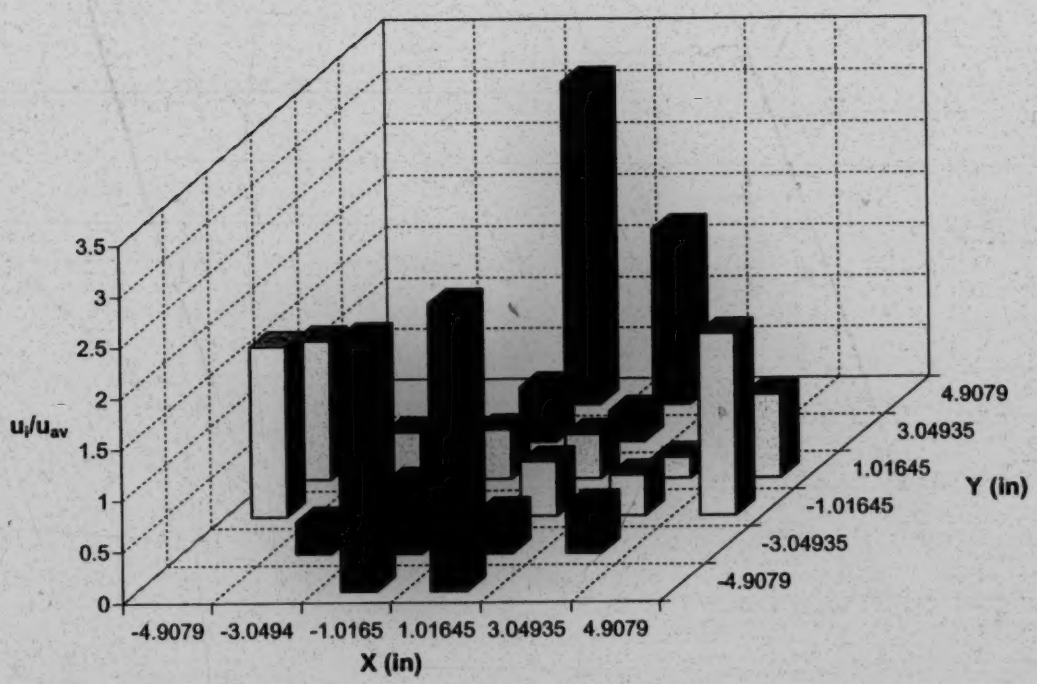

Figure 4.20 Liquid distribution for L: 0.002 m^3/m^2s, G: 1.1 m^3/m^2s and bed height: 1.056 m

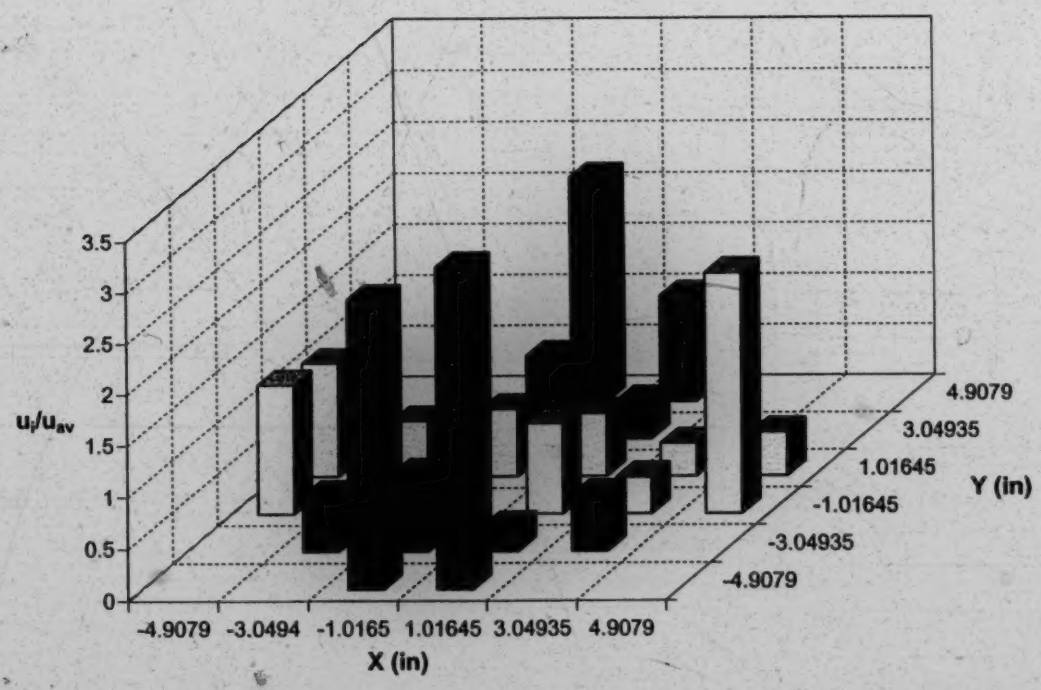

Figure 4.21 Liquid distribution for L: 0.002 m^3/m^2s, G: 2.2 m^3/m^2s and bed height: 1.056 m

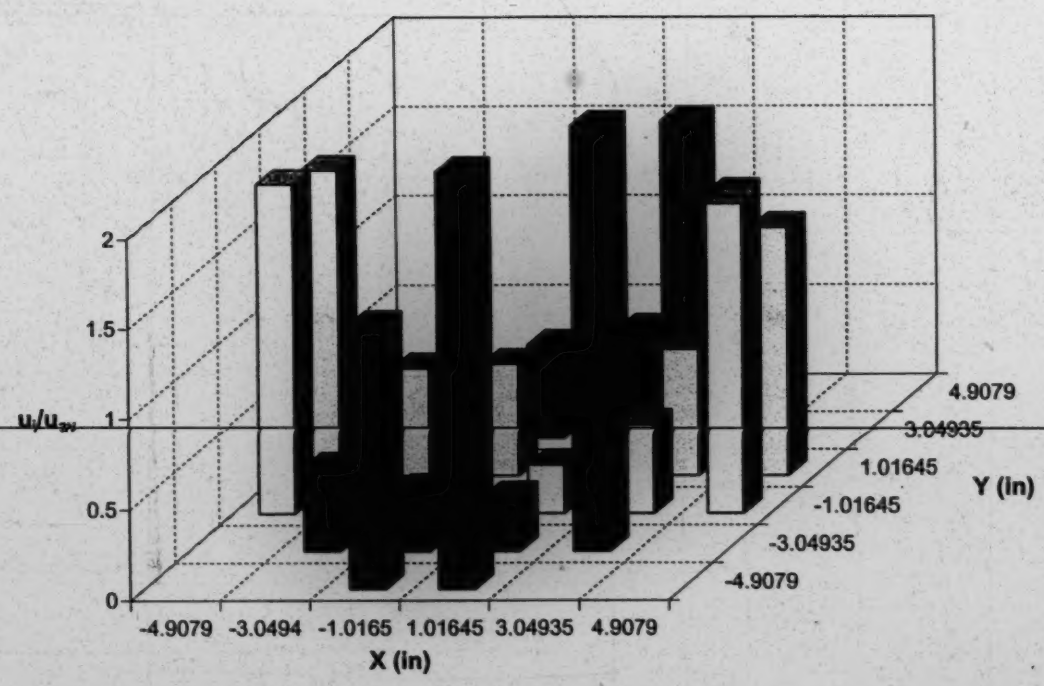

Figure 4.22 Liquid distribution for L: 0.004 m^3/m^2s G: 2.2 m^3/m^2s and bed height: 1.056 m (single pipe or point flow)

4.4.6 Quantification of Liquid Maldistribution

The liquid flow distribution in packed distillation columns can be further characterized by maldistribution factor. Maldistribution factors are calculated from the detailed liquid flow distribution profiles. It is a measure of the severity of the liquid maldistribution in a section of a packed column. The larger the *Mf*, the poorer the liquid flow distribution.

The definition of maldistribution factor (*Mf*) proposed by Hoek et al. (1986) was used in the calculations and shown below,

$$Mf = \sqrt{\frac{1}{m}\sum_{i=1}^{m}\left(\frac{u_i - \bar{u}}{\bar{u}}\right)^2} \qquad (4.5)$$

where,

Mf = maldistribution factor,

m = number of cells = $\frac{A}{Ai}$,

i = cell index,

u_i = liquid flow rate based on section area in cell i and,

$\bar{u}$ = average liquid flow rate based on section area

Obviously, when the liquid has a uniform distribution over the column cross-section, *Mf* equals zero. A higher value of *Mf* means higher degree of liquid maldistribution.

The liquid flow distributions shown in Figures 4.6 to 4.22 were further assessed by the maldistribution factor (*Mf*) and the results were plotted in Figure 4.23 as a function of packed bed height. The calculation of the maldistribution factors were based on 24 sampling cells over the column cross section, the same as the liquid collector used in the hydraulic experiments.

From the nature of the plot, it can be told that, the initial flow distributions for all gas and liquid loads were good (all *Mf's* are lower than 0.35 for bed height 0.264 m). It can also be seen that, for the liquid load, L = 0.002 m^3/m^2s and the gas load, G = 2.2 m^3/m^2s and also for the liquid load, L = 0.001 m^3/m^2s and gas load, G = 2.2 m^3/m^2s, after two layers of the packing (packed bed height = 0.528 m) *Mf* reached the minimum values of 0.26 and 0.14 respectively, which demonstrated the good liquid spreading ability of the packing from a good initial distribution. But for the liquid load, L = 0.002 m^3/m^2s and the gas load, G = 1.1 m^3/m^2s and also for the liquid load, L = 0.001 m^3/m^2s and gas load, G = 1.1 m^3/m^2s, *Mf* increased to 0.37 and 0.19 respectively that means liquid spreading ability of the packings was decreased. In all four cases, below the second element, *Mf* increased due to the development of liquid wall flow. The measured liquid flow distributions can provide a useful guide for modifying any packing geometry.

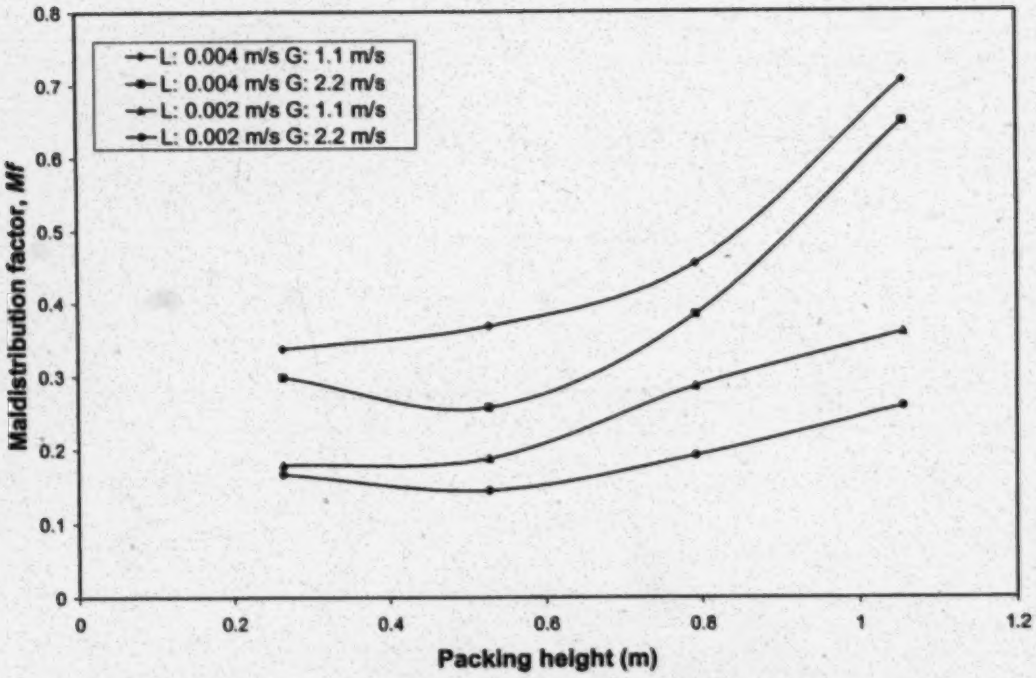

Figure 4.23 Plot of maldistribution factor vs. packing height

4.5 Experimental Measurements of Liquid Dispersion

4.5.1 Introduction

Dispersion in a packed column is usually studied through tracer experiments. Most of the previous studies on dispersion were carried out in small diameter columns packed with spherical particles or first generation random packings such as Raschig rings and Berl saddles. There is a lack of experimental data on dispersion in large scale columns filled with commercially important structured and random packings, such as flexipac, melapac, pall rings and mini rings, etc., especially when the columns are operated with both gas and liquid two-phase flow. Furthermore, more attention has been given to the axial, but not radial dispersion in the literature. Only the work by Yin et al. (2002) has investigated the radial dispersion of liquid phase in a large scale packed column filled with 25.4 mm metal pall rings.

4.5.2 Experimental Procedure and Range of Operating Parameters

Four experiments were conducted with the dry packing elements (two or four) being loaded into the column to a desired height to study the liquid radial dispersion using the steady state tracer technique. Just like the liquid distribution experiments, water the flow rate of which was set to a predetermined value, was first introduced into the column through the liquid distributor. The air blower was then started and adjusted to the desired value to provide air into the column as counter-current flow. A check was made regularly on the gas and liquid flow rates to ensure that the conditions did not vary during the operation. About 20 minutes were needed for the liquid to reach a steady state in the column.

The non-reactive aqueous solution of 0.45 N potassium chloride (KCl) was used as tracer in these experiments. It was pumped from the tracer storage tank by a centrifugal pump

and then injected/introduced into the column as a steady/continuous point source on the top of the packing along the column axis. It disperses radially as it flows downwards through the column due to the presence of the packing materials, molecular and turbulent mixing. The flow rate of the tracer was controlled by a needle valve.

Two liquid flow rates were used in this study those are, 1.996 kg/m^2s and 3.992 kg/m^2s. The gas flow rates were 1.1302 kg/m^2s and 2.6059 kg/m^2s. The concentration of KCl (tracer) solution was 0.45 N and flow rates were 5% and 10% of liquid flow rate. Packed bed heights used in the experiments were 0.528 and 1.056 m. The position of the liquid distributor and tracer inlet pipe were adjusted accordingly with the variation of the packed bed height.

To measure the liquid radial dispersion, the liquid samples were collected at each of collector cells at the bottom of the column. And the outlet tracer concentrations at each of the cells were measured by measuring the conductivity of the samples collected from each cells. After the tracer concentration on each collecting region was measured, the bar graphs were constructed in terms of relative tracer concentration on each of the measuring cells against the coordinates of the cells.

4.5.3 Results and Discussion

The results are shown as bar plots of variation of the tracer relative concentration with the coordinates of the cells in Figure 4.24 to Figure 4.27. From the Figures 4.24 and 4.25, it can be seen that, for the gas and liquid loads, 0.004 m^3/m^2s and 1.1 m^3/m^2s respectively, with the increase in bed height (from 0.528 m to 1.056 m), as tracer flowed downward it dispersed in all radial direction so relative radial concentration gradient decreased due to dispersion of tracer. So the outlet relative concentration of tracer will be almost equal in each cell.

In Figures 4.26 and 4.27, liquid dispersion was shown for four elements of packings i.e. bed height 1.056 m, with liquid load 0.002 m^3/m^2s, and for two different gas loads, such as, 1.1 m^3/m^2s and 2.2 m^3/m^2s respectively. As the tracer flowed downward through unperforated packing elements due to the continual changes in direction/orientation it dispersed in all radial direction. But due to increase in gas flow rate, liquid wall flow developed and so circumferential concentrations showed higher value.

It can be concluded that, although the tracer was introduced into the column as a continuous point source, due to the corrugations of the packings, liquid flowing downward through a packing element spreaded/dispersed in all radial directions. Since, in the structured packings, each element of the packings is rotated at 90° angle with respect to the element above or below, the dispersion was not uniform/homogeneous due to the complex geometry of the packings and continuous changes in flow direction.

4.6 Conclusion

The results of hydrodynamics experiments showed that, these can help us to get a complete visualization of complex flow phenomena inside the structured packed distillation column.

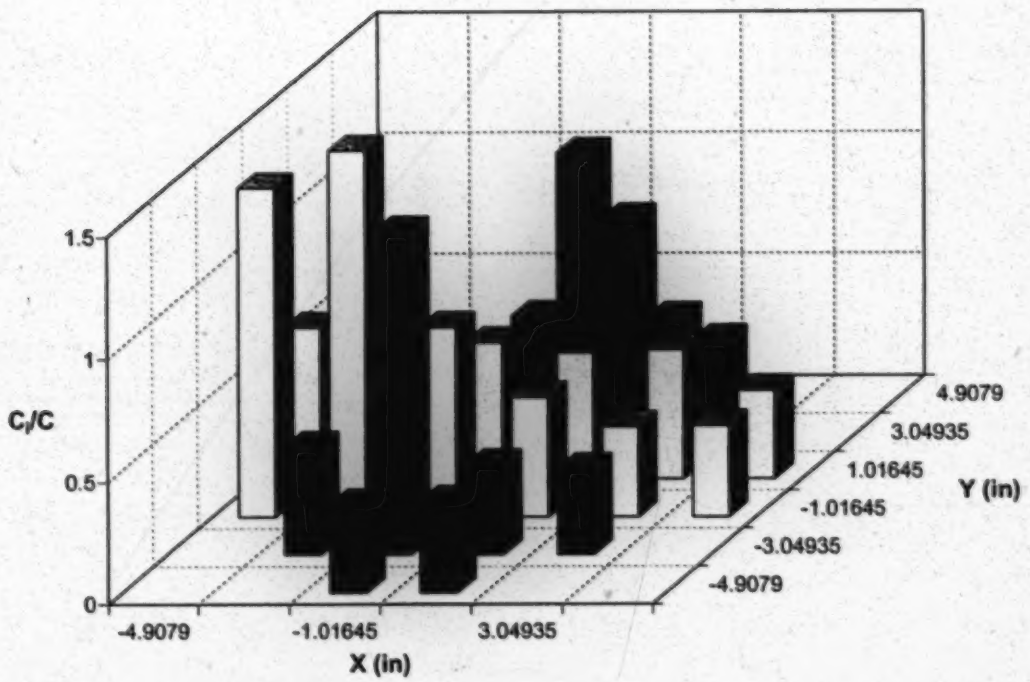

Figure 4.24 Liquid dispersion for L: 0.004 m^3/m^2s, G: 1.1 m^3/m^2s and bed height: 0.528 m

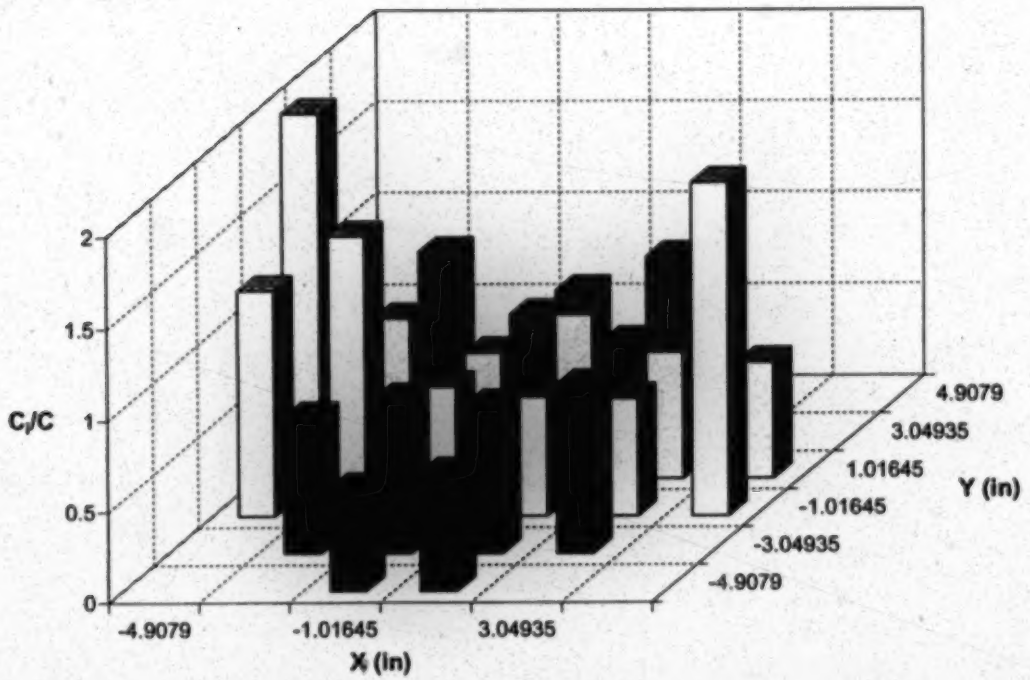

Figure 4.25 Liquid dispersion for L: 0.004 m^3/m^2s, G: 1.1 m^3/m^2s and bed height: 1.056 m

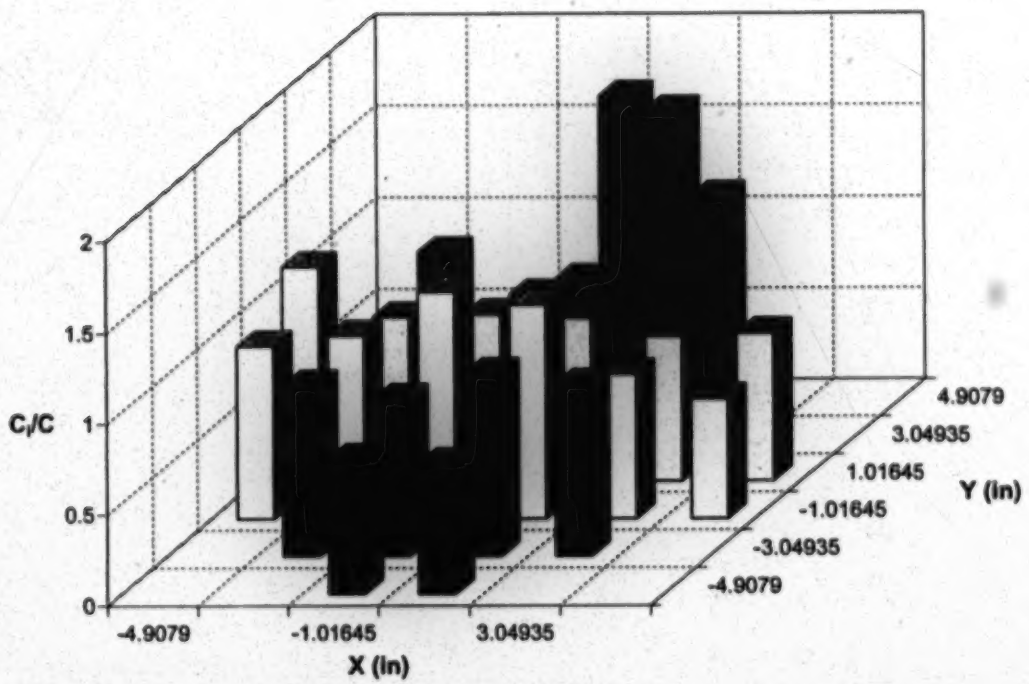

Figure 4.26 Liquid dispersion for L: 0.002 m^3/m^2s, G: 2.2 m^3/m^2s and bed height: 1.056 m

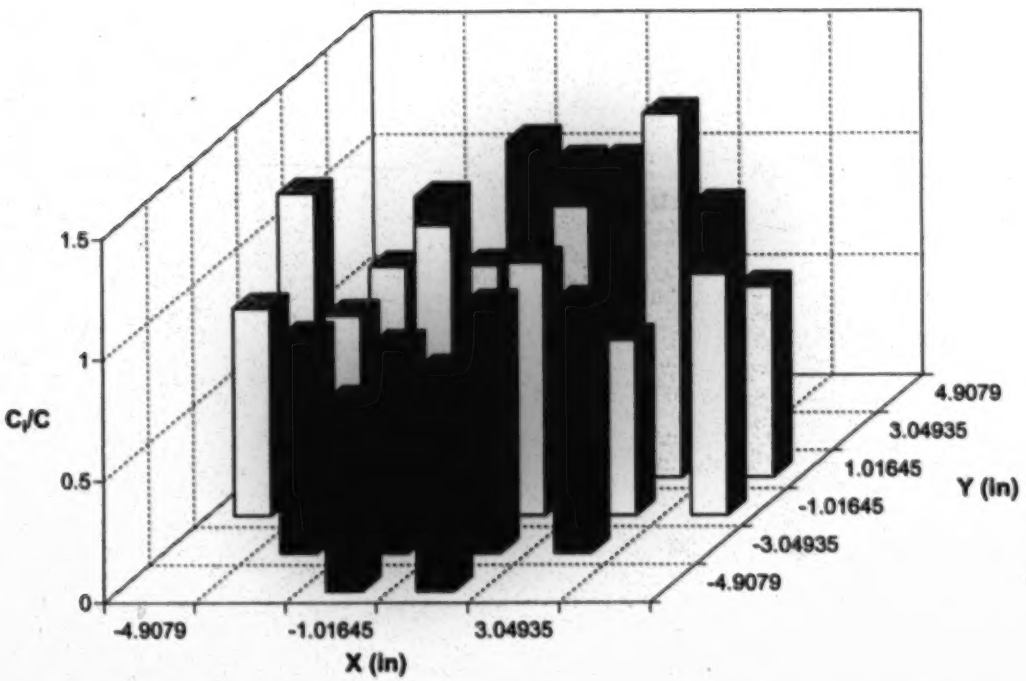

Figure 4.27 Liquid dispersion for L: 0.002 m^3/m^2s, G: 1.1 m^3/m^2s and bed height: 1.056 m

Chapter 5 CFD Simulations of Pressure Drop and Tracer Dispersion

5.1 Introduction

In this chapter, the essential features of CFD simulations of single and two-phase pressure drop model for both Zogg's (Zogg, 1972) and UofA's models are given. The features for single-phase tracer dispersion in UofA's model are also given. The models presented have a sound physical basis.

5.2 Description of flow geometry and operating conditions

5.2.1 Pressure Drop in Zogg's and UofA's Models

The geometry and operating conditions of UofA's model were based on the experimental work that was carried out at University of Alberta's distillation laboratory in a 0.3 m diameter column packed with Flexipac 3Y type structured packings. Air and water were used as the medium fluids. Similarly, for the Zogg's model (Zogg, 1972), experimental setup with Sulzer wire-mesh BX type structured packings, described in his dissertation was used. The model consists of two sheets of sulzer mesh pack. The fluid (gas) flows only through the inner channel. The outer channels were kept blocked. Schematic diagrams of the flow geometries with the boundaries used in the simulations are shown in Figure 5.1 and Figure 5.2. The geometrical characteristics of both types of packings are given in Table 5.2.

5.2.2 Tracer Dispersion in UofA's Model

The geometry and operating conditions of this model are same as that of UofA's pressure drop model. The geometry was modified a little bit to make a new inlet boundary for tracer entrance. Schematic diagram of the flow geometry with the boundaries used in the simulations is shown in Figure 5.3. Air was used as medium fluid whereas carbon-dioxide (CO_2) was used as tracer.

5.3 Assumptions Made During Simulations

1. Fluid Properties - The physical properties of air, water and carbon-dioxide (CO_2) are assumed to be constant. The assumption is valid, since there are no significant variations of physical properties due to any physical processes. Thus the fluids, such as, air, water and carbon dioxide (CO_2) are assumed to be incompressible fluids. The physical properties of air, water and carbon-dioxide used in the simulations are given in Table 5.1.

2. Energy Transfer – Isothermal flow is assumed. Since fluid flow is incompressible, the hydrodynamics can be studied without solving the energy equation.

3. In tracer dispersion simulations, instead of full multi-component diffusion dilute approximation was considered. So, a constant value of mass diffusivity (1.77×10^{-5} m^2/s) for CO_2 was used (Sherwood et al., 1975).

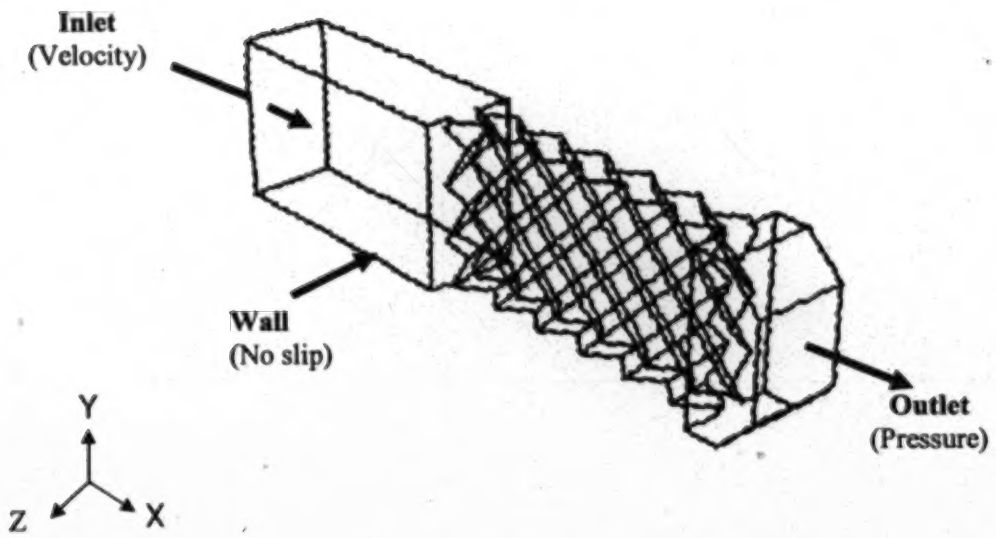

Figure 5.1 Schematic diagram of Zogg's model

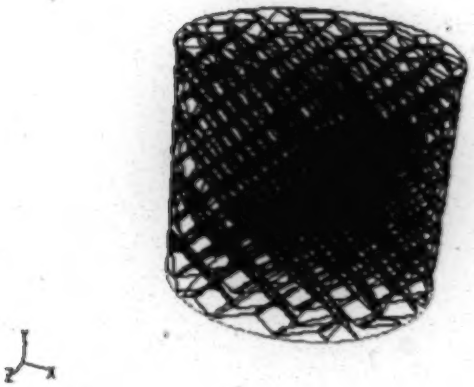

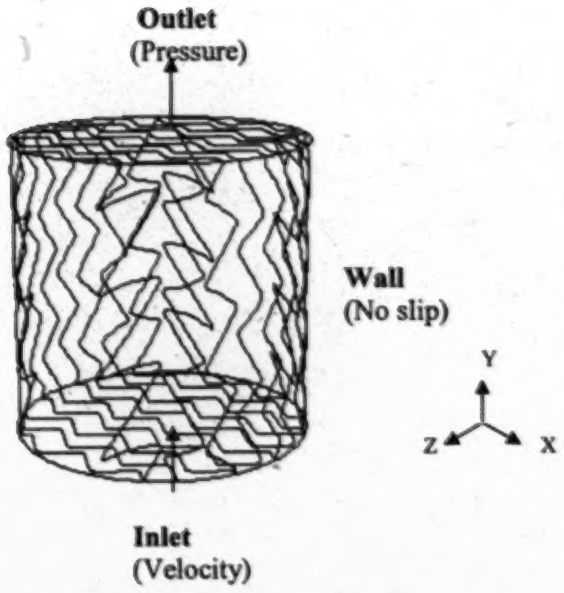

Figure 5.2 Schematic diagram of UofA's model

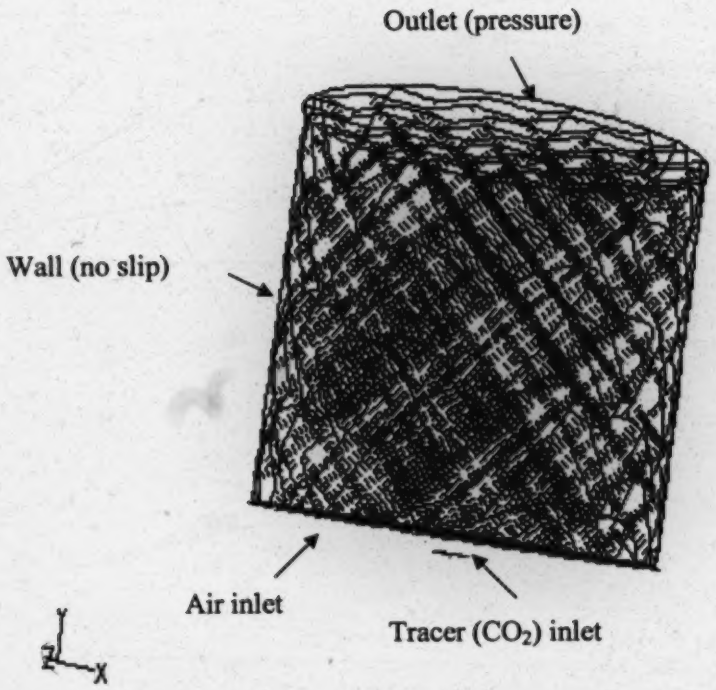

Figure 5.3 Schematic diagram of UofA's model for tracer dispersion

Table 5.1 Physical properties of air, water and carbon-dioxide (CO_2)

Physical properties	Air	Water	Carbon-dioxide
Density (kg/m^3)	1.1845	998.2	1.7774
Viscosity (kg/m-s)	1.8444×10^{-05}	1.003×10^{-3}	1.4831×10^{-5}
Mass diffusivity (m^2/s)			1.77×10^{-5}

Table 5.2 Geometrical characteristics of the packings used in the simulation

	Sulzer wire-mesh pack- BX	Flexipac-3Y
Crimp angle (deg)	78	
Crimp height, h (m)		0.0266
Base length, b (m)	0.0102	0.0504
Side length, S (m)		0.0366
Corrugation angle (deg)	45	45
Porosity, ε_p (%)	99.9	97.7
Specific surface area, a_p (m^2/m^3)	500	110
Equivalent diameter, d_h (m)	0.00793	0.03663
Element height (m)		0.264

5.4 Model Equations Solved by CFD Software's

The model equations solved by computational fluid dynamics or CFD software's such as, Fluent and CFX are discussed in Chapter 3. Modern packings, such as, random and structured, have some common features, as for example, complex geometric structure, large specific area and high void fraction (generally larger than 0.9). These characteristics not only ensure a large gas-liquid contact area but also intensify the two phase mixing due to the continually change of flow direction and interruption of the fluids over the packing surface. For flow through a packed column, the Reynolds number can be calculated as (Billet, 1995),

$$\mathrm{Re}_L = \frac{L}{a_p \mu_L} \tag{5.1}$$

$$\mathrm{Re}_G = \frac{G}{a_p \mu_G} \tag{5.2}$$

where,

L = liquid superficial flow rate per unit cross sectional area, [kg/m^{2}s]

G = gas superficial flow rate per unit cross sectional area, [kg/m^{2}s]

a_p = total surface area of packing per unit volume, [m^2/m^3]

Re_G = Reynolds number for the gas phase, and

Re_L = Reynolds number for the liquid phase

Based on numerous experimental measurements on 50 different types of packings, Billet (1995) found that the critical Reynolds number for the transition of flow region from laminar to turbulent is about 10. Since the high capacity operation is the main objective in the design and operation of packed columns, the condition of $\mathrm{Re}_{cr}<10$ is rarely encountered in practice. And, so, in this study, the Reynolds number for most of cases was normally much greater than 10, i.e. the flows were in the turbulent region.

The models considered the flow of both gas and liquid as turbulent. And standard k-ε turbulence (dispersed multi-phase model for two-phase) model was used. Air (gas) was considered as the continuous phase whereas, water (liquid) was taken as dispersed phase. Since, the flow is isothermal and our focus was mainly on the hydrodynamic behavior and mass dispersion in structured packings, energy equation was not solved. Thus the single and two-phase continuity, momentum and species equations were numerically solved.

5.5 Boundary Conditions used in the Simulations

The definition of the boundaries is necessary to isolate the flow computational domain from its surroundings. The boundary conditions are information specified on any boundary, such as, flow boundary, wall boundary and symmetry boundary etc. The flow boundary is such a boundary that is used to define the conditions at the entrance and/or exit of the flow domain. At the entrance of the flow domain, the flow boundary is known as the inlet boundary, and at the exit, it is known as the outlet boundary. For countercurrent multi-phase (liquid and gas) flow, it is possible to have flows that enter and leave the same flow boundary simultaneously. Therefore special treatment is required at these boundaries.

For both models, the inlet boundary was specified at the bottom of the column. Mathematically, it is referred to as 'Dirichlet boundary'. So, all the variables such as, pressure, velocity, volume fraction, mass fraction and turbulent quantities etc. was specified at this boundary. However, for incompressible flow, the specified inlet pressure value was not used; instead its value was extrapolated from downstream. In case of turbulent flow, the values of turbulent quantities at the inlet boundary were specified. For the two-equation k-ε model, the inlet values for k and ε were calculated as follows,

$$k_{inl} = c_{pl} u_{inl}^2 \qquad (5.3)$$

$$\varepsilon_{inl} = \frac{k_{inl}^{1.5}}{c_{p2} D_H} \tag{5.4}$$

The hydraulic diameter, D_H is defined as,

$$D_H = \frac{4A_f}{P} \tag{5.5}$$

and, for the flow through any porous media, it is related to the void fraction, ε_p and the wetted surface area per unit volume of the bed, a_p as (Bird et al., 1960)

$$D_H = \frac{4\varepsilon_p}{a_p} \tag{5.6}$$

where,

c_{p1} and c_{p2} are empirical constants and is set to $c_{p1} = 0.002$ and $c_{p2} = 0.3$

u_{inl} = mean inlet velocity, [m/s]

A_f = cross sectional area available for flow, [m^2] and

P = wetted perimeter of the flow domain, [m]

To predict the multi-phase flow fields, such as gas and liquid flow within the flow domain, three different boundary conditions were specified at the bottom, top and wall of the packed bed. For counter-current multi-phase flow, both inlet and outlet flows were defined at the same inlet boundary. If a positive velocity value was specified for the inlet flow, then for the outlet flow, a negative value was assigned. In this way, the outflow was defined to have a direction pointing away from the computational domain.

For a typical simulation with the liquid volumetric flow rate, L and gas volumetric flow rate, G, the boundary conditions were specified as follows:

(1) At the bottom of the column, the inlet boundary was specified. At this boundary the appropriate values for velocity components, volume fractions, turbulence quantities, etc. were specified for both the gas and liquid phase. For the gas phase, flow entered the flow domain, and the velocity components were specified as follows:

$$U_G = \frac{G}{\rho_G \gamma_G \varepsilon_P}; V_G = 0; W_G = 0; \tag{5.7}$$

And for the liquid phase, flow left the flow domain, so, the x-component of velocity was assigned a negative value, that is,

$$U_L = -\frac{L}{\rho_L \gamma_L \varepsilon_P}; V_L = 0; W_L = 0; \tag{5.8}$$

The inlet volume fraction of secondary phase (liquid in this case) was difficult to specify since there was no measured value available. However, it can be estimated from the liquid holdup based on the liquid flowrate as follows (Kister, 1992),

$$h_L = \frac{0.4184}{\varepsilon_p}\left(\frac{\mu_L}{\rho_L}\right)^{\frac{1}{3}}(u_L a_p)^{0.5} \tag{5.9}$$

$$\gamma_L = \frac{h_L}{\varepsilon_p} \tag{5.10}$$

The volume fraction of gas phase can then be determined as

$$\gamma_G = 1 - \gamma_L \tag{5.11}$$

where,

h_L = liquid holdup

u_L = liquid superficial velocity, [m/s]

a_p = specific surface area of packing, [m^2/m^3]

γ_L = liquid volume fraction

γ_G = gas volume fraction

The values of turbulent kinetic energy, k and turbulent dissipation rate, ε for both the phases were calculated using equations (5.3) and (5.4).

(2) At the top of the column, the pressure outlet boundary was specified. So, the pressure values for both of the phases were specified at this boundary. Operating pressure was set to 101325 Pa and gauge pressure was 0.

(3) At the column wall, the 'no-slip' boundary conditions were specified to the velocities of both the gas and liquid phase. For other variables, such as volume fractions and mass fractions, no flux conditions were specified. Turbulent kinetic energy and turbulent dissipation rate were calculated using the logarithmic wall functions.

5.6 Initial Values, Discretization Schemes and Flow Field Initialization

It is important to have good initial guesses for the flow variables – not only to avoid numerical divergence but also to reduce computational time significantly. For all equations, first order upwinding scheme were used for discretization, but for the pressure equation standard scheme was used and pressure velocity coupling was obtained by applying simple algorithm.

5.7 Simulation of Single-Phase Pressure Drop in Zogg's and UofA's Models

Simulations of dry pressure drop were carried out for both models. For both models, all simulations were carried out using commercial CFD package, Fluent-6.1.22 and for

geometry creation and mesh preparation Gambit 2.1.6 was used. In both cases, default segregated solver was used and for turbulence, standard k-ε turbulence model was used.

For the Zogg's model, geometry was meshed with a mesh size of 0.001 m which gave a total mesh volume of 2,656,010. For the UofA's model, due to limitations of computer memory, full length of packed column was not simulated; instead only one element of packing consisted of ten sheets of packing was used in the simulations. Packing element was meshed with 0.0045 m which gave a total mesh volume of 1,184,037. In both cases, tetrahedral type unstructured mesh was used.

5.8 Simulation of Two-Phase Pressure Drop in Zogg's Model

For the two-phase that means irrigated pressure drop simulations, geometry of Zogg's model was used. The commercial CFD software package, CFX-5.7.1 was used and only the packing section was considered. Due to the limitations of computer memory, packing element was meshed with 0.001 m tetrahedral mesh, which gave a total mesh volume of 860,000. Steady flow was considered and Eulerian multiphase model was chosen. For turbulence, standard two equation k-ε dispersed multi-phase turbulence model was considered. Water-air was taken as medium, where water flowed downward as a thin film over the packing surface due to gravity and gas was trickled through the packing to upward due to the pressure difference. So, water behaved as dispersed phase (secondary) and gas as continuous (primary) phase and counter-current operation was observed. The value of average liquid holdup for any packed column found in literature is usually 4-6%. According to this, volume fraction of water was taken as 0.04, and so for air it was 0.96. The water bubble diameter was taken as 0.0013 m. In the simulations gas flow rates were varied from 3.96 m/s to 9.95 m/s and liquid flow rate was taken as 0.002 m/s.

For the fluid-fluid interaction term, i.e., the inter-phase momentum transfer term or the inter-phase drag force per unit volume, Schiller-Naumann model was used. For the multi-phase flow, Sun et al. (2000) used the volume averaged continuity and Navier-Stokes

equation to describe the gas and liquid two phase flow through any packed bed or porous media. In the Navier Stokes equation, they considered both the gravity and the flow resistance offered by the packing elements as the body force, i.e., they did the volume-averaging over all 3-phases (gas, liquid and solid). But in our case, we considered the multi-phase flow through exact geometry and so the volume-averaging was done only over two-phases (only gas and liquid) and so only fluid-fluid interaction terms were considered.

5.9 Simulation of Single-Phase Tracer Dispersion in UofA's Model

The CFD simulations for single-phase tracer dispersion were carried out with one element of circular Flexipac-3Y type packings with ten sheets. Due to the limitations of computer memory, packing element was meshed with a mesh size of 0.003 m which gave a total mesh volume 1,837,163.

At first, hydrodynamics (flow and turbulence equations) for single-phase flow (air) were solved by using Fluent 6.1.22. Since, hydraulics is not coupled with mass transfer; flow problem was first solved by solving momentum and turbulence equations. The result of the flow field, i.e., velocity from that problem was then used in the species transport equation to get the solution for species concentration. Carbon dioxide (CO_2) which was used as tracer was introduced into the column with the same velocity as air. Since air-CO_2 mixture model was not a default one for fluent, it was created by applying mixing law for all properties, such as, density and viscosity. After the set up for species transport has been done, only the equation of conservation of species (tracer) was solved.

5.10 Results and Discussions

5.10.1 Single-Phase Pressure Drop in UofA's Model

The validity of any theoretical models is evaluated through comparing the predicted and measured pressure drops values at different gas and liquid loads. The comparison of UofA's dry pressure drop experiments data with the simulations are illustrated Figure 5.4. In this figure, pressure drop per unit length of column ($\Delta P/L$) are plotted as a function of F-factor, which is defined as, $u_G\sqrt{\rho_G}$ where u_G is the superficial gas velocity over the column cross section. The nature of the plot showed that pressure drop increased linearly with the increase in gas flow-factor which can be seen in any literature.

Due to the limitations of computer memory, at first the simulations were carried out with only two sheets of packing. But the results showed that, for the same gas flow-factor, the predicted pressure drop value is higher than experimental one. We know that, pressure drop occurs mainly due to frictional losses of fluid with the packings. So, the number of sheets then increased gradually. With the increase in number of sheets i.e., packing surface area, the ratio, S_p:S_w will increase. So more friction of gas with the packings occurred and so less pressure drop. For two sheets, the ratio, S_p:S_w = 3.60215:1, where, S_p= surface area of the packings and S_w = surface area of the container and for four and circular ten sheets, this ratio, S_p:S_w is equal to 5.971:1 and 104.08:1 respectively. For the same gas flow-factor, pressure drop decreases with the increase in the ratio, S_p:Sw i.e. packing surface area or number of sheets. It can be seen in Figure 5.4 that, experimental dry pressure drop (per unit length of packing) data almost exactly matched with simulations for ten sheets circular element.

The simulations results are also shown graphically in Figure 5.5 to Figure 5.8. The contour plots of velocity magnitude at planes x = 0 m, y = 0 m and z = 0 m are shown in Figure 5.5 and Figure 5.6. It can be seen from these plots that magnitude of velocity varies from 0.0 m/s to 6.12 m/s in these planes. The effects of packing corrugation on

velocity can be seen from these figures. It was seen that, velocity is almost 0.0 at the packing surface due to no-slip condition and flow was only through the channels.

The Figure 5.7 and Figure 5.8 showed contour plots of velocity vector colored by velocity magnitude of air inside packing at planes x = 0 m and y = 0 m. The arrowhead indicates that fluid is going up and the effects of corrugation can be seen through zigzag nature of vectors.

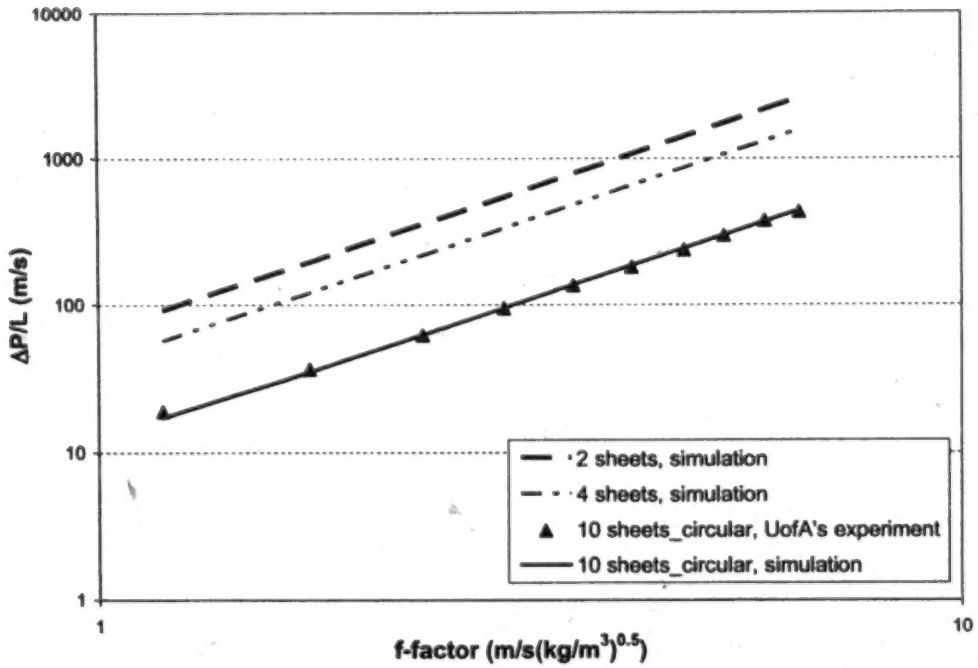

Figure 5.4 Comparison of dry pressure drop in UofA's model, experiments vs. simulations

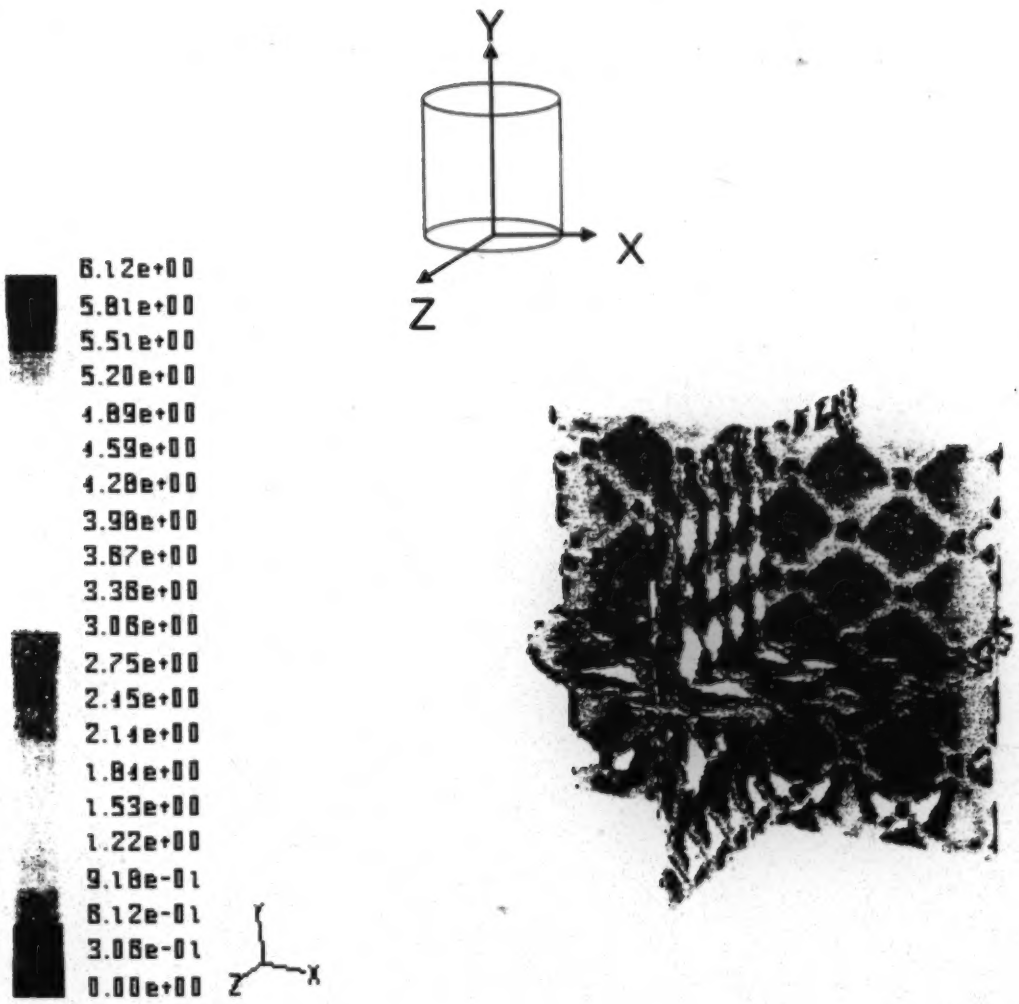

Figure 5.5 Contour plots of velocity magnitude (m/s) at X = 0.0 m, Y = 0.0 m and Z = 0.0 m planes

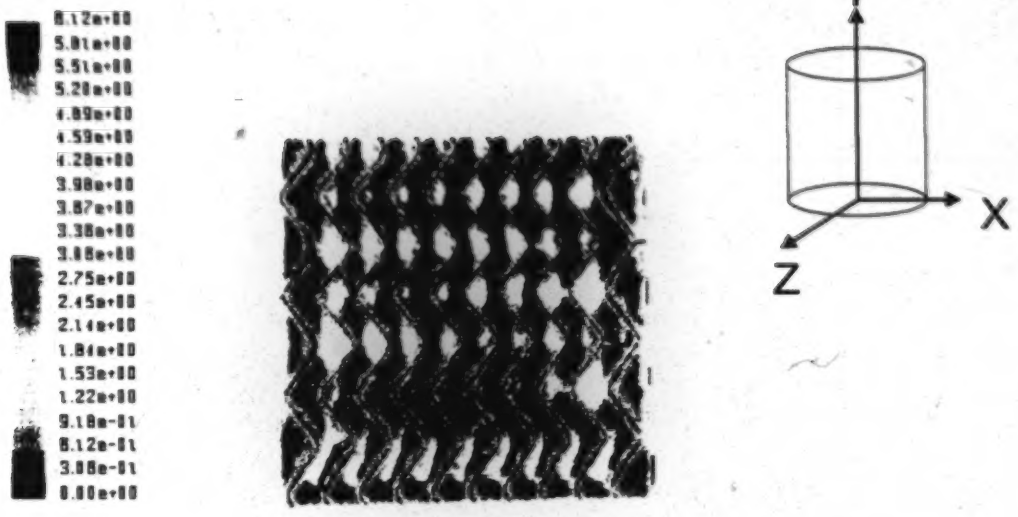

(a)

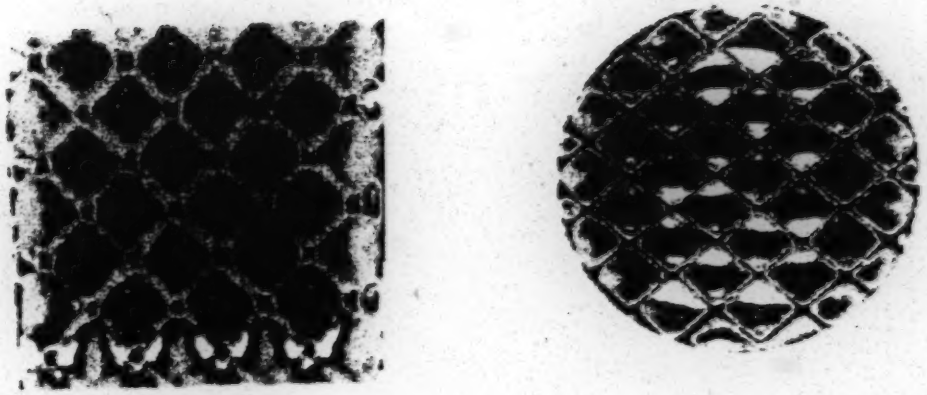

(b) (c)

Figure 5.6 Contour plots of velocity magnitude (m/s) at (a) X = 0.0 m, (b) Z = 0.0 m and (c) Y = 0.0 m planes

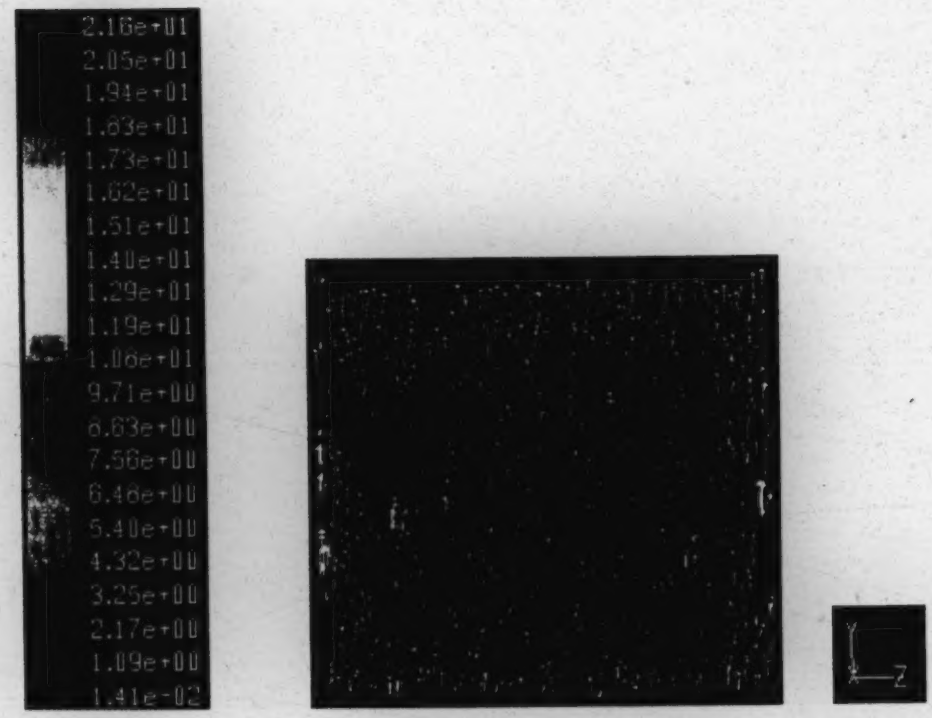

Figure 5.7 Contour plots of velocity vectors colored by velocity magnitude (m/s) at plane X = 0.0 m

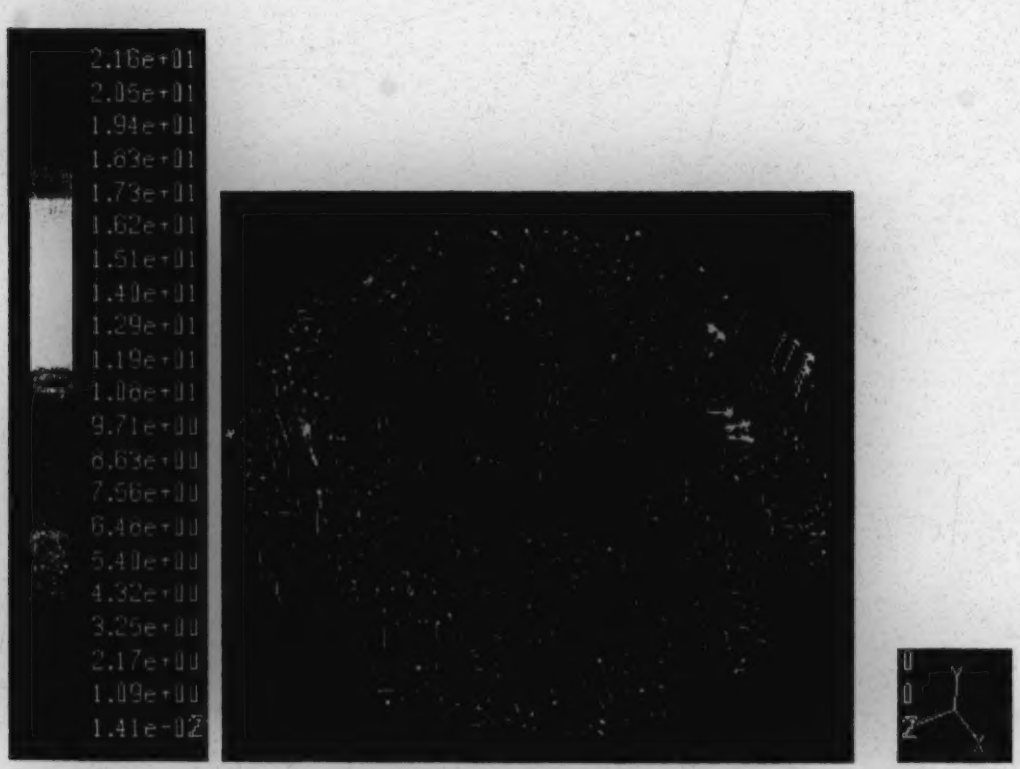

Figure 5.8 Contour plots of velocity vectors colored by velocity magnitude (m/s) at plane Y = 0.0 m

5.10.2 Single-Phase Pressure Drop in Zogg's Model

Zogg (Zogg, 1972) plotted his experimental results for single-phase pressure drop in terms of friction factor, C_{fM} vs. Reynold's number, Re_g for different corrugation angle and different width of sheets, where, friction factor and Reynold's number were defined as follows,

$$C_{fM} = \frac{\Delta P_M}{\frac{\rho_g}{2}\overline{v_g'}^2 \frac{L}{d_h'}} \tag{5.12}$$

and,

$$\mathrm{Re}_g = \frac{\overline{v_g'}\rho_g d_h'}{\eta_g} \tag{5.13}$$

where,

ΔP_M = pressure drop around packing, [Pa]

L = length of packing, [m]

v_g' = average gas velocity, [m/s]

d_h' = equivalent diameter, [m]

η_g = viscosity of gas, [kg/m-s]

To compare the simulations, the results were plotted as friction factor, C_{fM} vs. Reynold's number, Re_g for corrugation angle of 45° and for sheet width, $B = 0.13$ m so $\frac{B}{d_h'} = 16{,}325$, as shown in Figure 5.9. The nature of graph showed that, frictor factor, C_{fM} decreased with the increase in gas Reynolds number, Re_g and it showed good agreement with the experimental data.

The contour plots of velocity magnitude and velocity vectors for air for the simulation results of Zogg's model at different planes of Z = -0.003 m, Z = 0 m and Z = 0.003 m were shown in Figure 5.10 and Figure 5.11 respectively. In Figure 5.10, the magnitude of

velocity varies from 0.0 to 5.33×10^{-3} m/s in these planes. The highest velocity is observed in the middle of the channels and zero velocity was observed at the packing surfaces due to no-slip conditions. In Figure 5.11, the arrow heads of velocity vectors indicated the upward direction of gas flow. The effects of corrugation due to opposite orientation of the two sheets can be visualized from 1st and 3rd figures in Figure 5.10 and Figure 5.11 . The middle figure indicated that there were no sheets in the plane Z = 0 m and so the corrugation effects from both the sheets were active here.

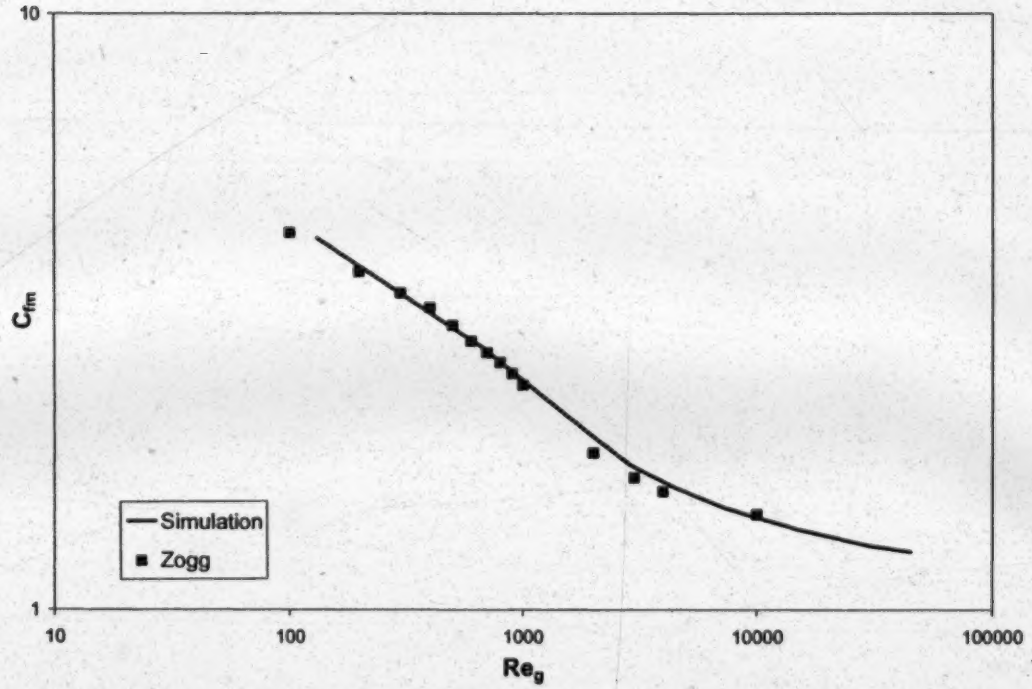

95

Figure 5.9 Comparison of CFD simulation result for single phase pressure drop with Zogg's experiment

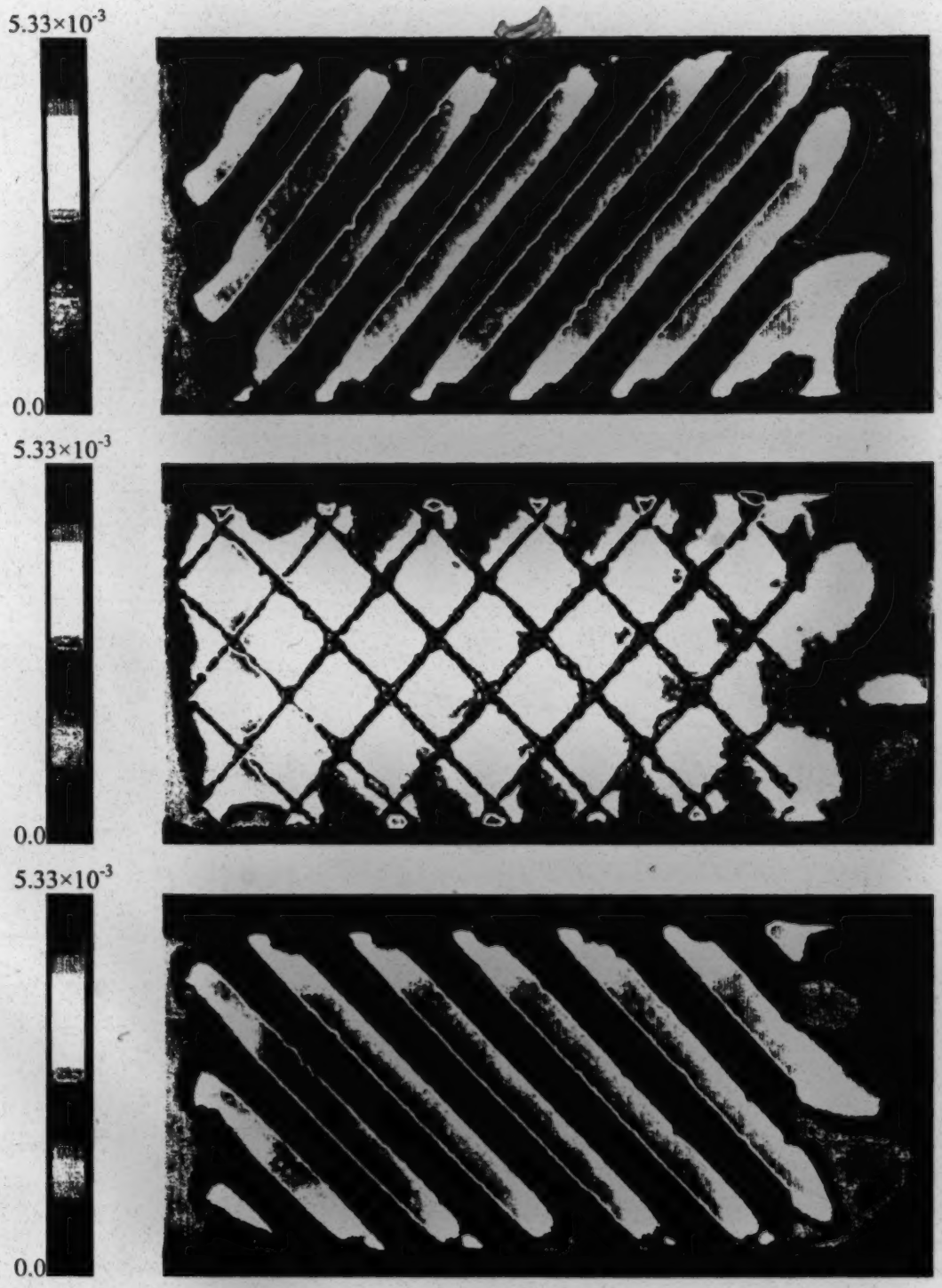

Figure 5.10 Contour plots of velocity magnitude (m/s) at Z = - 0.003, Z = 0.0 and Z = - 0.003 planes (for Zogg's model)

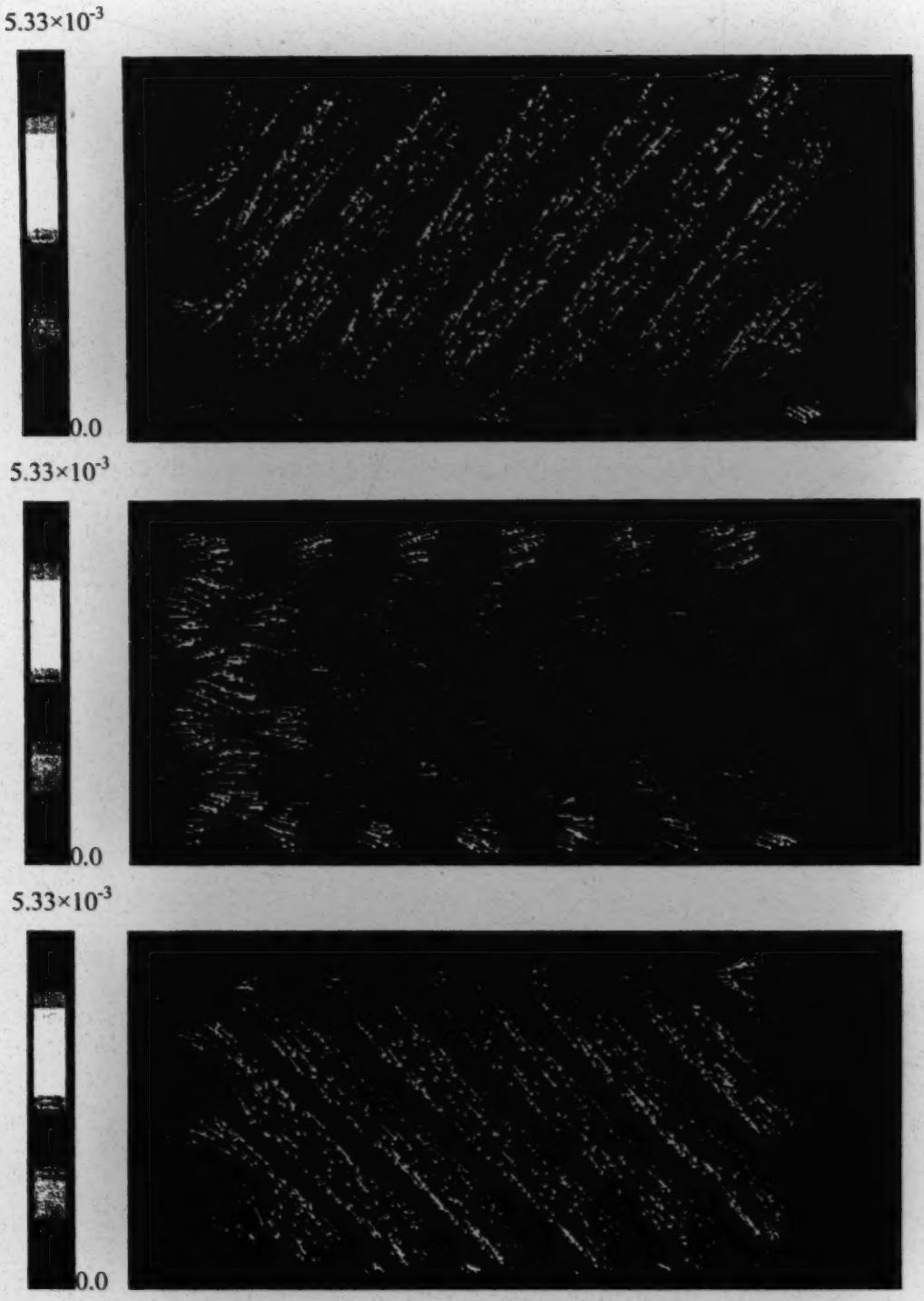

Figure 5.11 Contour plots of velocity vector colored by velocity magnitude at Z = 0.003 m, Z = 0.0 m and Z = -0.003 m planes (for Zogg's model)

5.10.3 Two-phase Pressure Drop in Zogg's Model

The simulation results for two-phase pressure drop in Zogg's model were plotted in terms of pressure drop per unit length (ΔP/L) against gas flow-factor ($v\sqrt{\rho}$) as shown in Figure 5.12. The nature of the plot showed that, ΔP/L increases almost linearly with the increase in $v\sqrt{\rho}$, so it agreed well with any literature. But, due to lack of two-phase pressure drop data from Zogg's experiments, the simulations results couldn't be compared. It was also seen that, due to the convergence problem of the simulations, the 'loading or flooding point' for any given liquid flow rate could not be detected.

The simulation results are shown graphically in Figure 5.13 and Figure 5.14 as velocity vectors of both air and water at the planes z = -0.003 m z = 0 m and z = 0.003 m. The magnitude of velocities for air and water in these planes were varied from 0 to 5.91 m/s and 0 to 1.562 m/s respectively. The direction of arrowheads of velocity vectors for both air (upward) and water (downward) indicated counter-current flow through channels of the packings.

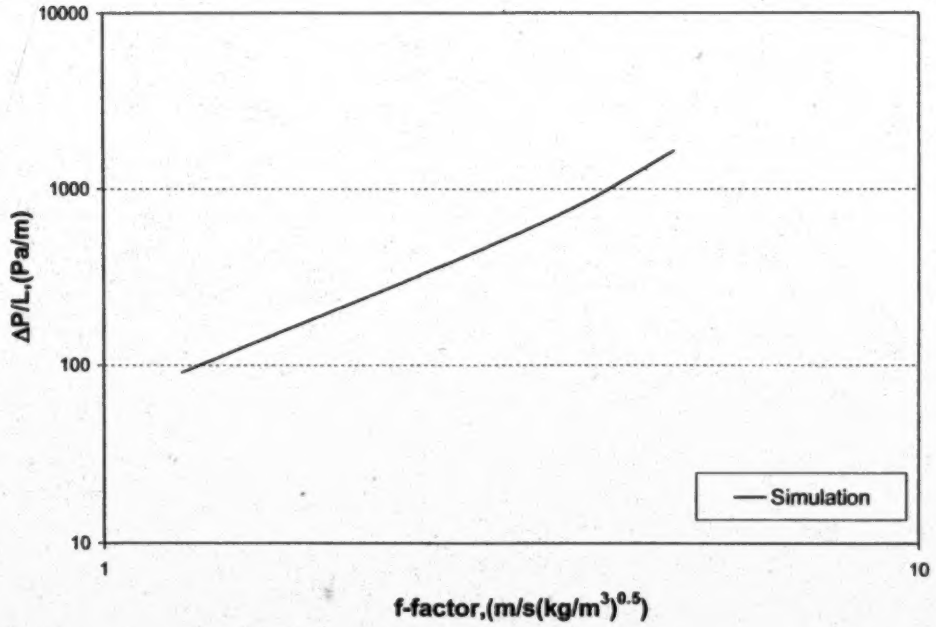

Figure 5.12 CFD simulation result for two-phase pressure drop vs. f-factor for Zogg's model for L: 0.002 m/s and G: 3.95-9.96 m/s

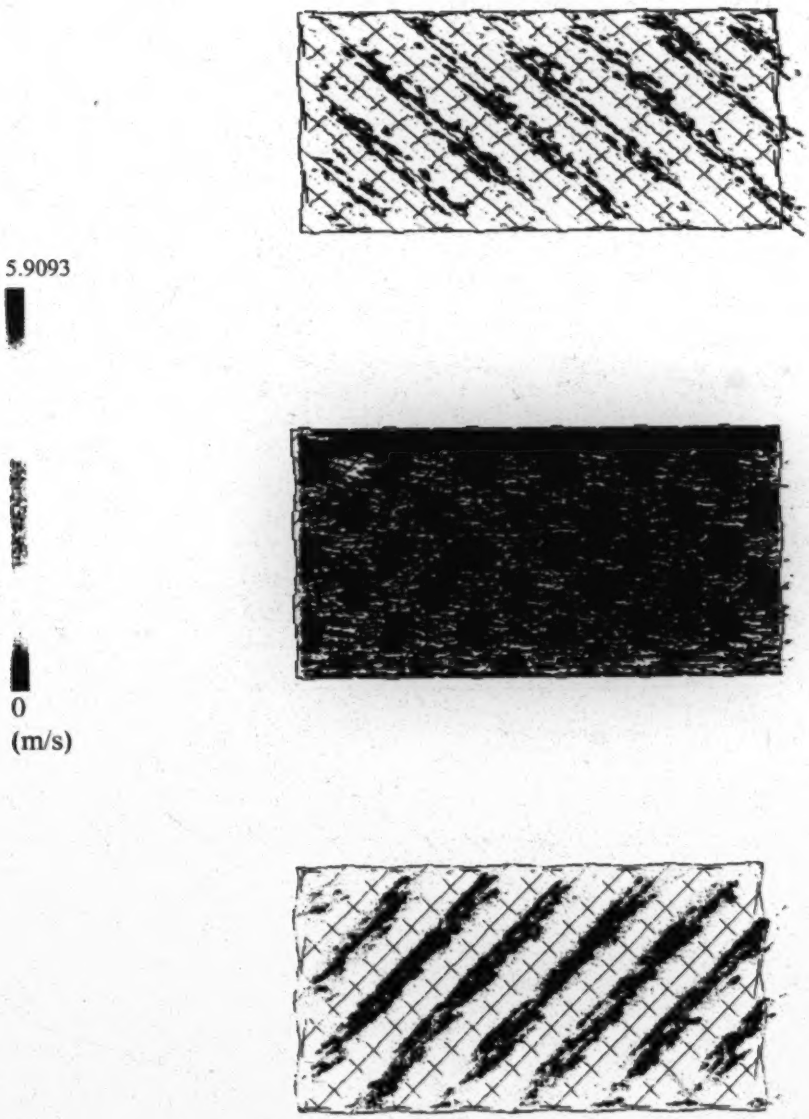

Figure 5.13 Contour plots of velocity vectors for air colored by velocity magnitude (m/s) at planes Z = - 0.003 m, Z = 0 m and Z = 0.003 m for two-phase flow in Zogg's model

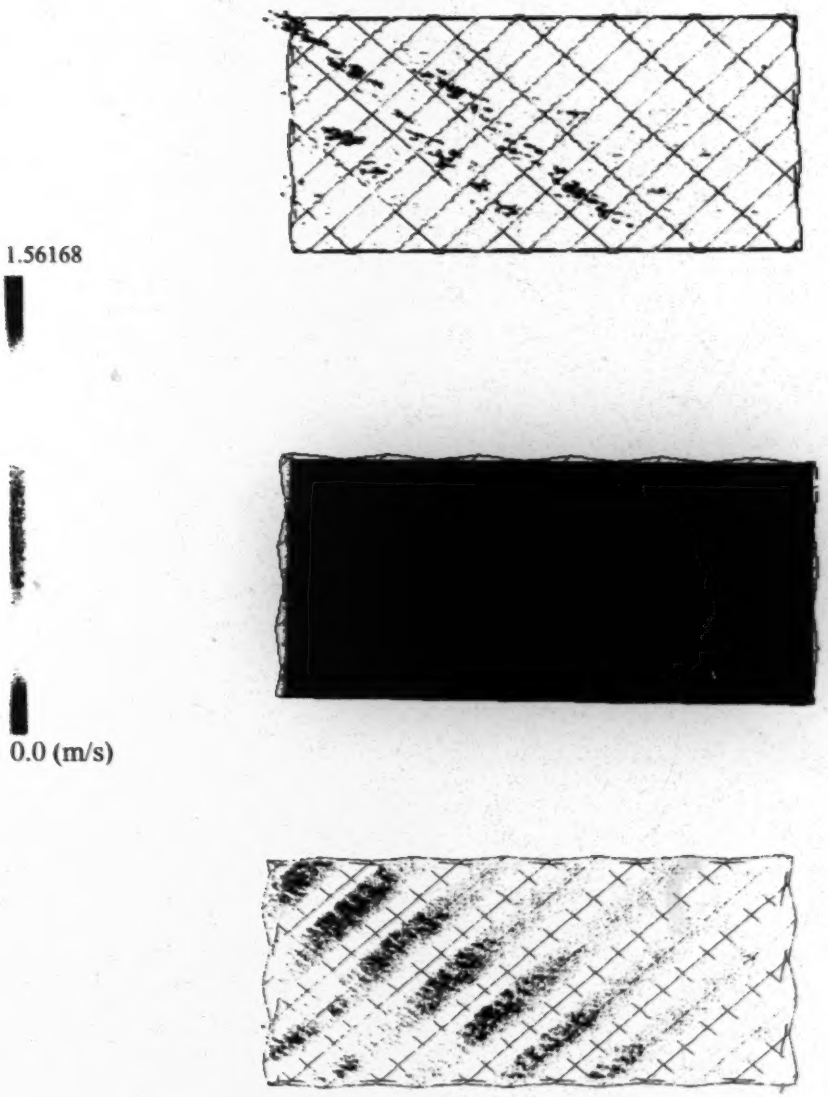

Figure 5.14 Contour plots of velocity vectors for water colored by velocity magnitude (m/s) at planes Z = - 0.003 m, Z = 0 m and Z = 0.003 m for two phase flow in Zogg's model

5.10.4 Single-phase Tracer Dispersion in UofA's Model

Upon completion of the simulations of tracer dispersion, the mass fraction of carbon dioxide (CO_2) at different cross sectional planes was observed to check the dispersion of carbon dioxide (CO_2) into air. To analyze the result, surface plots were created. Matlab was used to convert unstructured grids into structured ones. The results were shown in Figure 5.15 to Figure 5.25.

The Figure 5.15 and Figure 5.16 are showing the contour plots of mass fraction of carbon dioxide (CO_2) and air at x = 0 m plane respectively. From the nature of plot, we can see that CO_2 was introduced into the column as a point source. The location of the centre of the point source was along the column axis and it positioned in between two adjacent sheets. Since the sheets are unperforated, CO_2 was dispersed along x direction only. Figure 5.15 showed that the whole column was occupied with air and CO_2 occupied only a small place.

The development of tracer (CO_2) concentration profiles along the packed bed height in different Y-planes is shown in Figure 5.17 to Figure 5.22 as the contour plots of mass fraction of CO_2 at different cross sectional planes in Y-direction. It can be seen that the maximum tracer concentration (almost 1.0) was seen in the middle of the column at Y = -0.12 m plane and it was reduced with the increase in packed bed height (along positive y-direction) and at Y = 0 m plane it was almost 0.25. The tracer concentrations at other radial positions (along X axis) away from the column axis showed an increase, indicating that tracer was dispersed away along X axis from the high concentration region (column center) to the low concentration region (column wall). At the bottom of the column, the radial dispersion is relatively fast due to the higher tracer concentration gradient. As the tracer (CO_2) was transported upwards (positive Y direction), more and more tracer was dispersed towards the column wall, thus smoothing the radial tracer concentration gradient and reducing the rate of radial tracer dispersion.

The 3-D surface plots shown in Figure 5.23 and Figure 5.24 also showed the dispersion of CO_2 in X-direction. Dispersion in random packings is homogeneous due to isotropic behavior of the packings. But like random packings, dispersion in structured packing is not homogeneous. It may be due to the anisotropic behavior of structured packings. Due to this anisotropic behavior, unlike Yin et al (2002), we had to carry out 3-D simulations to observe the non-homogeneous dispersion of tracer.

In Figure 5.25, dispersion of CO_2 at different y-planes was visualized from z-direction and mass fraction of CO_2 at different y-planes was plotted against radial position. It can be seen that, as CO_2 flows upward in y-direction, it dispersed more into air and so with the increase in distance in y-direction the value of mass fraction of CO_2 decreased in that cross-sectional plane. And, in some planes more than one peak was seen which may be arised due to corrugation of the packings which are in alternate/opposite directions/orientations, so flow changed their directions at channel crossings. There was a small gap of 1 mm in between the packings and the column wall and so, near the column wall, where there were channel openings present, flow changed their directions.

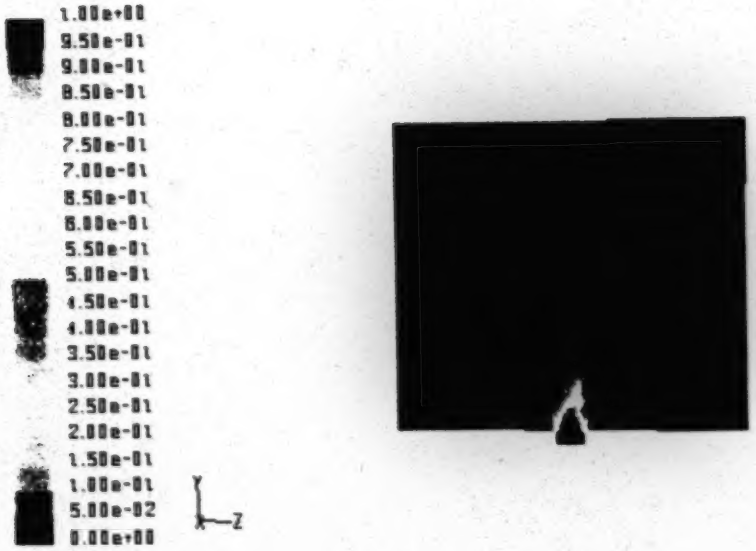

Figure 5.15 Contour plot of mass fraction of CO_2 at X = 0.0 m plane

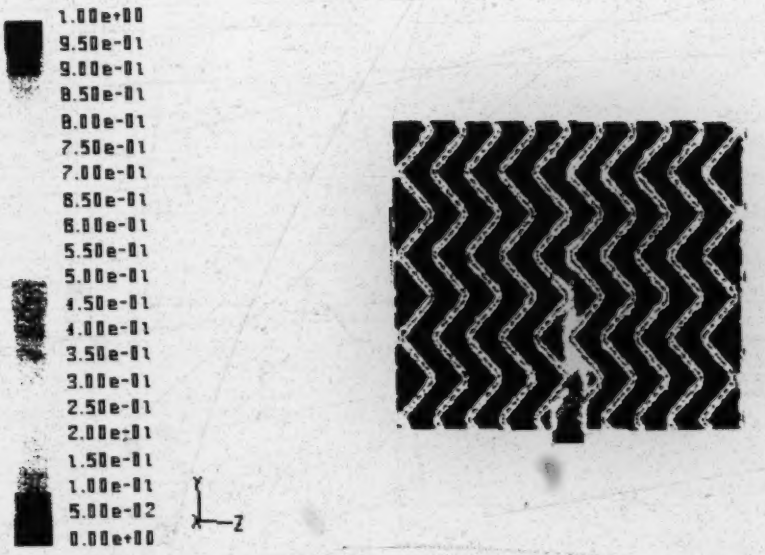

Figure 5.16 Contour plot of mass fraction of air at X =0.0 m plane

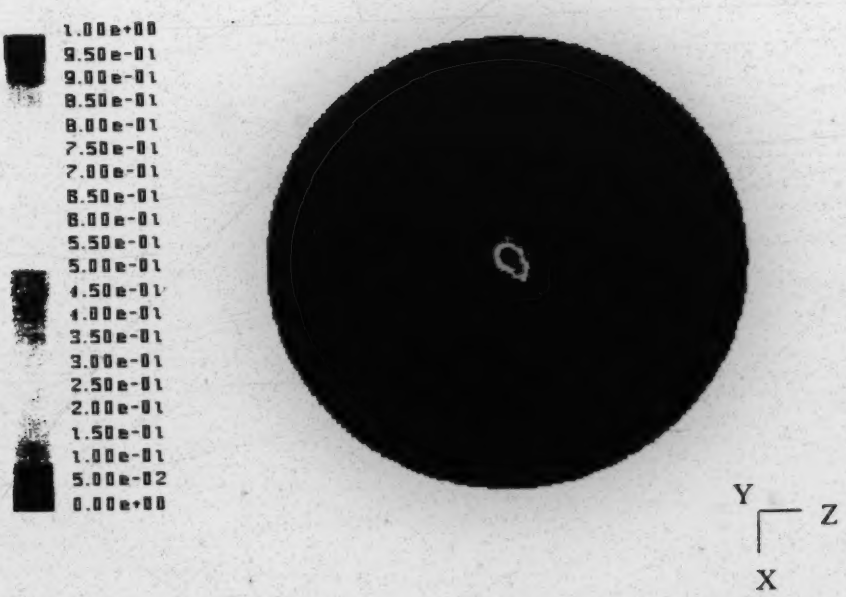

Figure 5.17 Contour plot of mass fraction of CO_2 at Y = - 0.12 m plane

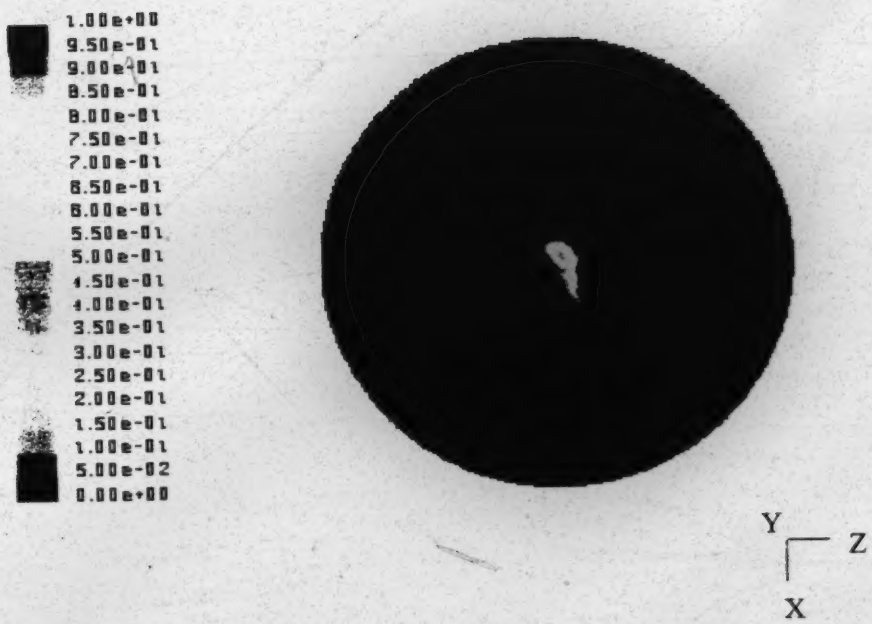

Figure 5.18 Contour plot of mass fraction of CO_2 at Y = - 0.11 m plane

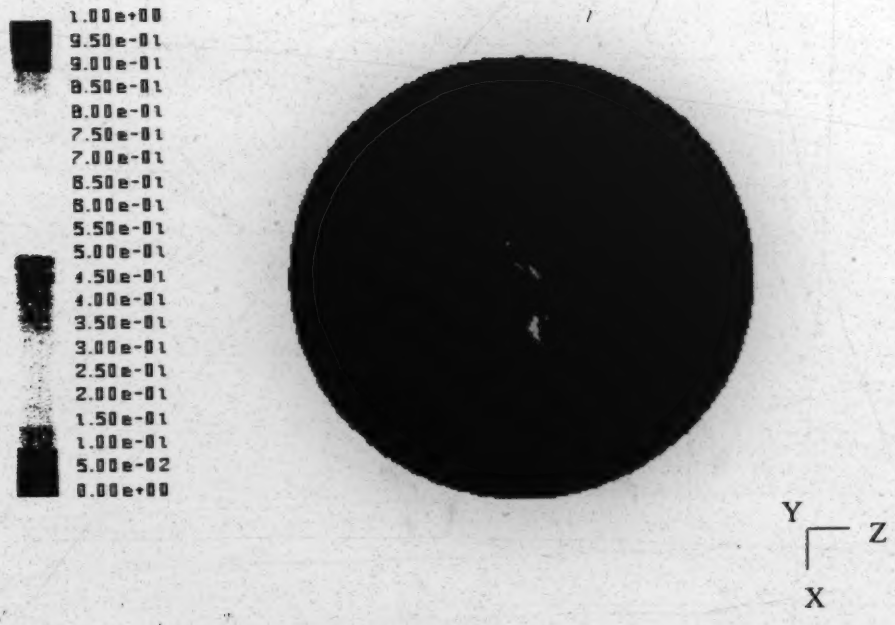

Figure 5.19 Contour plot of mass fraction of CO_2 at Y = - 0.08 m plane

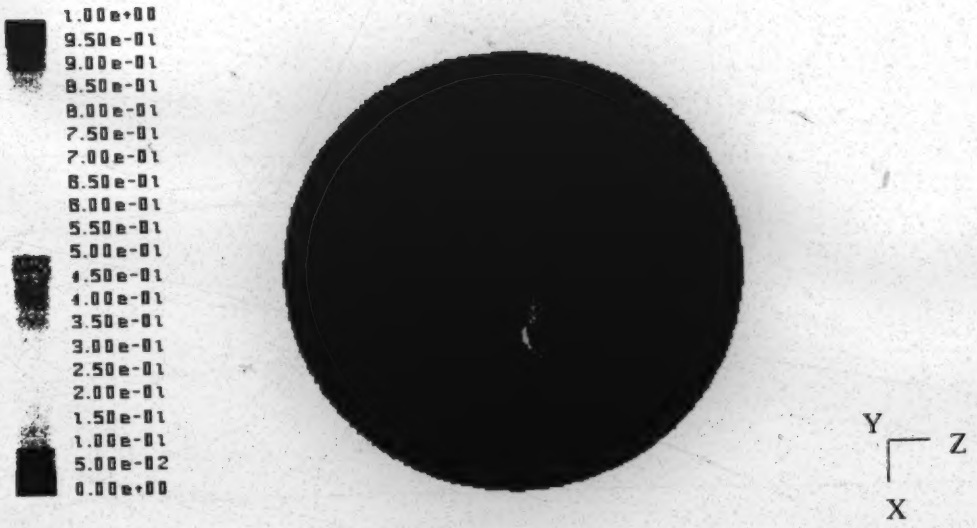

Figure 5.20 Contour plot of mass fraction of CO_2 at Y = - 0.06 m plane

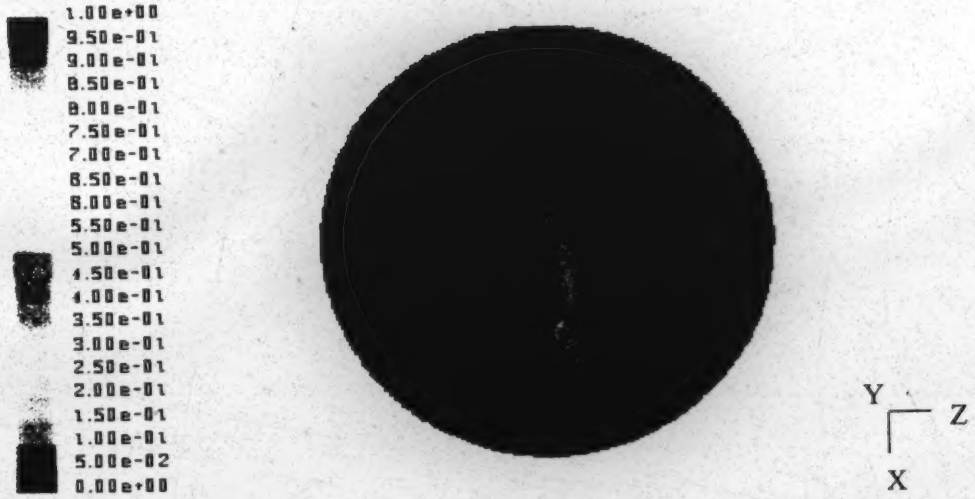

Figure 5.21 Contour plot of mass fraction of CO_2 at Y = - 0.04 m plane

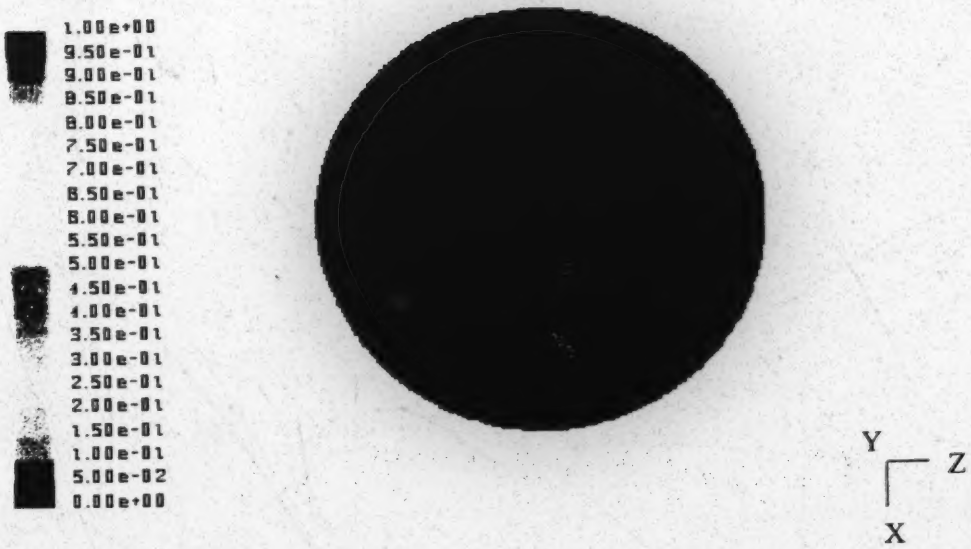

Figure 5.22 Contour plot of mass fraction of CO_2 at Y = 0.0 m plane

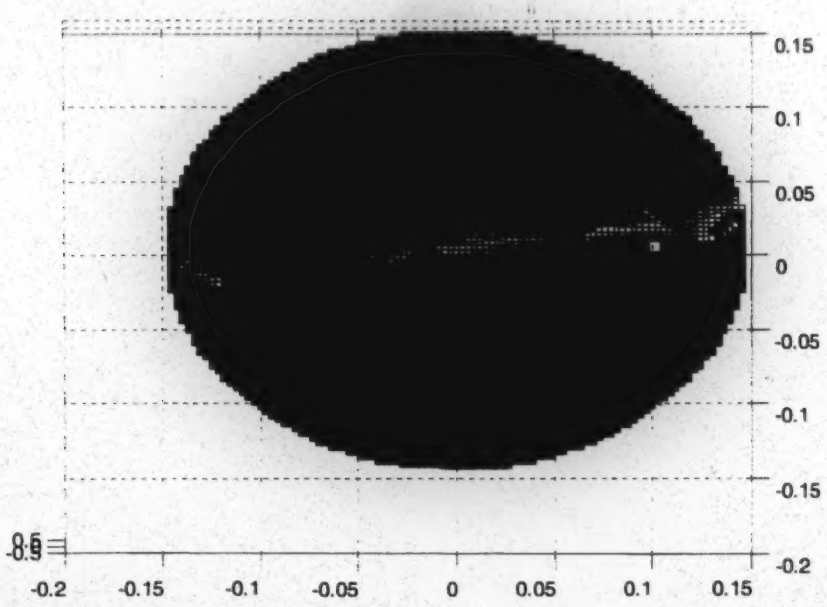

Figure 5.23 Surface plot at Y = 0.0 m (birds' eye view)

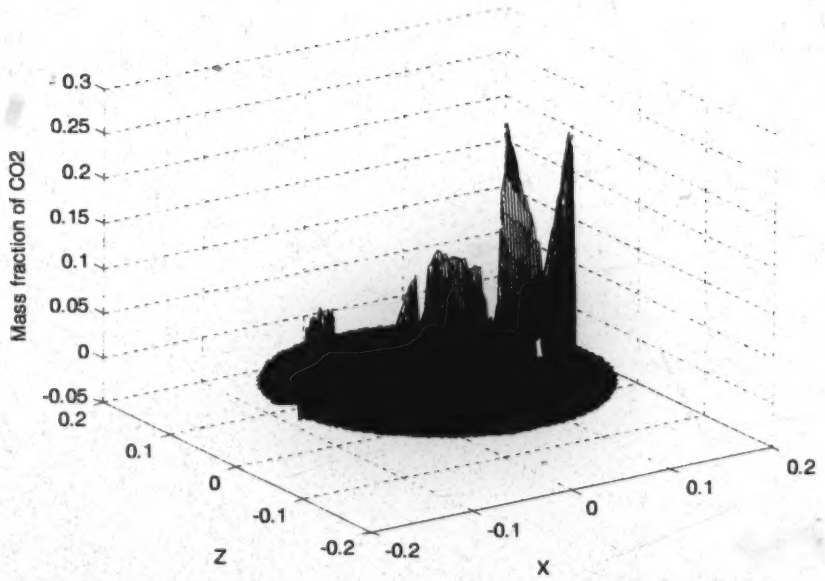

Figure 5.24 Surface plot at Y = 0.0 m plane (3D view)

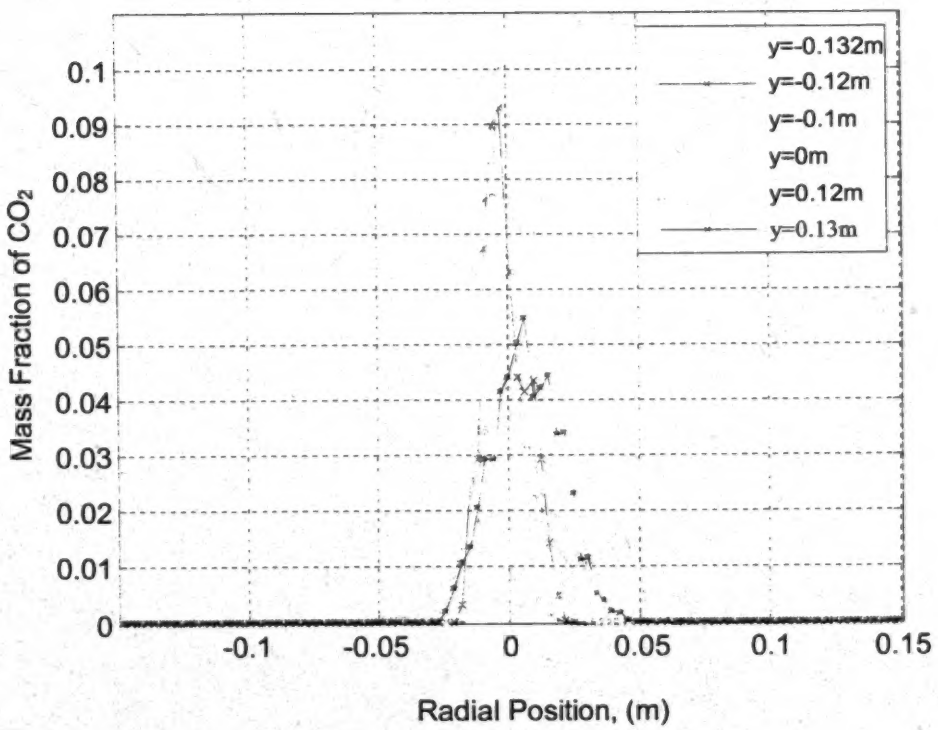

Figure 5.25 Mass fraction of CO_2 at different Y planes

5.11 Conclusions

The simulations for two-phase pressure drop with UofA's model were not successful due to the complicated nature of structured packings geometry. Although the simulations with Zogg's model were successful, the results could not be compared due to the unavailability of multiphase pressure drop data for this model (Zogg, 1972).Similarly, the simulations results for single phase tracer dispersion with UofA's model could not be compared. Although two-phase tracer dispersion experimental data was available for the whole column of UofA's model, we could not do the two-phase tracer dispersion simulations since the hydrodynamics simulations for two-phase flow with this model was not successful.

Chapter 6 Future Work

6.1 Mass Transfer Modeling

Our future work on structured packing will focus mainly on modeling of the interphase mass transfer and the prediction of mass transfer efficiencies in structured packed column. The main goal in packed column design is to maximize the separation efficiency. CFD can play a great role in respect of that. With the help of CFD, inter-phase mass transfer in packed column can be modeled and thus the mass transfer efficiency can be predicted. After the species conservation equations have been solved numerically, the composition of the phases can be predicted from which the mass transfer efficiencies can be computed. Experimental data will be needed to validate the model. One can also use experimental data from literature, such as, Baten et al. (2001, 2002) ,Billet et al. (1999), Cavatorta et al. (1999, 2000), Nawrocki et al. (1991), Rocha et al. (1996), Wronski et al. (1998), Zogg (1973) etc.

The success of mass transfer model depends on the success of the hydrodynamics model since the values of velocity and volume fractions obtained from the hydrodynamics simulation are used in species transport simulations.

6.2 Prediction of Mass Transfer efficiency

Height equivalent to theoretical plate (HETP) is one of the most often used measures to characterize the separation efficiency of a packed column. The success of any hydrodynamics and mass transfer model relies on its ability to predict HETP accurately. The comparisons between the measured and simulated HETPs will be made at a given operating condition and packed bed height for a specific packing types. The variation of HETP with the loading is also an important concern in mass transfer modeling. The flow

maldistribution also need to be considered in order obtain a better prediction of mass transfer efficiency.

To date, few researchers have attempted to predict the mass transfer performance from the fluid flow mechanism inside the packed bed. A model of liquid flow in structured packing based on a wetted-wall analogy was developed and tested by Bravo et al. (1985). It focused mainly on gauge-type structured packing. An equivalent diameter for the packing was defined in this paper and was used along with the correlations given by Johnstone et al. (1942) and Higbie (1935) for the gas and liquid side mass transfer coefficient respectively.

6.3 Prediction of Residence Time Distributions

Residence time distribution (RTD) has been extensively used to characterize mixing and flow non-idealities in process vessels. Computational fluid dynamics (CFD) can play a major role to predict the residence time distributions of the gas or liquid phase (single phase flow) and of the liquid and gas phases (two phase flow) in structured packed column. In this case, the flow is assumed unsteady, so the time component in the transport equations should be considered.

Bibliography

Baten, J. M. and Krishna, R., 2002, Gas and liquid phase mass transfer within KATAPAK-S structures studied using CFD simulations, *Chemical Engineering Science*, 57: 1531–1536.

Baten, J. M., Ellenberger, J. and Krishna, R., 2001, Radial and axial dispersion of the liquid phase within a KATAPAK-S structure: experiments vs. CFD simulations, *Chemical Engineering Science*, 56: 813-821.

Baten, J.M. and Krishna, R., 2001, Liquid phase mass transfer within KATAPAK-S structures studied using CFD simulations, *Catalysis Today*, 69: 371-377.

Bear, J., 1972, *Dynamics of fluids in porous media*, (Elsevier, New York).

Billet, R. and Schultes, M., 1999, Prediction of mass transfer columns with dumped and arranged packings, *Trans IChemE*, 77-A: 498-504.

Billet, R., 1995, *Packed towers in processing and environmental technology*, (VCH Publishers, Weinheim, Germany).

Billet, R., 1989, Predicting mass transfer in packed columns. In: *Packed column design and analysis*. Bochum: Ruhr University Bochum.

Bird, R.B., Stewart, W.E. and Lightfoot, E.N., 1960, *Transport Phenomena*, (Wiley, New York).

Bravo, J.L., Rocha, J.A. and Fair, J.R., 1992, A comprehensive model for the performance of columns containing structured packings, *Institute of Chemical Engineering Synp. Ser.*, A489:128.

Bravo, J. L., Rocha, J. A. and Fair, J. R., 1986, Pressure drop in structured packings, *Hydrocarbon Processing*, 45-49.

Bravo, J.L., Rocha, J.A. and Fair, J.R., 1985, Mass transfer in gause packings, *Hydrocarbon Processing* 64: 91.

Brunazzi, E. and Paglianti, A., 1997, Mechanistic pressure drop model for columns containing structured packings, *AIChe Journal*, 43: 317.

Brunazzi, E., Nardini, G., Paglianti, A. and Petarca, L., 1985, Interfacial area of mellapak packing: absorption of 1,1,1-trichloroethane by genosorb 300, *Chemical Engineering and Technology*, 18: 248.

Cavatorta, O.N. and Bohm, U., 2000, Systems with structured packing: fluid dynamics and liquid-solid mass transfer, *Chem. Eng. Technol.*, 23(11): 1021–1026.

Cavatorta, O. N., Bohm, U. and M.C., Giorgio, 1999, Fluid-dynamic and mass transfer behavior of static mixers and regular packings, *AIChe Journal*, 45(5): 938 – 948.

Courant, R., Isaacson, E. and Rees, M., 1952, On the solution of non-linear hyperbolic differential equations by finite differences, *Comm. Pure Appl. Math.*, 5: 243.

Crowe, C., Sommerfield, M., and Tsuji, Y., 1998, *Multiphase flows with droplets and particles* (CRC Press, Boca Raton).

Fair, J. R., Seibert, A. F., Behrens, M., Saraber, P. P. and Olujic, Z., 2000, Structured packing performance – Experimental evaluation of two predictive models, *Ind. Eng. Chem. Res.* 39: 1788-1796.

Greenkorn, R. A. and Kessler, D. P., 1969, Dispersion in heterogeneous nonuniform anisotropic porous media, *Ind. and Eng. Chem.*, 61(9): 14-32.

Higbie, R., 1935, The rate of absorption of a pure gas into a still liquid during short periods of exposure, *Trans. Am. Inst. Chem. Eng.*, 31: 365-389.

Hoek, P.J., Wesselingh, J.A. and Zuiderweg, F.J., 1986, Small scale and large scale liquid maldistribution in packed columns, *Trans IChemE, Chem Eng Res Des*, 64: 431–449.

Iliuta, I., Petre, C. F. and Larachi, F., 2004, Hydrodynamic continuum model for two-phase flow structured-packing-containing columns, *Chemical Engineering Science*, 59: 879–888.

Iliuta, I. and Larachi, F., 2001, Mechanistic model for structured-packing-containing columns: irrigated pressure drop, liquid holdup, and packing fractional wetted area, *Ind. Eng. Chem. Res*, 40: 5140-5146.

Iliuta, I., Larachi, F. and Al-Dahhan, M. H., 2000, Double-slit model for partially wetted trickle flow hydrodynamics, *AIChE Journal*, 46(3): 597-609.

Johnstone, H. F. and Pigford, R. L., 1942, Distillation in a wetted-wall column, *Trans. Am. Inst. Chem. Eng.*, 38: 25-50.

Kister, H. Z., 1992, *Distillation Design*, (McGraw-Hill, New York).

Larachi, F., Petre, C. F., Iliuta, I. and Grandjean, B., 2003, Tailoring the pressure drop of structured packings through CFD simulations, *Chemical Engineering and Processing*, 42: 535-541.

Liu, S. J. and Masliyah, J. H., 1996, Single fluid flow in porous media, *Chem. Eng. Comm.*, 148-150: 653-732.

Nardini, G., Paglianti, A., Petarca, L. and Viviani, E., 1996, Sulzer BX Gause: fluodynamics and absorption of acid gases, *Chemical Engineering and Technology*: 19, 20.

Olujic, Z., 1999, Effect of column diameter on pressure drop of a corrugated sheet structured packing, *TransIChemE*, 77: 505.

Olujic, Z., 1997, Development of a complete simulation model for predicting the hydraulic and separation performance of distillation columns equipped with structured packings, *Chemical and Biochemical Engineering Quarterly*, 11: 31.

Nandakumar, K., Chuang, K. T., Song, M. and Yin, F. H., 1999, Recent advances on modeling separation processes in random packed columns, *Recent Res. Devel. Chemical Engg.*, 3: 87-106.

Nawrocki, P. A., Z. P. Xu and Chuang, K. T., 1991, Mass transfer in structured corrugated packing, *Canadian Journal of Chemical Engineering*, 69(12): 1336-1343.

Olujic, Z. and de Graauw, J., 1989, Appearance of maldistribution in distillation columns equipped with high performance packings, *Chem. Biochem. Eng.* Q3 (4): 181-196.

Onda, K., 1968, Mass transfer coefficients between gas and liquid phases in packed columns, *J. Chem. Eng. Jpn.*, 1: 56-62.

Petre, C. F., Larachi, F., Iliuta, I. and Grandjean, B. P. A., 2003, Pressure drop through structured packings: Breakdown into the contributing mechanisms by CFD modeling, *Chemical Engineering Science*, 58: 163–177.

Ranke, H., Lerzer, R. and Becker, O., 2000, Hydraulic calculations for cross-channeled packings in distillation units based on a physical model, *Chem. Eng. Technol.*, 23(8): 691.

Reynolds, O., 1895, On the dynamical theory of incompressible viscous fluids and the determination of the criterion, *Philosophical Transactions of the Royal society of London, Series A*, 186: 123.

Robins, L.A., 1991, Improve pressure-drop prediction with a new correlation, *Chemical Engineering Progress*, 87, 87.

Rocha, J. A., Bravo, J. L. and Fair, J. R., 1996, Distillation columns containing structured packings: a comprehensive model for their performance. 2. Mass-transfer model, *Ind. Eng. Chem. Res.* 35: 1660-1667.

Rocha, J. A., Bravo, J. L. and Fair, J. R., 1993, Distillation columns containing structured packings: a comprehensive model for their performance. 1. Hydraulic model, *Ind. Eng. Chem. Res.*, 32: 641-651.

Romkes, S. J. P., Dautzenberg, F. M., Van den Bleek, C. M. and Calis, H. P. A., 2003, CFD modelling and experimental validation of particle-to-fluid mass and heat transfer in a packed bed at very low channel to particle diameter ratio, *Chemical Engineering Journal*, 96: 3–13.

Sherwood, T.K., Pigford, R.L. and Wilke, C.R., 1975, *Mass Transfer*, (McGraw-Hill, USA).

Shi, M. G. and Mersmann, A., 1985, Effective interfacial area in packed column, *Ger. Chem. Eng*, 8: 87-96.

Slattery, J. C., 1969, Single-phase flow through porous media, *AIChE J.*, 15: 866-872.

Spiegel, L. and Meier, W.A., 1992, Generalized pressure drop model for structured packings, *Institute of Chemical Engineering Symposium Series*, 128: B85.

Spiegel, L., Meier, W.A., 1987, Correlations of the performance characteristics of the various mellapak types, 104, A203.

Stichlmair, J., Bravo, J.L. and Fair, J.R., 1989, General model for prediction of pressure drop and capacity of countercurrent gas/liquid packed columns. *Gas Separation and Purification*, 3: 19.

Strigle, R. F., 1994, *Pollution control. in packed tower design and applications: random and structured packing*, Gulf Publishing Company, (Houston, TX).

Sun, C. G., Yin, F. H., Afacan, A., Nandakumar, K. and Chuang, K. T., 2000, Modeling and simulation of flow maldistribution in random packed columns with gas-liquid countercurrent flow, *Trans. IChemE*, 78: 378-388.

Uresti-Melendez, J., Alvarado, F. J. and Rocha, J. A., 1994, Effect of packing material in distillation with structured packings, *In Separation Technology*, Vansant, E. F.,Ed., Elsevier Science, Amsterdam, The Netherlands, 153-162.

Van Doormal, J. P. and Raithby, G. D., 1984, Enhancements of the SIMPLE method for predicting incompressible fluid flows, *Numer. Heat Transfer*, 7: 147.

Wankat, P.C., 1988, *Equilibrium staged separations*, Prentice-Hall Inc., (Englewood Cliffs, New Jersey).

Whitaker, S., 1966, The equations of motion in porous media, *Chem. Eng. Sci.*, 21: 291-300.

Wilcox, D. C., 1993, *Turbulence modeling for CFD*, DCW Industries, Inc., (La Canada, California).

Woerlee, G.F., Berends, J., Olujic, Z. and Graauw, J., 2001, A comprehensive model for the pressure drop in vertical pipes and packed columns, *Chemical Engineering Journal* 84: 367–379.

Wronski, S. and Molga, E., 1998, Mass transfer model for the film countercurrent flow of two liquid phases in a packed bed column, *Chemical Engineering and processing*, 37: 47-54.

Yin, F. H., Afacan, A., Nandakumar, K., and Chuang, K. T., 2002, CFD simulation and experimental study of liquid dispersion in randomly packed metal pall rings, *Chem. Eng. Process.*, 41: 473-483.

Zogg, M., 1973, Stoffaustausch in der Sulzer-Gewebepackung, *Chemie-Ing-Techn.*, Jahrg., 45(2): 67-74.

Zogg, M, 1972, *Strömungs-und stoffaustauschuntersuchungen an der Sulzer-Gewebepackung*, Diss. No. 4886, Technische Hochscule Zürich.

Appendix

Matlab Script for Tracer Dispersion:

```
clear all
close all
clc
load('outlet.mat');
surface_area=0.0706788; % got from fluent
n=30;
a=surface_area/n;
for i=1:n
   r(i)=i*a/pi;
end
N=size(Vy,1)
for i=1:N
   rr(i)=x(i)*x(i)+z(i)*z(i);
end
k=find(rr<=r(1));
cu(1)=sum(co2(k).*Vy(k));
%c(1)=sum(co2(k));
u(1)=sum(Vy(k));
for j=2:n
   k=find(rr<=r(j) & rr>r(j-1));
   cu(j)=sum(co2(k).*Vy(k));
   c(j)=sum(co2(k))/length(k);
   u(j)=sum(Vy(k));
end
C=cu./u;
R(1)=0.5*r(1);
for m=2:n
   R(m)=0.5*(r(m-1)+r(m));
end
columnrad=sqrt(R);
plot(columnrad,C);
figure
xlin=linspace(min(x),max(x),100);
zlin=linspace(min(z),max(z),100);
[X,Z]=meshgrid(xlin,zlin);
CO2=griddata(x,z,co2,X,Z,'cubic');
surf(X,Z,CO2);
figure
plot3(x,z,co2,'.')
n=30;
xn=linspace(min(x),max(x),n);
for j=2:n
```

```
  k=find(x<=xn(j) & x>xn(j-1));
  cu2(j)=sum(co2(k).*Vy(k));
  c2(j)=sum(co2(k))/length(k);
  u2(j)=sum(Vy(k));
end
C2=cu2./u2;
for m=2:n
  Xn(m)=0.5*(xn(m-1)+xn(m));
 end
figure
plot(Xn,C2);
zn=linspace(min(z),max(z),n);
for j=2:n
  k=find(z<=zn(j) & z>zn(j-1));
  cu3(j)=sum(co2(k).*Vy(k));
  c3(j)=sum(co2(k))/length(k);
  u3(j)=sum(Vy(k));
end
C3=cu3./u3;
for m=2:n
  Zn(m)=0.5*(zn(m-1)+zn(m));
end
figure
plot(Zn,C3);
```